

AD-A194 692

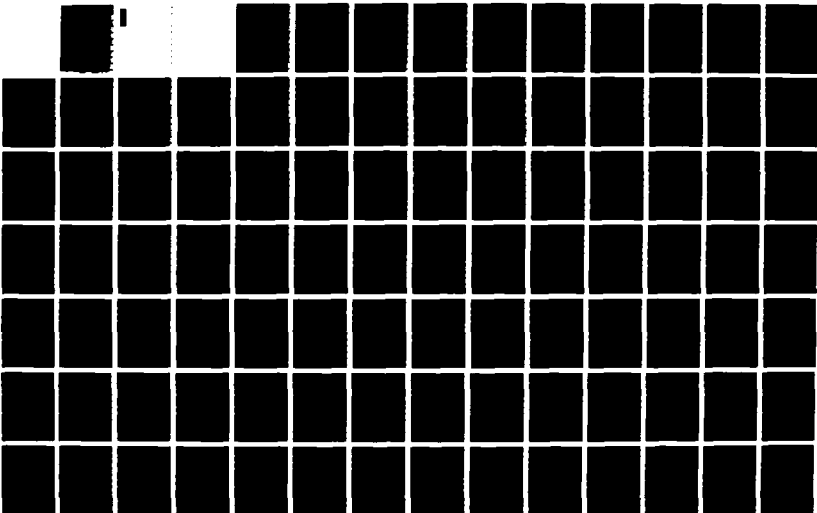
THERMAL CONDUCTIVITY EFFECTS ON SHS (SELF-PROPAGATING
HIGH-TEMPERATURE SY. (U) ARMY BALLISTIC RESEARCH LAB
ABERDEEN PROVING GROUND MD T KOTTKE ET AL. MAR 88
BRL-TR-2089

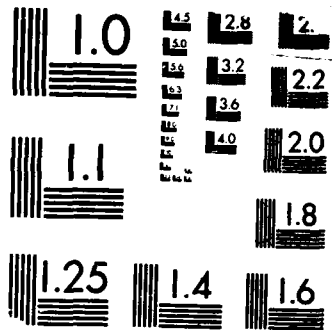
1/2

UNCLASSIFIED

F/G 20/13

ML





MICROCOPY RESOLUTION TEST CHART
 NATIONAL BUREAU OF STANDARDS-1963-A

UNCLASSIFIED

SECURITY CLASSIFICATION OF THIS PAGE

ADA194692

REPORT DOCUMENTATION PAGE

Form Approved OMB No. 0704-0188

1a. REPORT SECURITY CLASSIFICATION Unclassified		1b. RESTRICTIVE MARKINGS	
2a. SECURITY CLASSIFICATION AUTHORITY N/A		3. DISTRIBUTION / AVAILABILITY OF REPORT	
2b. DECLASSIFICATION / DOWNGRADING SCHEDULE N/A			
4. PERFORMING ORGANIZATION REPORT NUMBER(S) BRL-TR-2889		5. MONITORING ORGANIZATION REPORT NUMBER(S)	

6a. NAME OF PERFORMING ORGANIZATION USA Ballistic Research Laboratory	6b. OFFICE SYMBOL (if applicable) SLCBR-TB	7a. NAME OF MONITORING ORGANIZATION	
6c. ADDRESS (City, State, and ZIP Code) Aberdeen Proving Ground, Maryland 21005-5066		7b. ADDRESS (City, State, and ZIP Code)	

8a. NAME OF FUNDING / SPONSORING ORGANIZATION USA Ballistic Research Lab	8b. OFFICE SYMBOL (if applicable) SLCBR-D	9. PROCUREMENT INSTRUMENT IDENTIFICATION NUMBER	
8c. ADDRESS (City, State, and ZIP Code) Aberdeen Proving Ground, Maryland 21005-5066		10. SOURCE OF FUNDING NUMBERS	
		PROGRAM ELEMENT NO.	PROJECT NO.
		TASK NO.	WORK UNIT ACCESSION NO.

11. TITLE (Include Security Classification)
Thermal Conductivity Effects on SHS Reactions

12. PERSONAL AUTHOR(S)
Dr. T. Kottke a Dr. A. Niiler

13a. TYPE OF REPORT TR	13b. TIME COVERED FROM _____ TO _____	14. DATE OF REPORT (Year, Month, Day)	15. PAGE COUNT
---------------------------	--	---------------------------------------	----------------

16. SUPPLEMENTARY NOTATION

17. COSATI CODES			18. SUBJECT TERMS (Continue on reverse if necessary and identify by block number) SHS → Powder Compact Density; → Solid Combustion; Thermal Conductivity, → Ceramics; Propagation Velocity.
FIELD	GROUP	SUB-GROUP	
11	02		

19. ABSTRACT (Continue on reverse if necessary and identify by block number)
→ The effects of green compact thermal conductivity on SHS reaction initiation and propagation velocity have been modeled for the titanium and carbon system. This modeling predicts that, for a given filament power input, the time required to ignite an SHS reaction is a strong function of the green compact thermal conductivity. It also predicts that, for systems where the mass diffusion rate is high, the green compact thermal conductivity controls the reaction front velocity. Thermal conductivities of mixed titanium and graphite powder compacts have been measured for compact densities ranging from 58% to 81% of maximum theoretical density and have been found to increase by a factor of four in this density range. Modeling results suggest this change in thermal conductivity with density is sufficient to have marked affect on SHS initiation and reaction velocity. An anisotropy of the mixed titanium and graphite powder compact thermal conductivities, which increase with increasing compaction density, was also observed. This anisotropy is thought to be the result of graphite powder particle orientation and pore deformation (con't on reverse side)

20. DISTRIBUTION / AVAILABILITY OF ABSTRACT <input checked="" type="checkbox"/> UNCLASSIFIED/UNLIMITED <input checked="" type="checkbox"/> SAME AS RPT <input type="checkbox"/> DTIC USERS		21. ABSTRACT SECURITY CLASSIFICATION UNCLASSIFIED <i>→ next page</i>	
22a. NAME OF RESPONSIBLE INDIVIDUAL Dr. Thomas Kottke		22b. TELEPHONE (Include Area Code) 301/278-2557	22c. OFFICE SYMBOL SLCBR-TB-EP

UNCLASSIFIED

19. Abstract (con't)

resulting from the uniaxial compacting force. The importance of controlling green compact thermal conductivities, methods of accomplishing this by varying the ratio of crystalline to amorphous carbon in the powder mixture and the application of this control to processing and final product material characteristics are discussed. *Keywords:*

UNCLASSIFIED

ACKNOWLEDGEMENTS

The authors would like to thank Laszlo Kecskes, Michael Riley and Frederick Bart Pierce for assisting with the experimental measurements and Dr. John Powell for useful discussions concerning the analysis of the thermal conductivity data.



Accession For	
NTIS GRA&I	<input checked="" type="checkbox"/>
DTIC TAB	<input type="checkbox"/>
Unannounced	<input type="checkbox"/>
Justification	
By _____	
Distribution/	
Availability Codes	
Dist	Avail and/or Special
A-1	

TABLE OF CONTENTS

	Page
ACKNOWLEDGEMENTS.....	iii
LIST OF FIGURES.....	vii
LIST OF TABLES.....	ix
1. INTRODUCTION.....	1
2. REACTION MODELING.....	2
2.1 Model Overview.....	2
2.2 Model Verification.....	4
2.3 Model Input Parameters.....	7
2.4 Propagation Velocity Modeling.....	13
2.5 Reaction Initiation Modeling.....	14
2.6 Summary of Modeling Results.....	22
3. EXPERIMENTAL TECHNIQUES.....	25
3.1 Experimental Overview.....	25
3.2 Heat Stage.....	25
3.3 Sample Stage.....	29
3.4 Sample Preparation.....	29
3.5 Apparatus Calibration.....	29
3.6 Data Acquisition.....	33
3.7 Data Analysis.....	34
4. EXPERIMENTAL RESULTS AND DISCUSSION.....	35
5. SUMMARY.....	47
REFERENCES.....	51
APPENDIX A - SHS Reaction Initiation and Propagation Simulation Software.....	55
APPENDIX B - Electronic Component Values.....	69

	PAGE
APPENDIX C - Thermal Conductivity Apparatus Calibration Program.....	71
APPENDIX D - Thermal Conductivity Data Acquisition Program.....	79
APPENDIX E - Thermal Conductivity Data Analysis Program.....	85
DISTRIBUTION LIST.....	91

LIST OF FIGURES

FIGURE	PAGE
1 Comparison of numerical analysis model results (black circles) and partial differential equation results (solid line) for the test case of a slab of initially constant temperature bounded by temperature reservoirs at 0 C.....	6
2 Comparison of numerical analysis model results (black circles) and partial differential equation results (solid line) for the test case of a slab with an initial linear temperature distribution bounded by temperature reservoirs at 0 C.....	8
3 Comparison of numerical analysis model results (black circles) and partial differential equation results (solid line) for the test case of a slab, initially at 0 C, with adiabatic walls and energy flux F at the $x=L$ region.....	9
4 Geometry of space volumes used for SHS propagation velocity modeling.....	15
5 Position versus time plot for simulation of TiC SHS reaction propagating through an array of space volumes.....	16
6 Predicted dependence of SHS propagation velocity on powder compact thermal conductivity for the titanium and carbon system. Dotted line added to guide the eye.....	17
7 Computed TiC SHS ignition time versus array matrix dimension. Dotted line added to guide the eye.....	18
8 Computed SHS reaction propagation velocity versus iteration time interval for the titanium and carbon system. Thermal conductivity values are in W/m-K. Dotted lines are added to guide the eye.....	20
9 Computed TiC SHS reaction initiation time versus filament power density. Open symbols represent filament power densities which are predicted to lead to filament failure before reaction initiation. Dotted lines are added to guide the eye.....	21
10 Volume element temperatures of a 0.5 W/m-K thermal conductivity titanium and graphite powder compact array following 0.08 second of filament heating from ambient temperature.....	23
11 Volume element temperatures of a 9.2 W/m-K thermal conductivity titanium and graphite powder compact array following 0.08 second of filament heating from ambient temperature.....	24
12 Overall schematic of thermal conductivity measuring apparatus.....	26
13 Thermal conductivity apparatus heat stage.....	27

FIGURE	PAGE
14 Schematic of heat stage thermocouple electronics. Component values are listed in Appendix B.....	28
15 Schematic of sample thermocouple electronics. Component values are listed in Appendix B.....	30
16 Titanium/graphite powder mixture green compact density versus compaction pressure for 1/2-inch diameter opposed anvil die.....	31
17 Experimental data of temperature at $x = 0$ surface versus time and plot of Eq. 25 for best fit thermal conductivity value.....	35
18 Thermal conductivity of titanium and graphite powder compacts in the directions parallel and perpendicular to the direction of compaction as a function of powder compact density and percent theoretical compaction density.....	37
19 Thermal conductivity versus powder compact density for $2\text{Fe}_2\text{O}_3 + 3\text{Ti} + 2.26\text{TiO}_2$ (squares), $2\text{Cr}_2\text{O}_3 + 3\text{Zr} + 2.8\text{ZrO}_2$ (circles) and $\text{Cr}_2\text{O}_3 + 2\text{Al} + 0.64\text{Al}_2\text{O}_3$ (triangles) systems as measured by Butakova et. al. ³³	38
20 Possible effect of non-isostatic pressure on pore geometry.....	42
21 Observed green compact thermal conductivity anisotropy versus density.....	43
22 Thermal diffusivity of titanium and graphite powder compacts in the direction perpendicular to the direction of compaction as a function of powder compact density.....	46
23 Predicted dependence of SHS propagation velocity on powder compact density for the titanium and carbon system.....	47

LIST OF TABLES

	PAGE
1 Ti+C Powder Compact Attributes.....	32
2 Ti+C Powder Compact Thermal Conductivities.....	39

1. INTRODUCTION

Self-propagating high-temperature synthesis (SHS) is a relatively new process for producing refractory ceramic materials. This method usually involves mixing and compressing powders into green compacts which are then synthesized into the final product by an exothermic self-sustaining reaction wave. As opposed to conventional ceramic processing techniques which often require extended times at high temperatures, the SHS process is rapid and potentially energy efficient. A fast heat pulse such as that provided by a heated filament, spark or laser, is generally all that is required to initiate the exothermic synthesis reaction which then propagates through the remainder of the green compact without additional external energy

requirements.¹ One promising feature of this technique is the potential for simultaneous material synthesis and product fabrication by forming the precursor green compacts into the shape of the desired piece. The final products of SHS reactions that are synthesized without external containment are often very porous. Thus commercial applications of this process have been limited to the production of ceramic powders. However, more recent SHS studies have focused on methods for producing fully dense materials by various compaction schemes during or shortly following the synthesis reaction.^{2,3,4,5}

The thermal conductivity of the precursor powder compacts has been studied for the importance of its role in controlling the characteristics of both the SHS reaction and the final products. The green compact thermal conductivity and the mass diffusion rates of the reactant materials are the predominant limiting factors which determine the rate of synthesis or propagation velocity of the synthesis wave.⁶ Solid combustion of energetic materials, for which mass diffusion rates are high, has been shown to be rate limited by the thermal conductivity of the unreacted material with small additions of high thermal conductivity material greatly increasing reaction velocities. The properties of materials produced by the SHS method are determined in part by this synthesis rate or propagation velocity of the reaction zone in the green compact. One factor which is thought to be partially responsible for the highly porous nature of many SHS final products is the expulsion of volatiles from the precursor powders while the green compact is being heated prior to the arrival of the synthesis reaction wave.^{7,8,9} The temperature profile of the green compact ahead of the advancing synthesis zone, both in time and space, is controlled by the thermal conductivity of the green compact. The rate of green compact outgassing, which is temperature dependent, and thus the final product porosity is therefore also expected to be partially controlled by the green compact thermal conductivity. In addition, the ease with which an SHS reaction can be initiated within a given green compact also depends on the green compact thermal conductivity.¹⁰

The aim of this study has been to investigate the possible effects of green compact thermal conductivity on the SHS initiation process and propagation rate. This task was performed in two concurrent steps. The SHS synthesis process was modeled to determine what magnitude of thermal conductivity variations would be required to appreciably affect the SHS ignition conditions and combustion wave velocity. In addition, the thermal

conductivity of mixed titanium and carbon powder compacts was measured as a function of compaction density. This was done to determine whether the actual green compact thermal conductivities were in fact in the range to affect SHS initiation and reaction rates as predicted by the modeling study. The relative importance of thermal conductivity versus mass diffusion as rate limiting factors in SHS reactions is also discussed.

2. REACTION MODELING

2.1 Model Overview:

A numerical analysis model was developed for simulating exothermic heat generation and transport through a green compact where the powder compact was treated as a three-dimensional array of finite homogeneous cubic volume elements. Systems with convenient geometries and well defined boundary conditions might be analyzed more elegantly and easily using the standard differential equations of heat conduction. However, the ultimate goal of this modeling exercise is to have flexibility in simulating the contained reaction of SHS samples, mimicking conditions similar to those of experiments being performed in the laboratory. Experimental realities include unusual sample geometries with multiple layers of thermal insulation and containing walls, heats of transformation, temperature dependent thermal conductivities and specific heats. Since these unavoidable factors may present problems for a strictly analytical treatment, a numerical approach has been followed from the start. A Cartesian coordinate system was similarly chosen for this modeling because of its direct applicability to proposed simulations of experimental geometries.

In this finite element approach, the powder compact is subdivided into volume cells on the scale of the powder particles of which it is composed and the time scale of the SHS reaction is divided into units which are small enough to allow for an accurate approximation to a continuous time evolution. During each interval of time, the thermal interactions between all pairs of interacting volume cells are calculated separately. The thermal interactions for each space volume are then combined to yield the total thermal interaction. In this way, the flow of heat through the three dimensional array is reduced to the calculation and combination of many two-body heat flow problems which, although requiring careful bookkeeping, is quite simple.

When two bodies interact thermally, heat energy is transferred from the warmer to the cooler body at a rate which depends on the temperature difference between the two, their thermal conductivities, and their geometries, including the shared cross-sectional area. The change in temperature of these bodies as a result of this heat energy transfer depends on their masses and specific heats. This time dependent transfer of heat energy can be treated as being analogous to the transfer of charge between two electrical capacitors through a resistor. The results of circuit theory¹¹ give:

$$V_1(t) = i_{V_1} + \frac{(i_{V_2} - i_{V_1})}{1 + \frac{C_1}{C_2}} (1 - \exp(-\frac{1}{R}(\frac{1}{C_1} + \frac{1}{C_2})t)) \quad (1)$$

Following this analogy, if the electrical potential (V) is equivalent to temperature, electrical resistance (R) is equivalent to the thermal resistance, or inverse thermal conductivity, and the capacitance (C) is equivalent to the heat capacity, which is the mass times the specific heat, then Eq. 1 becomes:

$$T_1(t) = i_{T_1} + \frac{(i_{T_2} - i_{T_1})}{1 + \frac{m_1 c_1}{m_2 c_2}} (1 - \exp(-\frac{k_{eff} A}{L}(\frac{1}{m_2 c_2} + \frac{1}{m_1 c_1})t)) \quad (2)$$

where T is the block temperature with the superscript i representing an initial condition, t is the time, m is the block mass, c is the block specific heat, k_{eff} is an effective combined thermal conductivity for the two blocks, A is the cross-sectional area shared by the blocks, L is the distance between the centers of mass of the blocks and the subscripts denote the block number. Briefly considering some limiting cases of Eq. 2:

- a) If the initial temperatures of the blocks are the same, then the temperature of block one remains constant.
- b) For $t=0$, the temperature of block one is equal to its initial temperature.
- c) If $m_1 c_1 \gg m_2 c_2$, then the change in temperature of block one over a given period of time will be small.
- d) For infinitely long times and blocks with equal heat capacities, the final temperature of the blocks is the average of their initial temperatures.

This cursory analysis of Eq. 2 agrees with physical intuition. The validity of Eq. 2 and the analogy between heat transport and electrical transport will be considered and tested in greater detail later.

The effective thermal conductivity has the property that if $k_1 = k_2 = k_{eff}$, the flow of heat energy would be impeded by the same amount as in the case for the two individual thermal conductivities. An expression for the effective thermal conductivity is derived by considering that the linear heat flow between the two blocks is related to the thermal conductivity of the two blocks in the same manner as electrical current passing through two resistors in series.

$$R_{eff} = R_1 + R_2 \quad (3)$$

$$= \frac{L_1}{A k_1} + \frac{L_2}{A k_2} \quad (4)$$

where R_{eff} is the combined effective thermal resistance of the two blocks, R_1 and R_2 are the individual block thermal resistances, subscripted L is the block dimension, A is the cross-sectional area shared by the blocks and subscripted k is the individual block thermal conductivity. For blocks of the same physical dimensions, $L_1 = L_2$. Substituting into Eq. 4:

$$R_{\text{eff}} = \frac{L}{A} \left(\frac{1}{k_1} + \frac{1}{k_2} \right) = \frac{L_{\text{eff}}}{A_{\text{eff}}} \left(\frac{1}{k_{\text{eff}}} \right) \quad (5)$$

The effective length of the combined blocks is twice the individual length and the shared area remains the same.

$$R_{\text{eff}} = \frac{2L}{A} \left(\frac{1}{k_{\text{eff}}} \right) = \frac{L}{A} \left(\frac{2}{k_{\text{eff}}} \right) \quad (6)$$

Comparing Eq. 5 and Eq. 6:

$$\left(\frac{1}{k_1} + \frac{1}{k_2} \right) = \frac{2}{k_{\text{eff}}} \quad (7)$$

Yielding the final expression for the effective thermal conductivity:

$$k_{\text{eff}} = \frac{2k_1k_2}{(k_1 + k_2)} \quad (8)$$

Again considering limiting cases:

- a) If the thermal conductivities of the two individual blocks are equal, then the effective thermal conductivity is equal to the thermal conductivity of the individual blocks.
- b) If the thermal conductivity of either block is zero, the effective thermal conductivity of the series pair is also zero.
- c) As the thermal conductivity of either block approaches infinity, the effective thermal conductivity of the pair is twice the value of the other block's thermal conductivity.

These limiting cases also agree with physical intuition.

2.2 Model Verification:

In any computer aided numerical analysis modeling exercise there are abundant opportunities for errors to be introduced into the simulation. These errors can be broadly divided into those due to incorrect assumptions on which the simulation is based and errors introduced during software development. It is therefore imperative that computer based models be sufficiently tested so that their results can be accepted with confidence. One convenient method for testing a numerical analysis model is to simulate a test case for which the answer can also be obtained using analytic techniques and then compare the two results. The heat transport software, which is outlined and listed in Appendix A, has been verified against several test cases.

The first test case is linear heat flow in a solid bounded by two parallel planes at $x=0$ and $x=L$ where the bounded region is initially at a positive constant temperature and the unbounded region is kept at zero temperature. Solving the differential equation:

$$\frac{dT}{dt} = \left(\frac{k}{pc}\right)\left(\frac{d^2T}{dx^2}\right), \quad 0 < x < L \quad (9)$$

with $T = 0$ when $x = 0$ and $x = L$ for all t , and $T = T_0$ for $0 < x < L$ when $t = 0$, the temperature at position x and time t can be expressed as:¹²

$$T(x,t) = \frac{4T_0}{\pi} \sum_{n=0}^{\infty} \frac{1}{(2n+1)} \exp(-(k/pc)(2n+1)^2 \pi^2 t/L^2) \sin \frac{(2n+1)\pi x}{L} \quad (10)$$

where k is the thermal conductivity, p is the mass density and c is the specific heat.

This test case can also be easily simulated by the numerical analysis model. All the volume cell temperatures, except for the volume cells representing the bounding planes, are set to the initial temperature, T_0 .

The bounding plane volumes are set to zero temperature and given artificially large values of mass and specific heat to maintain this initial temperature. A bounded region 32 blocks wide is used for the test simulation with the block dimension scaled to the size of powder particles used in making laboratory green compacts. In order to test the numerical analysis model under conditions similar to those that it will eventually be run under, values of thermal conductivity, specific heat and density which were representative of powder compacts were also used. The predicted temperatures from the numerical analysis simulation (black circles) and Eq. 10 (solid line), after an elapse time of 0.05 second, are both shown in Fig. 1. Parameters used in this numerical analysis computation were: (1) block size - 88 microns; (2) time interval - 10 microseconds; (3) mass density - 3750 kg/m^3 ; (4) specific heat - 900 J/kg-K ; (5) thermal conductivity - 9.2 W/m-K and (6) initial temperature - 400 C . As expected, the portions of the bounded region closest to the zero temperature surfaces have experienced the greatest amount of cooling. There is very close correlation between the results of the numerical analysis model and the partial differential equation solution.

A solid bounded by two parallel planes at $x=0$ and $x=L$ was also used for the second test case. However, now the initial temperature distribution was a linear function of the form $T(x) = T_0 x/L$ rather than a constant. The partial differential equation solution of this case can be expressed as:

$$T(x,t) = \frac{2T_0}{\pi} \sum_{n=1}^{\infty} \frac{(-1)^{n-1}}{n} \exp(-(k/pc)n^2 \pi^2 t/L^2) \sin \frac{n\pi x}{L} \quad (11)$$

The numerical analysis model was configured to this test case by setting the initial volume cell temperatures to the same linear function and again using

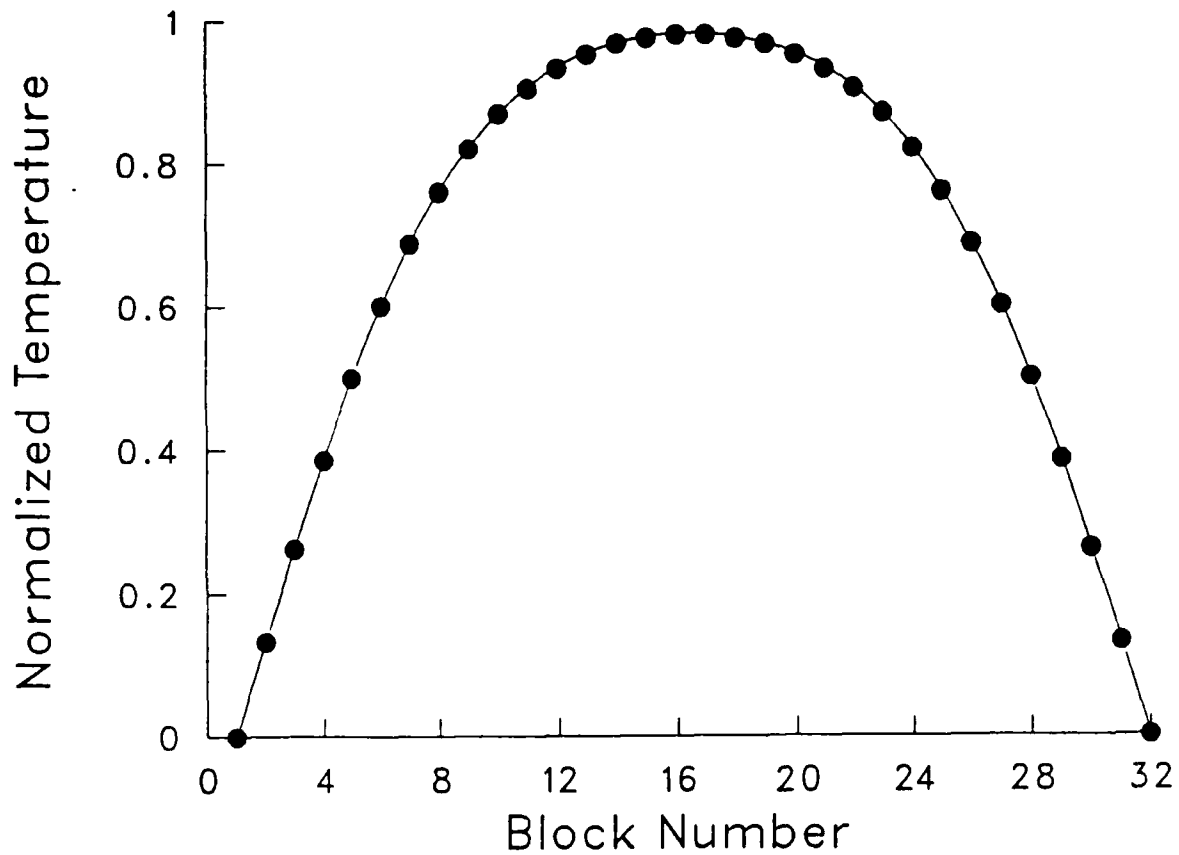


Figure 1. Comparison of numerical analysis model results (black circles) and partial differential equation results (solid line) for the test case of a slab of initially constant temperature bounded by temperature reservoirs at 0 C.

artificially large masses and specific heats for the end volumes to ensure that their temperatures remained at zero. The predicted temperatures after an elapse time of 0.025 second for the numerical analysis model (black circles) and Eq. 11 (solid line) are shown in Fig. 2. Parameters used in the numerical analysis computation were: (1) block size - 88 microns; (2) time interval - 10 microseconds; (3) mass density - 3750 kg/m³; (4) specific heat - 900 J/kg-K; (5) thermal conductivity - 9.2 W/m-K and (6) maximum initial temperature - 400 C. The correlation between the two methods of temperature prediction is again very close.

The final test case again assumes a volume bounded by planes at x=0 and x=L. But this time these planes are treated as adiabatic surfaces. A flat heater is assumed to be embedded in the bounded volume near the x=L plane which supplies a constant flux of heat energy, F, into the solid. The initial temperature of the bound region is assumed to be zero degrees Celsius. Analysis of this configuration using partial differential equations yields the expression:

$$T(x,t) = \frac{Ft}{\rho c L} + \frac{FL}{k} \left(\frac{3x^2 - L^2}{6L^2} - \frac{2}{\pi} \sum_{n=1}^{\infty} \frac{(-1)^n}{n^2} \exp(-(k/\rho c)n^2 \pi^2 t/L^2) \cos \frac{n\pi x}{L} \right). \quad (12)$$

To simulate this configuration using the numerical analysis model, the rise in temperature of the volume cells at the x=L positions was calculated for each interval of time from the heat energy input, mass and specific heat. The predicted results from the numerical analysis simulation (black circles) and the results from Eq. 12 (solid line) after an elapsed time of 0.05 second are both shown on Fig. 3. Numerical analysis parameters used in this computation were: (1) block size - 88 microns; (2) time interval -

- 10 microseconds; (3) mass density - 3750 kg/m³; (4) specific heat - 900 J/kg-K; (5) thermal conductivity - 9.2 W/m-K and (6) heat energy flux - 8.6E+8 W/m².

In all three test cases, the results of the numerical analysis simulation agree well with the analytic results obtained from a partial differential equations analysis. This close correlation indicates that the expression given in Eq. 2, which was arrived at using an analogy between heat transport and current flow in an electric circuit, is valid. In addition, the software that utilizes this expression to simulate heat flow, also appears to be free of errors.

2.3 Model Input Parameters:

No matter how much a numerical analysis simulation program is tested and verified, it is an inescapable reality that "garbage in gives garbage out". Since the simulated results depend directly on the input parameters, much emphasis must be spent on obtaining accurate input values. For the simulations of titanium carbide SHS initiation and reaction, input values were required for material properties such as specific heat, thermal conductivity, heats of reaction, heats of transformation, melting points and density. Wherever possible, the temperature dependence of these quantities was also considered because the SHS reaction involves temperature changes of thousands of degrees.

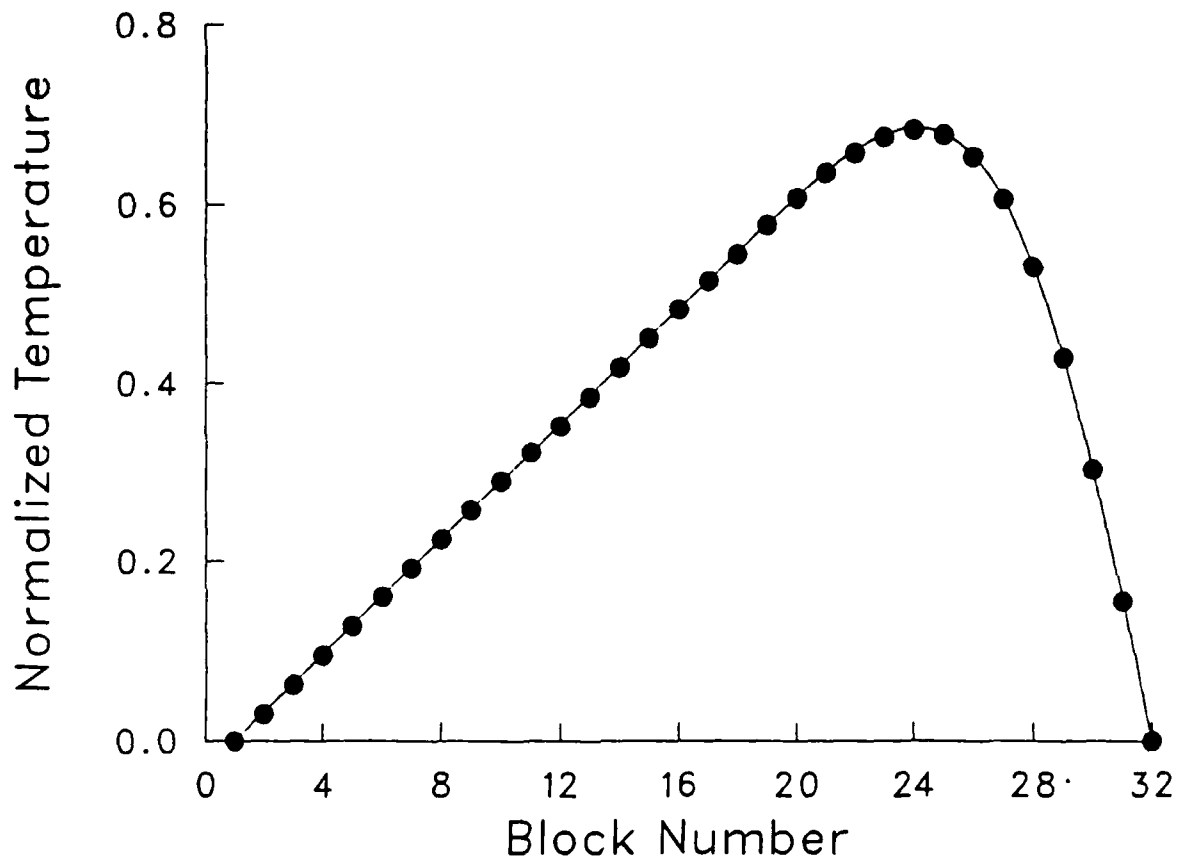


Figure 2. Comparison of numerical analysis model results (black circles) and partial differential equation results (solid line) for the test case of a slab with an initial linear temperature distribution bounded by temperature reservoirs at 0 C.

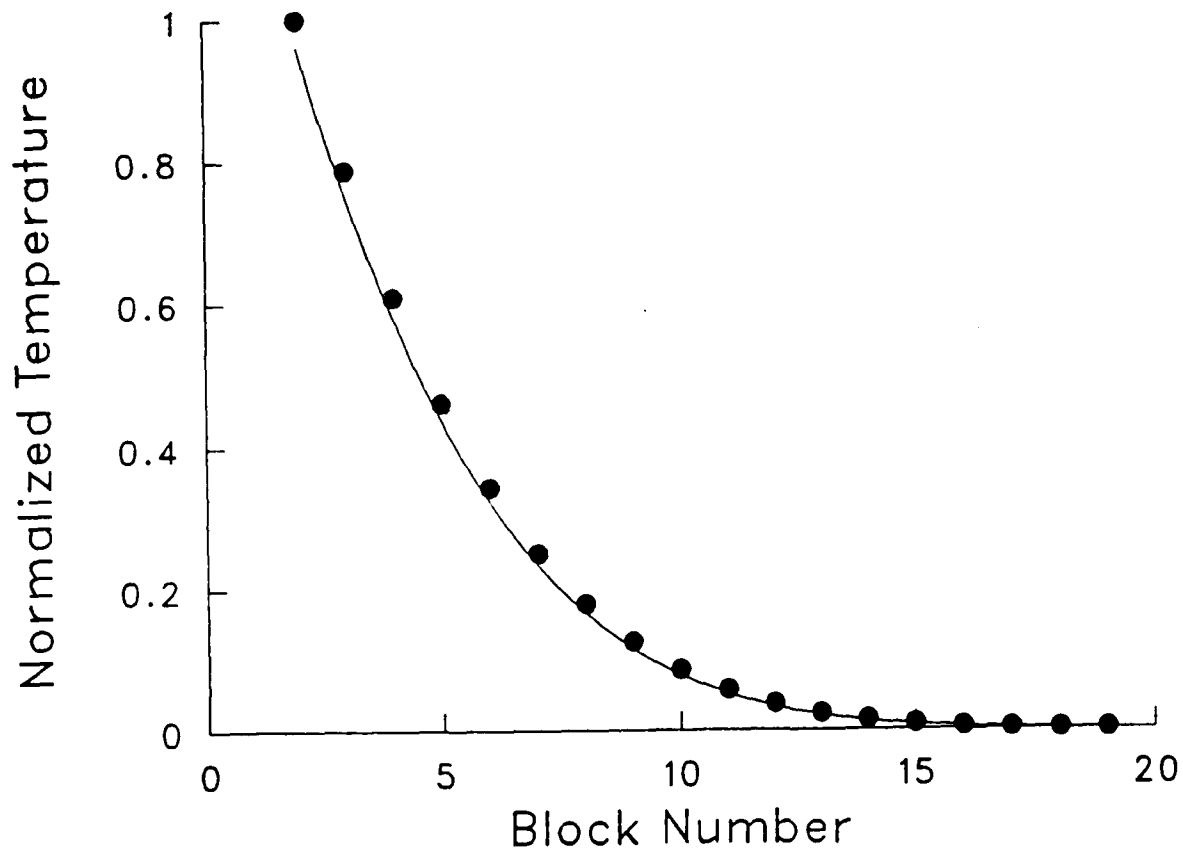


Figure 3. Comparison of numerical analysis model results (black circles) and partial differential equation results (solid line) for the test case of a slab, initially at 0 C, with adiabatic walls and energy flux F at the x=L region.

The specific heat of the mixed titanium and carbon powder compact was calculated from the mass weighted average of the individual components. The temperature dependent specific heat of carbon can be expressed as:¹³

$$c_C = 1430 + (0.356)T - (7.33E+7)/T^2 ; (J/kg-K) \quad (13)$$

over the entire temperature range of interest where T is the temperature expressed in degrees Kelvin. The specific heat of titanium is expressed over two temperature ranges due to an alpha to beta transformation at 1155 K. From room temperature to 1155 K the titanium specific heat is given as:

$$c_{Ti} = 458 + (0.22)T ; (J/kg-K) \quad (14)$$

and from 1155 K to 2000 K the titanium specific heat is:

$$c_{Ti} = 654 J/kg-K . \quad (15)$$

The atomic weight of titanium is four times that of carbon. The specific heat of a stoichiometric titanium and carbon powder mixture can therefore be expressed as:

$$c_{Ti+C} = \frac{4c_{Ti} + c_C}{5} . \quad (16)$$

Titanium undergoes two structural transitions over the temperature range of interest. As stated, titanium transforms from a hexagonal close packed alpha form to a body centered cubic beta form¹⁴ at 1155 K. This endothermic transformation has a heat of formation of 83000 J/kg. At 2000 K, beta titanium melts with a heat of formation of 400000 J/kg. When calculating the effect of these heats of formation on the heating or cooling rate of the powder compacts, it is important to keep in mind that only 80 % of the compacts mass is made up of titanium and that both components contribute to the specific heat.

The thermal conductivity values for the mixed titanium and carbon powder compacts were taken from experimental measurements discussed in detail in a later section. An anisotropy of the thermal conductivity was noted during these measurements. This anisotropy between the directions parallel and perpendicular to the compaction direction is due to the orientation of the graphite crystals under the uniaxial compaction force. Thermal conductivity values for the direction perpendicular to the compacting force were chosen for modeling input because larger samples are generally compacted on the largest outer surface to reduce mass density gradients and achieve a higher overall density. SHS reactions in such samples propagate perpendicular to these large outer surfaces and thus perpendicular to the direction of the compacting force. The measured thermal conductivity of porous materials is often found to have a power series relation to the sample porosity.¹⁵ The thermal conductivity of the mixed titanium and carbon powder compacts in the direction perpendicular to the compaction force was well fit by the power

series expression:

$$(\text{thermal conductivity in W/m-K}) = 1.013\text{E-}8(\% \text{ mass density})^{4.48} . \quad (17)$$

Thermal conductivities of low density compacts were limited by the ability of these highly porous compacts to hold together. Measurements of very high density compact thermal conductivities were limited by the structural strength of the die used for powder compaction. Equation 17 was used to extrapolate the value of mixed powder thermal conductivities for compact densities outside the obtainable range of mass densities.

Due to limitations of the apparatus used in measuring the powder compact thermal conductivities, all measurements were performed at room temperature. The consequent lack of knowledge concerning the temperature dependence of the thermal conductivity of the powder compacts represents the most serious uncertainty for the input parameters. It might be argued that since the thermal conductivity of titanium increases with temperature¹⁶ while that of graphite decreases¹⁷, the temperature dependences of the thermal conductivities of the individual components, at least partially, offset each other. However this line of reasoning does not take into account the porous nature of these compacts. For porous media, the variation of relative efficiency with temperature between conductive, convective and radiative heat transport adds an additional complication. Due to the uncertainty in the temperature dependence of the powder compact thermal conductivity, the results of these modeling exercises must be considered strictly valid only in terms of showing trends and relative magnitudes. This restriction can be removed as further information concerning the temperature dependence of these powder compact thermal conductivities becomes available.

The maximum mass density of the powder compacts was calculated from the atomic mass and densities of the individual components.

$$P_{\text{Ti+C}} = \frac{M_{\text{Ti+C}}}{V_{\text{Ti+C}}} = \frac{m_{\text{Ti}} + m_{\text{C}}}{v_{\text{Ti}} + v_{\text{C}}} = \frac{\frac{m_{\text{Ti}}}{P_{\text{Ti}}} + \frac{m_{\text{C}}}{P_{\text{C}}}}{\frac{m_{\text{Ti}}}{P_{\text{Ti}}} + \frac{m_{\text{C}}}{P_{\text{C}}}} \quad (18)$$

The density of titanium is 4540 kg/m^3 , the density of graphite is 2210 kg/m^3 and the ratio of the atomic masses of titanium and carbon is 4:1. Substituting into Eq. 18 for a stoichiometric mixture of titanium and carbon yields:

$$P_{\text{Ti+C}} = 3750 \text{ kg/m}^3 . \quad (19)$$

The exothermic titanium carbide SHS reaction initiates when the powder compact approaches the melting temperature of titanium where the endothermic transformation discussed previously occurs. Once molten, the titanium flows

around the graphite with sufficient mobility to diffuse into the edges of the graphite flakes.¹⁸ The exothermic SHS reaction then proceeds creating titanium carbide with a heat of formation of -3070000 J/kg .¹⁹

The amount of material that is expelled during the SHS reaction is small compared to the amount that remains as final product.⁹ For this reason the mass of the final product is taken to be the same as that of the precursor powder compact. Since the eventual goal of this modeling exercise is to simulate contained SHS reactions, the volume and thus the density of the powder compact and final product are also assumed equal.

Titanium carbide has a density of 4930 kg/m^3 which is considerably larger than the maximum theoretical density of the precursor titanium and carbon powder compact. Assuming constant mass and volume, the porosity of the final product must therefore be much greater than that of the unreacted compact. The high porosity of the final product titanium carbide affects the thermal conductivity. Highly porous materials are characterized by interconnected pores which readily transport gases and thus aid heat transport by gas conduction. Larger pore spaces also lead to greater radiation heat transfer between particles.²⁰ Radiative thermal conductivity in powders is generally treated as being strongly temperature dependent, increasing with the third power of the absolute temperature. However it has been shown that for some porous aggregates even this third power relationship may lead to an underestimation of the actual radiative thermal conductivity.²¹ At any rate, the large temperature increase associated with the SHS reaction leads to a substantial increase in the radiative thermal conductivity. The conduction thermal conductivity of titanium carbide also increases with temperature.²² For all these reasons, the thermal conductivity of the hot reacted product is expected to be much greater than that of the powder compact. For modeling purposes, the thermal conductivity of the SHS reacted material was set to a large value which allowed the reacted portion of the sample to act as a heat source from which thermal energy propagated into the remaining unreacted material.

Over the entire temperature range of interest the specific heat of the titanium carbide product can be expressed as:²³

$$c_{\text{TiC}} = 825 + 0.056T - 2.50E+7/T^2 ; \quad (\text{J/kg-K}) \quad (20)$$

where T is the absolute temperature.

Following laboratory practice, a resistively heated tungsten filament was assumed to be the heat source for the SHS reaction initiation. The electrical energy supplied to such a filament is converted to heat energy which increases the temperature by an amount which can be calculated from the filament's specific heat and mass. By interpolating over several widely spaced temperatures,¹³ a temperature dependent expression for the specific heat of tungsten becomes:

$$c_w = 128 + 0.0194T ; (J/kg-K) \quad (21)$$

where this specific heat is limited to a maximum value of 167 J/kg-K reached at $T = 2000$ K. The density of tungsten is 19300 kg/m^3 . At the temperatures of interest, the thermal conductivity of tungsten is much larger than that of the powder compacts that it is heating. Therefore the thermal conductivity of tungsten was set to a large constant value.

In addition to values representing physical quantities which are input into the numerical analysis program, parameters within the simulation code must also be defined. One such parameter is the interval of time that is assumed to pass between iterative recalculations of the volume cell temperatures. Since the continuous time variable is being approximated as a series of discretized intervals, the smaller the time interval the better the approximation. For situations where computer time is not a limiting factor, the time interval can be set very small. Then by running multiple test cases with slightly smaller time intervals and noting that the final result does not change, the chosen time interval could be assumed to be small enough to faithfully approximate a continuous time evolution. For cases where computer run times are excessively long, the upper limit of time interval values which give the same result as that of a very small value is determined. A value near the larger end of this range is then used to save processing time.

Another internal parameter of the simulation code is the size of the volume cell. This value is chosen to correspond to the physical system being modeled. The powders used in BRL experiments are sized as -325 mesh. This designation specifies that the powder has been sieved through a 44 micron screen. In reality this designation is rather open ended since it does not set a lower limit on the powder particle size and large filamentary particles can also be included as long as their minor axis dimension does not exceed the mesh size. The 44 micron dimension is therefore treated as an average value. In order for the titanium carbide reaction to occur, a particle of titanium and carbon must both be present. For this reason the volume cell cube dimension was chosen to be 88 microns which is a large enough volume to have a high probability of containing powder particles of both types. In the future, the effect of particle size may be investigated by varying the volume cell size.

2.4 Propagation Velocity Modeling:

SHS reaction zone velocities depend on the rate at which heat energy is conducted from the reaction zone to the unreacted green compact ahead of the advancing reaction zone and to the already reacted product. Thus the propagation velocity depends on thermal conductivity. The modeling of these velocities assumed an array of volume cells, initially at room temperature, to which heat energy was added via a tungsten filament. This filament heated the surrounding powder compact volume cells which eventually reached the SHS ignition temperature and reacted. The exothermic heat energy from this reaction heated and ignited additional cells and this process worked its way through the entire array. Following the initial transient ignition process, the self propagating reaction reached a steady state value which was taken as the propagation velocity of the SHS reaction.

The advance of a small segment of cylindrical reaction zone far from a filamentary ignition source approaches one-dimensional propagation. A linear array of volume cells could therefore have been used for the modeling of these velocities. However a two-dimensional array of volume cells was used to gain additional data on simulation instabilities which are apparent for long iteration time interval values. This information was useful for ignition studies to be described later. A 1 x 9 x 35 array of volume cells was used with the filament located as shown in Fig. 4. The length of this array was chosen to ensure that a steady state value of the propagation velocity would be achieved. Figure 5 shows a position versus time plot for a typical propagation velocity simulation. Numerical analysis parameters used in this simulation were: (1) compact density - 71.1% of maximum; (2) thermal conductivity - 2.0 W/m-K and (3) time interval - 40 microseconds. The actual propagation velocity value was obtained by fitting the linear portion of the data by linear regression and noting the slope. Propagation velocities were determined for the entire range of possible titanium and carbon powder compact thermal conductivities as determined by extrapolating Eq. 17. The predicted SHS propagation velocity as a function of powder compact thermal conductivity is shown in Fig. 6. An approximately linear dependence is predicted for the larger values of thermal conductivity. For smaller powder compact thermal conductivities the predicted propagation velocity decreases at an increasing rate.

2.5 Reaction Initiation Modeling:

The effects of green compact thermal conductivity and filament power on the SHS reaction initiation process were modeled using a square two-dimensional array of volume cells. A tungsten filament was assumed to be at the central position of the array and supplied heat energy to the surroundings at a rate which depended on the filament power density. For sufficiently high power densities, the filament could readily heat the surrounding volume cells to a temperature that was high enough to initiate the SHS reaction in these volumes. This exothermic reaction energy then combined with the heat energy from the filament to ignite additional cells. By "turning off" the filament after the reaction had propagated varying distances and following the reaction to see if it continued to propagate, the minimum required reaction volume and time for the initiation of a self sustaining reaction could be determined.

The SHS reaction initiation study was designed to simulate an electrical filament heating and eventually igniting a large powder compact. Because the outer surfaces of the modeling array were treated as adiabatic walls, an improper choice of the array dimension could affect the apparent ignition times. If too small an array is used, the heat from the filament could easily be transported to the outer surfaces of the array where further transport is blocked. Thus the heat energy from the filament would be artificially localized near the region of the filament yielding ignition times that were too short. An example of this is shown in Fig. 7 where ignition times were determined for a sample using volume cell arrays of varying size. The parameters used in this numerical analysis computation include: (1) powder compact density - 83% of maximum; (2) thermal conductivity - 4.0 W/m-K; (3) filament power - 20 kW/m; (4) cell size - 88 microns and (5) time interval - 80 microseconds. With increasing array size the computed ignition time asymptotically approaches a constant value.

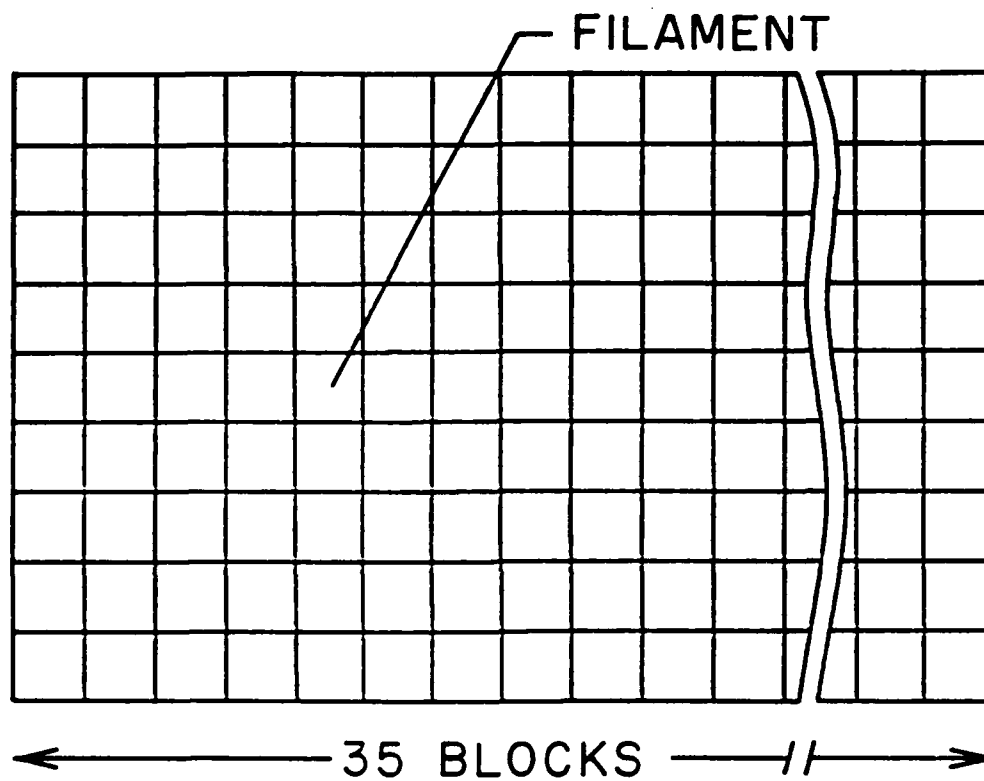


Figure 4. Geometry of space volumes used for SHS propagation velocity modeling.

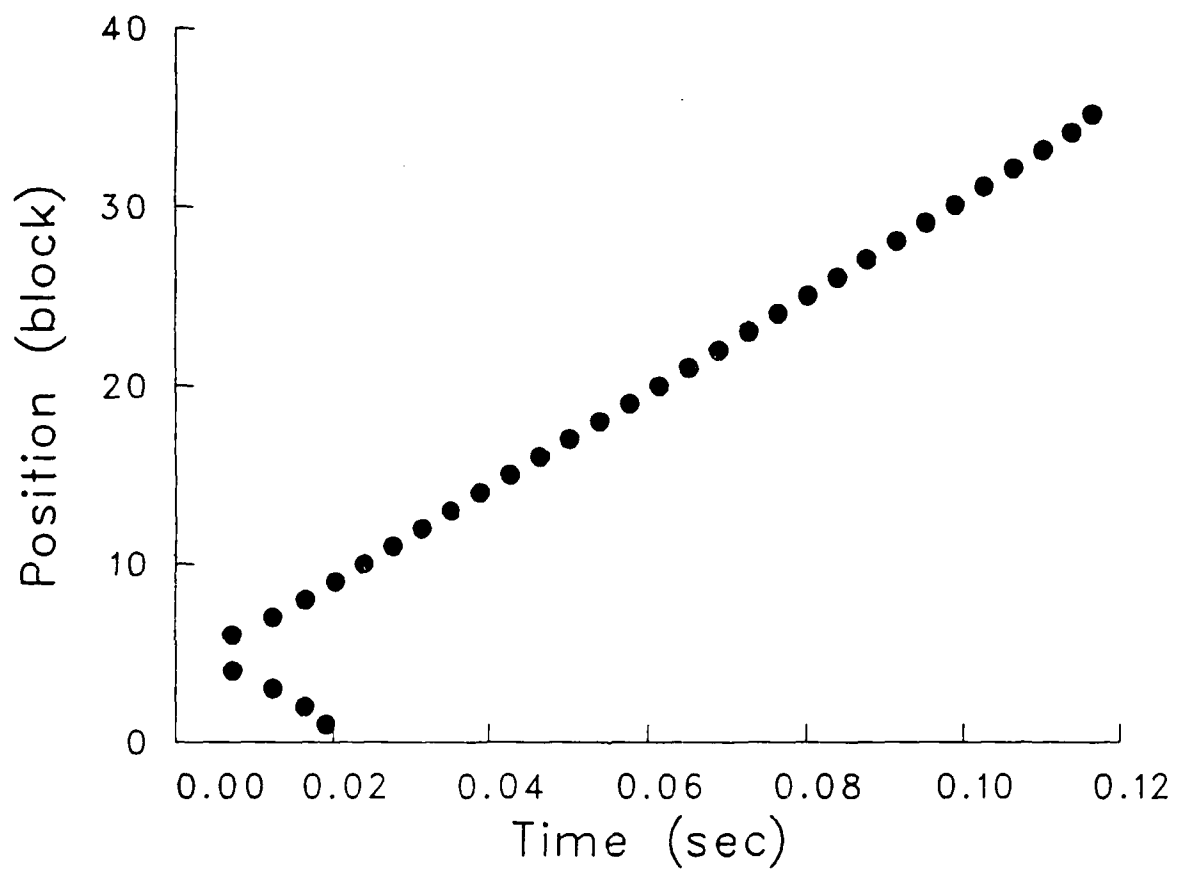


Figure 5. Position versus time plot for simulation of TiC SHS reaction propagating through an array of space volumes.

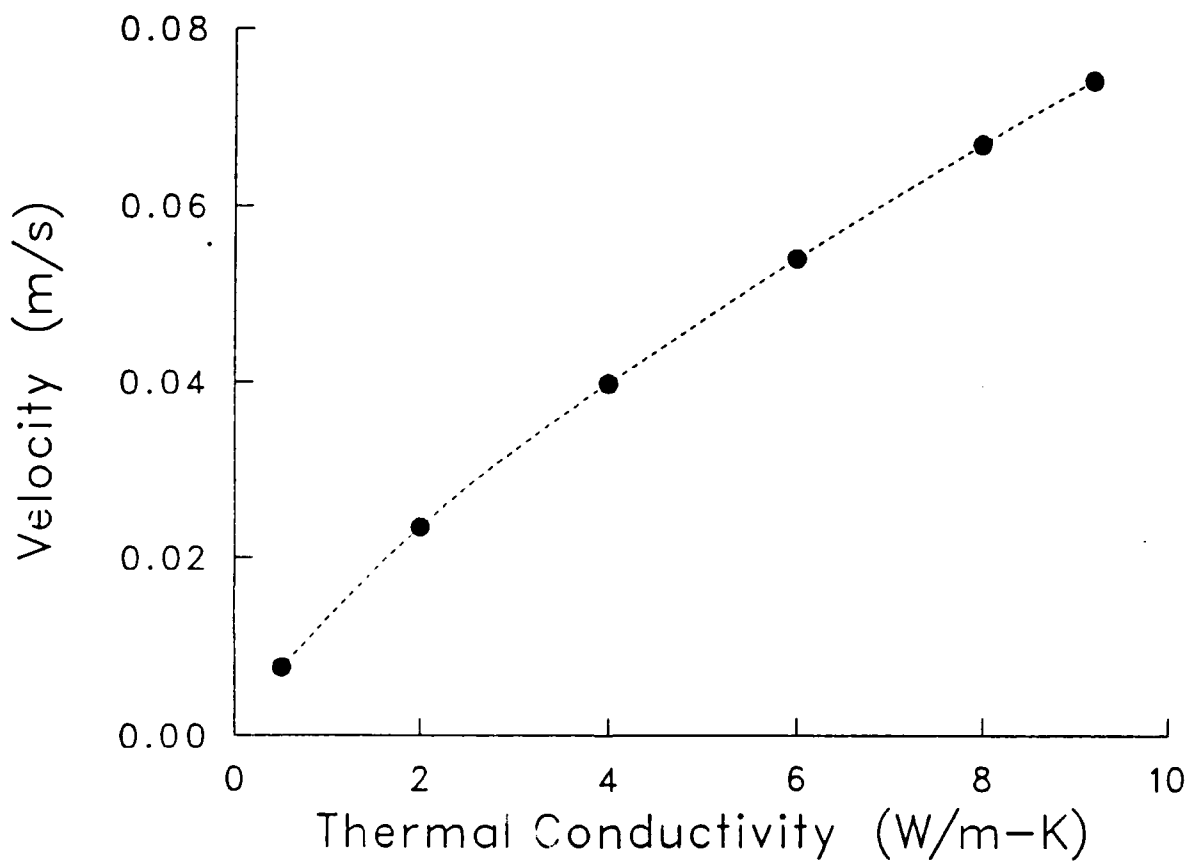


Figure 6. Predicted dependence of SHS propagation velocity on powder compact thermal conductivity for the titanium and carbon system. Dotted line added to guide the eye.

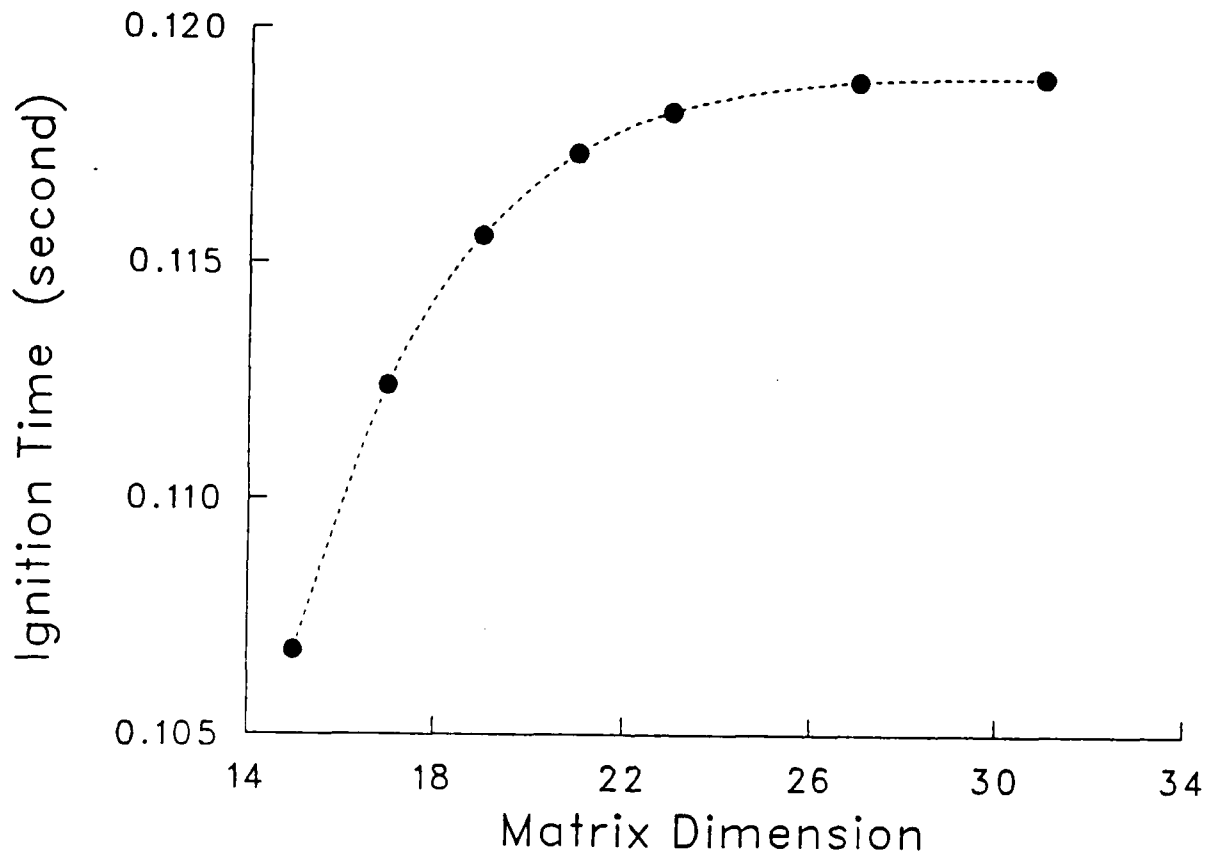


Figure 7. Computed TiC SHS ignition time versus array matrix dimension. Dotted line added to guide the eye.

An empirically determined guideline for choosing sufficiently large array sizes, which was followed for all SHS ignition modeling, was to choose arrays for which the temperatures of the outermost blocks did not exceed 100 C at the time of the SHS reaction initiation.

The condition that the temperature of the outer array elements remain relatively low required the use of fairly large array dimensions which led to relatively long computer run times. This was especially true for high thermal conductivity samples and low filament power densities where the heat energy from the filament could be transported a long distance before temperatures in the region of the filament were high enough to initiate the SHS reaction. In order to keep computer time to a minimum, iteration time intervals were used which were as large as possible while still allowing a valid approximation to a continuous time evolution. Conveniently, the valid range of iteration time intervals had already been investigated during the modeling of the reaction propagation velocity. Figure 8 shows the computed propagation velocity as a function of iteration time interval for various powder compact thermal conductivities. For sufficiently small time intervals the calculated velocities asymptotically approach a constant value indicating a valid approximation to continuous time evolution. As the time interval is increased, the calculated velocities initially remain fairly constant and then increase rapidly. This rapid increase in calculated propagation velocities is due to the assumption that heat energy is transferred only between nearest neighbors during each time interval. Overly long time intervals allow an unrealistic amount of heat energy to be transferred from newly reacted cells to neighboring unreacted cells without the transfer of this heat energy to the remainder of the unreacted array. Thus heat energy is artificially localized to the area of the green compact surrounding the reaction zone causing premature propagation. This effect is observed at smaller time intervals for low thermal conductivity powder compacts because of the inherent inefficiency of these compacts at conducting heat energy away from the reaction zone.

The results of the SHS reaction initiation simulation for the titanium and carbon system are shown in Fig. 9. The computed times required to initiate a self-sustaining reaction are plotted versus filament power density for the range of possible powder compact thermal conductivities as determined using Eq. 17. In addition to the apparent lower limit on ignition time for high filament power densities, overly high filament power is undesirable because of the possibility of burning out the filament before the reaction initiates. The possibility of filament failure was monitored by noting if the simulated filament temperature exceeded the melting point of tungsten. Both the power required to ignite a powder compact in a given period of time as well as the time to ignition at a given power level increase with the thermal conductivity of the compact.

The problem of heating volume elements surrounding an ignition filament to reaction initiation temperature while heat energy from these same elements is simultaneously being transported to volume elements farther away from the filament is equivalent to trying to fill a bucket with water when the bucket has a hole in the bottom. A bucket with a small hole can be rapidly filled with even a modest flow of water from a faucet. Similarly, for low thermal conductivity powder compacts, even relatively low filament power densities can soon heat the volume cells surrounding the filament to the ignition

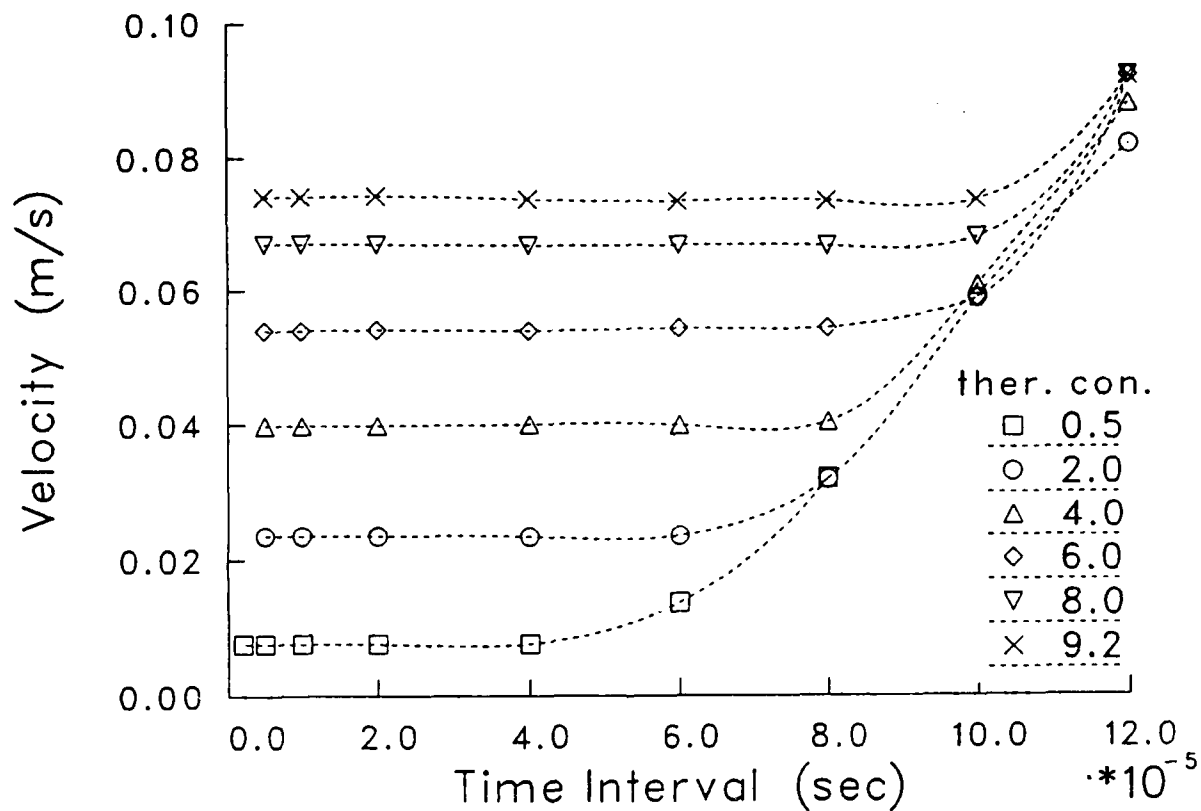


Figure 8. Computed SHS reaction propagation velocity versus iteration time interval for the titanium and carbon system. Thermal conductivity values are in W/m-K. Dotted lines are added to guide the eye.

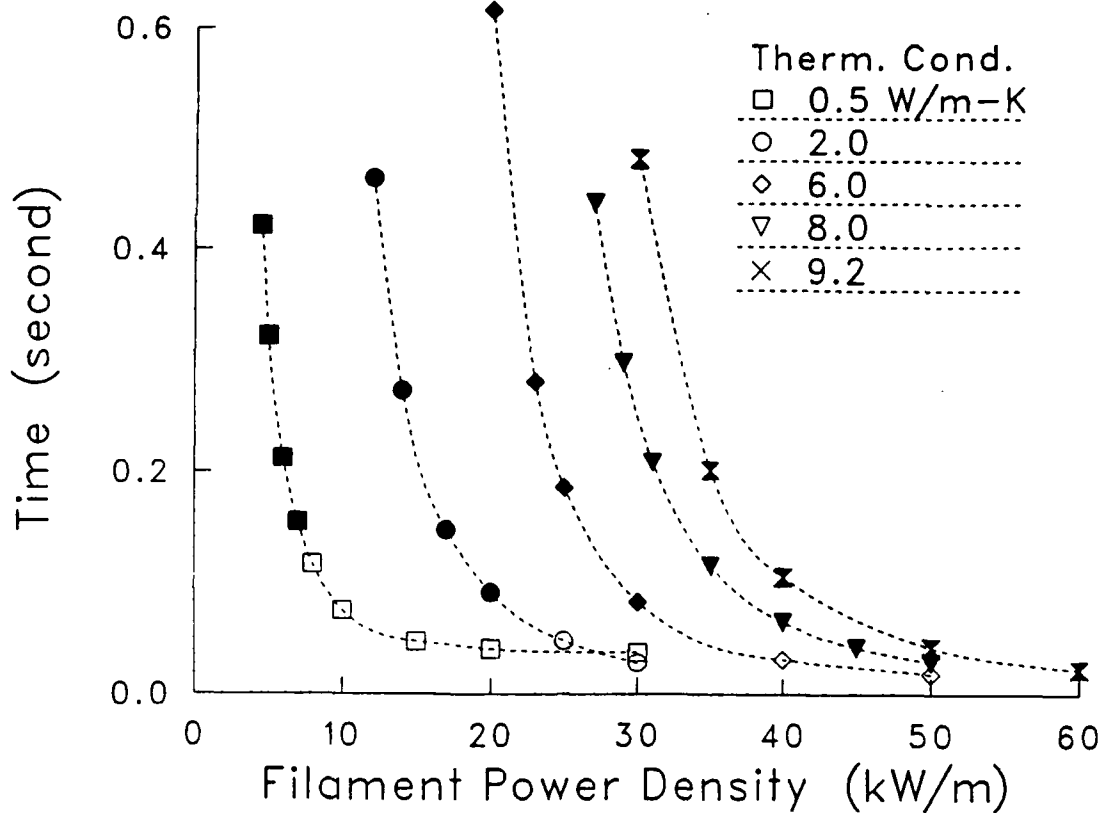


Figure 9. Computed TiC SHS reaction initiation time versus filament power density. Open symbols represent filament power densities which are predicted to lead to filament failure before reaction initiation. Dotted lines are added to guide the eye.

temperature because little heat energy is being lost from these volumes to the rest of the powder compact. As the hole in the bottom of the bucket increases in size, the time required to fill the bucket also increases or the flow of water from the faucet must be increased if the amount of time to fill the bucket is to remain the same. Analogously, powder compacts with larger thermal conductivities, which allow a greater amount of heat energy to pass from the material surrounding the filament to the remainder of the compact, also require either a longer time to initiation of the SHS reaction or higher filament power densities if the ignition time is to remain constant. If the hole in the bottom of the bucket becomes too large, then it may not be possible to fill the bucket even if the faucet is wide open. For powder compacts with high thermal conductivities, low filament power densities may not be sufficient to initiate the SHS reaction in a reasonable period of time. This effect is illustrated in Fig. 10 and Fig. 11 where the temperatures, in Celsius, of the volume cells for two samples of different thermal conductivity are plotted after 0.08 second of filament heating time at a power density of 5 kW/m. For the low thermal conductivity case shown in Fig. 10, the heat energy from the filament remains localized to the area surrounding the filament allowing these volumes to approach the ignition temperature while the volume cells on the edge of the matrix remain near the ambient temperature of 20 C. Heat energy from the filament in the high thermal conductivity case, shown in Fig. 11, has not been localized to the area surrounding the filaments. The volume cells surrounding the filament in this case are at a much lower temperature while the temperatures at the edge of the array are higher. Due to the high thermal conductivity, an effectively larger volume of the sample must be heated to the reaction initiation temperature, requiring a longer period of time.

2.6 Summary of Modeling Results:

A numerical analysis model has been developed for simulating SHS reaction initiation and propagation through a powder compact. The basic assumptions and software of this model have been tested by comparing the results of this model to those obtained for convenient test cases using the standard differential equations of heat conduction. Close agreement between these two methods of describing heat transport supports the validity of the numerical model. Considerable care has been exercised in choosing the best available external and internal parameters for input to the modeling simulations to allow a maximum level of confidence in the results.

For the mixed titanium and carbon powder system, the SHS propagation velocity is predicted to have a linear dependence on the thermal conductivity of the precursor powder compact for highly conductivity compacts. With decreasing thermal conductivity the propagation velocity is predicted to fall off at an increasing rate. The reaction initiation study indicates that the filament power density and time required to initiate an SHS reaction in a powder compact are strongly dependent on the thermal conductivity of the compact. High thermal conductivity powder compacts are predicted to require relatively high filament power density levels in order to initiate the reaction in a reasonable period of time. While low thermal conductivity powder compacts may be easier to ignite with modest filament power, the possibility of filament failure prior to reaction initiation is predicted to be more problematic for such compacts.

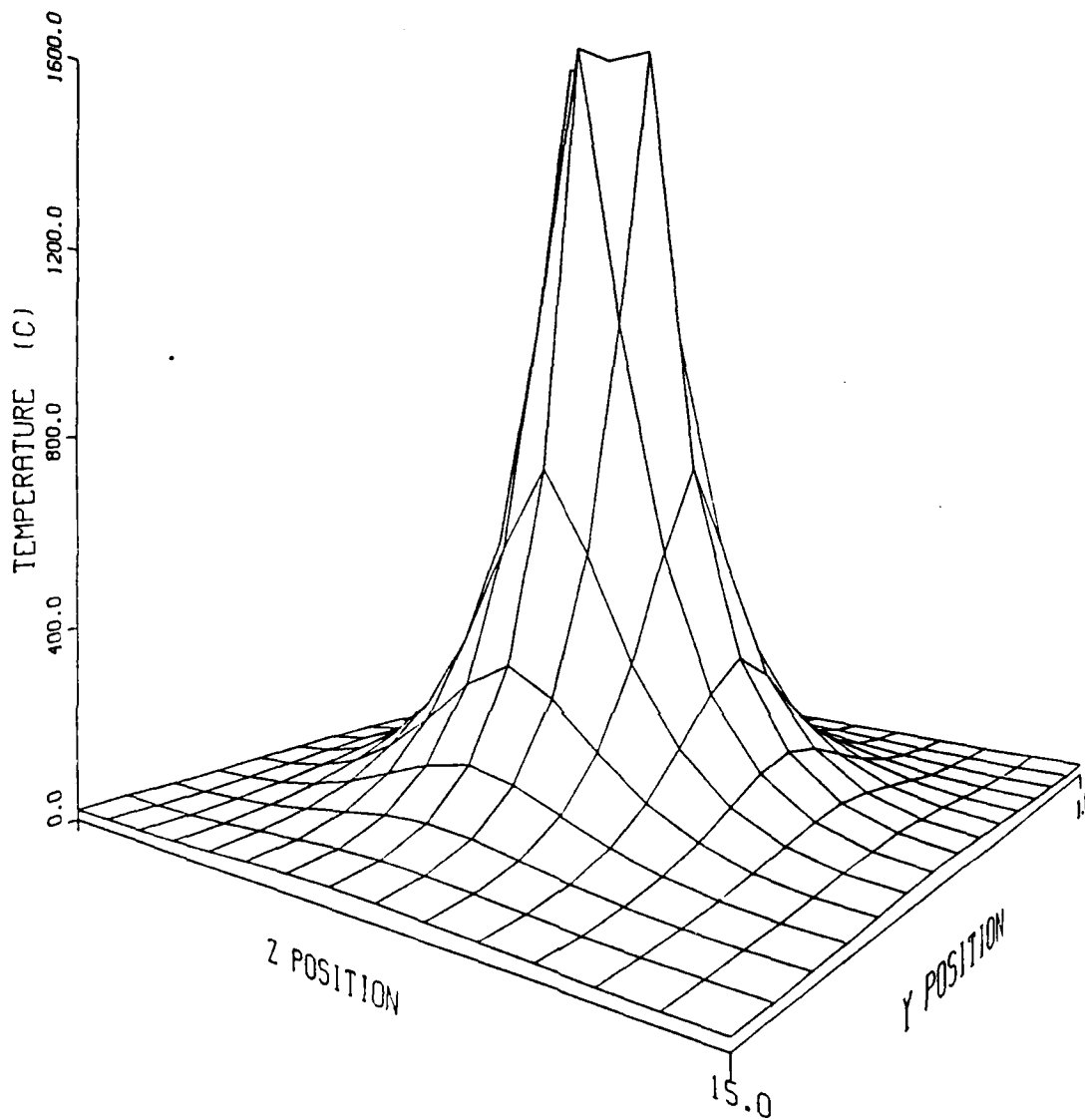


Figure 10. Volume element temperatures of a 0.5 W/m-K thermal conductivity titanium and graphite powder compact array following 0.08 second of filament heating from ambient temperature.

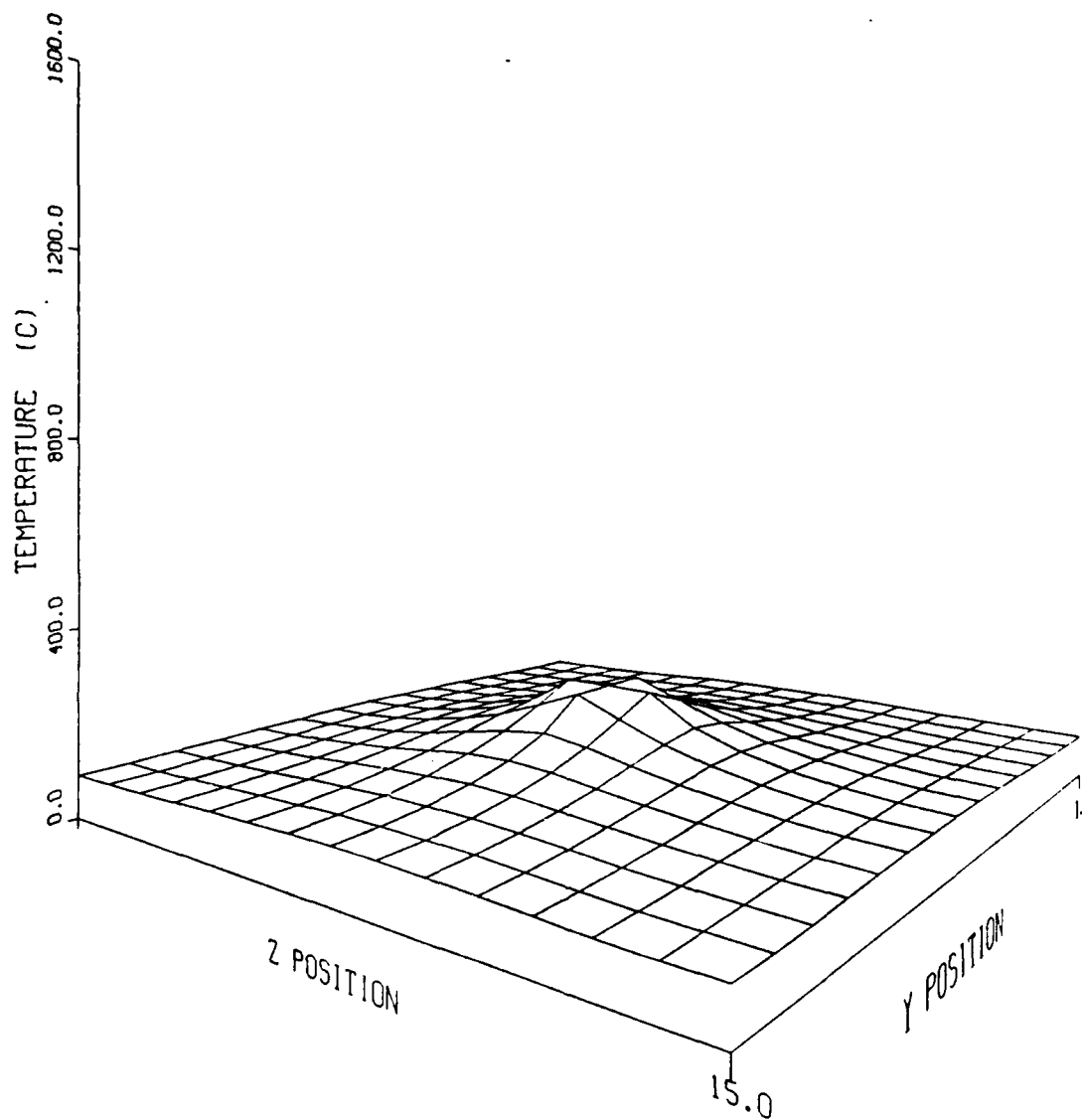


Figure 11. Volume element temperatures of a 9.2 W/m-K thermal conductivity titanium and graphite powder compact array following 0.08 second of filament heating from ambient temperature.

3. EXPERIMENTAL TECHNIQUES

3.1 Experimental Overview:

The thermal conductivity of green compacts was measured using a thermal heat pulse technique. Samples at some initial homogeneous temperature were brought into thermal contact with a heat reservoir of known temperature while the temperature of the far end of the sample was recorded as a function of time, Fig. 12. The thermal conductivity of the compact material was then deduced from the temperature-time response of this far end of the compact. The temperature regulation of the heat stage as well as the temperature measurement of the sample were both performed with the aid of an APPLE II²⁴ series computer. Following data acquisition, computer assistance was again utilized in data analysis.

3.2 Heat Stage:

To facilitate the maintenance of a constant heat stage temperature, the heat stage was fabricated with thick copper walls to increase the thermal inertia. The inside of the heat stage was bored out and fitted with a tungsten coil which was used to resistively heat the stage. This heating coil was wound around a cylindrical piece of boron nitride which provided thermal contact between the heating coil and the stage. This configuration also prevented the tungsten coil from shifting position and insulated it electrically from the surrounding copper walls, Fig. 13. A chromel-alumel thermocouple embedded near the working surface of the heat stage was used to monitor and regulate the temperature of the heat stage.

The Seebeck potential from this thermocouple was amplified to a magnitude that was sufficiently large enough to be monitored by the computer data logging system with the circuitry shown in Fig. 14.^{25,26} Operational amplifiers A1 and A2 act as buffers for the thermocouple signal and allow for zero signal offset by adjustment of potentiometer P1. This buffered thermocouple voltage is then differentially fed into A3 which preamplifies the voltage by a factor of 100. Use of a preamplifier with differential inputs provides a high degree of noise immunity. Potentiometer P2 fine tunes the input bias current into the noninverting input of A3 for maximum common mode rejection. The preamplified signal is then fed into the variable amplifier network of A4. Switches S1 and S2 each individually allow for amplification by a factor of 100 with potentiometer P3 offering additional continuously variable amplification of between 2 and 100. Since bipolar operational amplifiers were used, it was possible for amplified thermocouple voltages to be negative depending on the zero offset setting and the temperatures being measured. It is undesirable to feed negative voltages into the computer data logging system and so the amplified thermocouple signal was precision rectified by networks A6 and A7. The final output signal was a positive voltage between 0 and 5 volts which was in the voltage range that could be measured by the data logger.

For temperature regulation, the magnitude of the thermocouple signal, as read by the data logger, was compared to a preset value stored in the computer. Depending on whether or not the read value exceeded the preset value, the data logging system would toggle the heating coil in the heat stage on or off by means of an electrical relay in the heater circuit. This

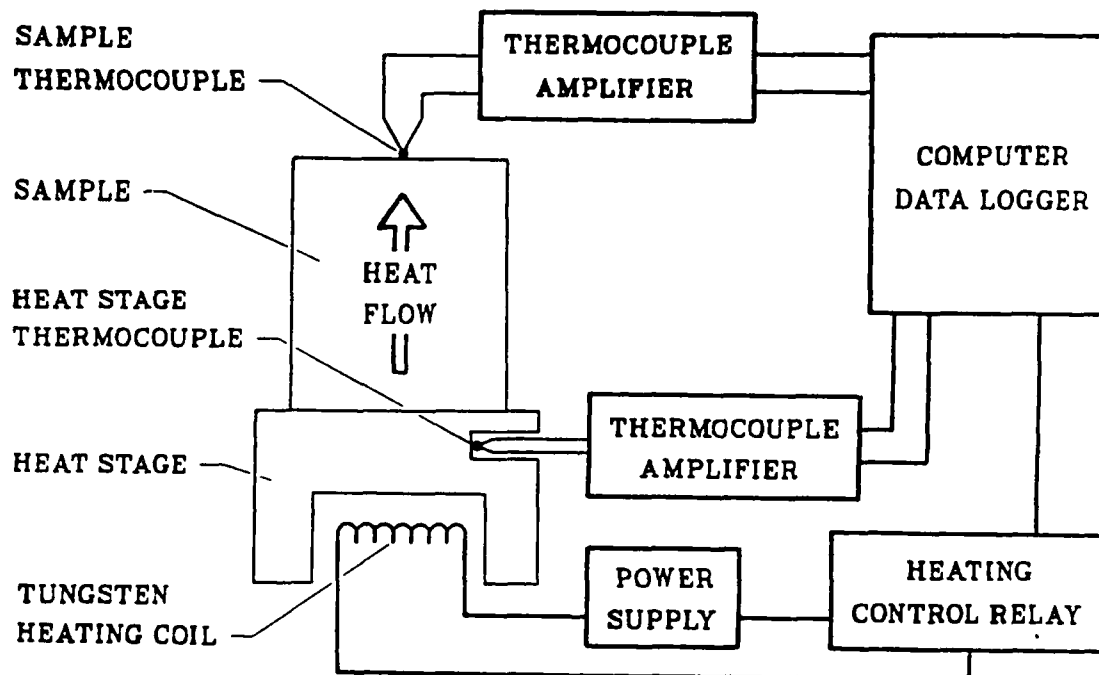


Figure 12. Overall schematic of thermal conductivity measuring apparatus.

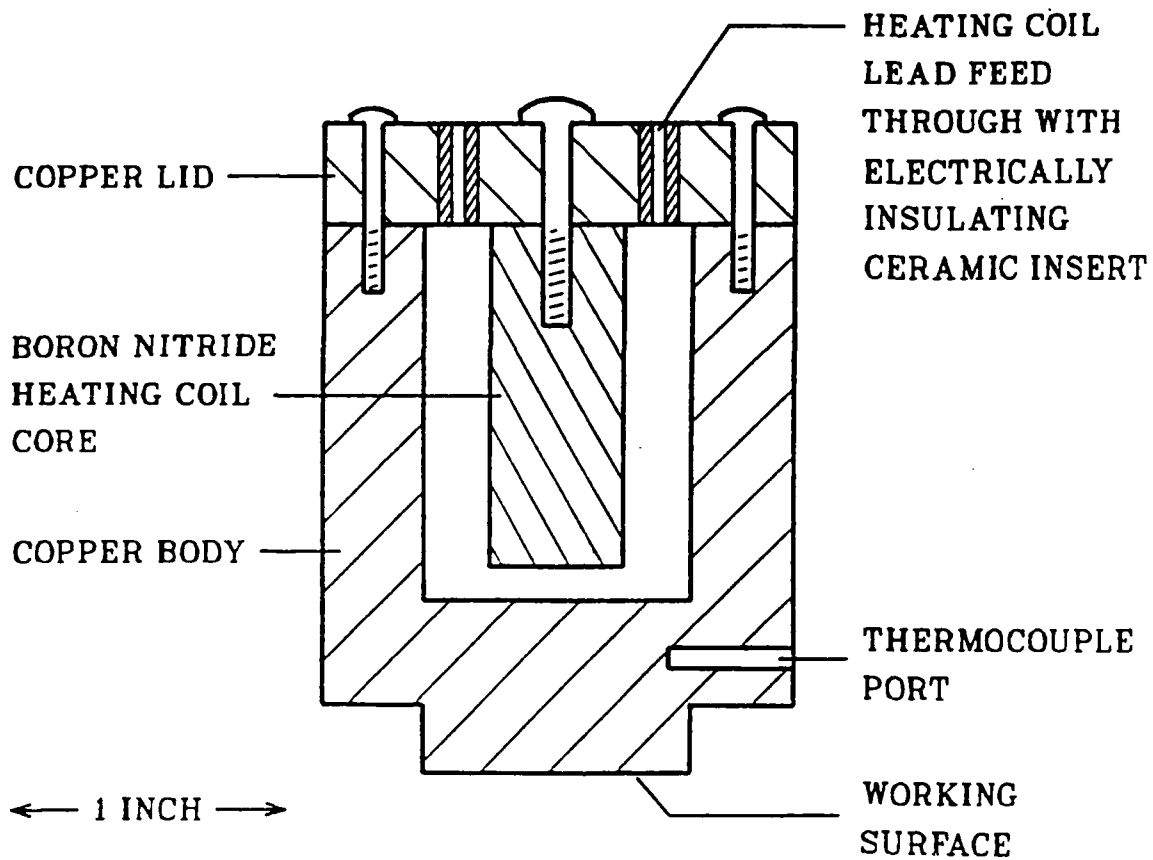


Figure 13. Thermal conductivity apparatus heat stage.

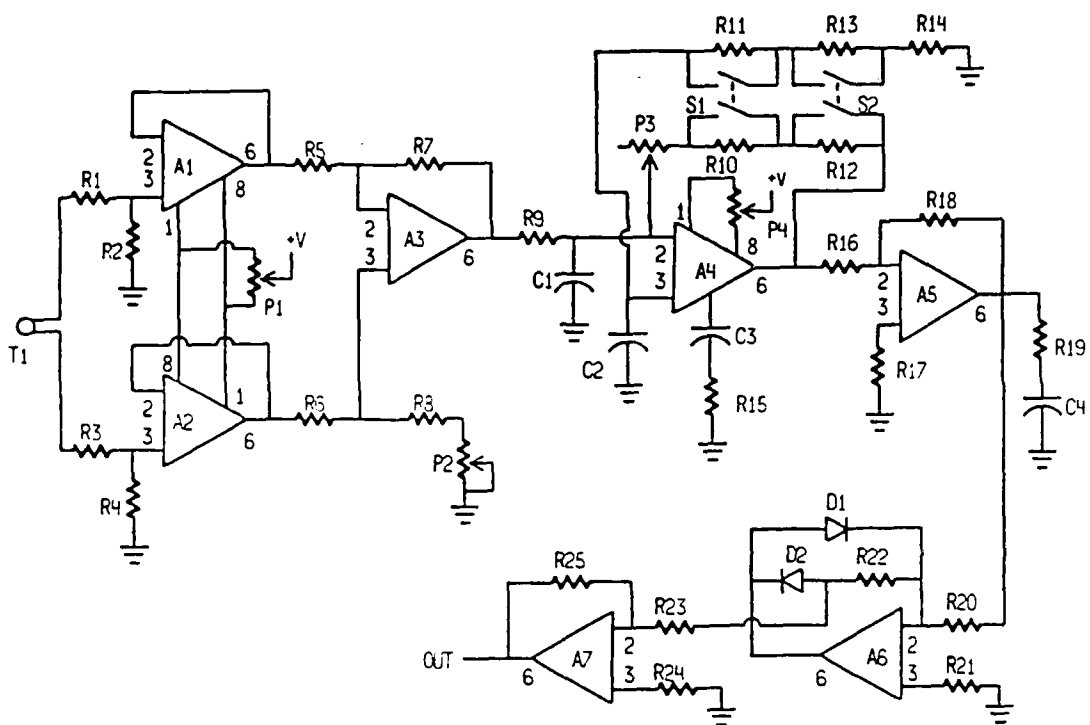


Figure 14. Schematic of heat stage thermocouple electronics. Component values are listed in Appendix B.

temperature regulation scheme, in combination with the thermal inertia of the heater stage, allowed the heat stage to be regulated to within 0.2 degree Celsius.

3.3 Sample Stage:

The sample holder was fabricated from phenolic and rubber to aid in thermally isolating the sample. A chromel-alumel thermocouple was again used as the sensor for sample temperature measurements. The sample thermocouple amplifier, as outlined schematically in Fig. 15, included a digital readout thermometer which was used to calibrate the entire system. This digital thermometer was equipped with a 1 mV/C analog output which required further amplification before being read by the computer data logger. As with the heat stage circuitry, the analog signal was buffered by two high impedance operational amplifiers before being differentially amplified by a factor of 100. Provisions for zero signal offset and common mode rejection adjustment were also provided. Samples as large as one-inch in diameter could be measured with the existing sample holder.

3.4 Sample Preparation:

All green compacts were made from stoichiometric mixtures of -325 mesh titanium and graphite powders. The titanium powder was from Atlantic Equipment Engineers²⁷ designated with can label T-1270. Oxidation resistant graphite from Consolidated Astronautics²⁸, lot number 412, of 99% purity was used as the source of carbon. These powders were mixed in a ball mill before being compacted in a 1/2-inch diameter opposed anvil cylindrical die. Figure 16 shows a plot of green compact density versus compaction pressure for this die configuration. Similar compaction pressure dependence of green compact densities has been reported for other die configurations.²⁹ Green compact densities were limited on the low end by failure of the compact to maintain structural integrity and on the high end by failure of the opposed anvil die. Roughly cubic samples of approximately one centimeter on a side were cut from these cylindrical shapes with care being taken to orient one orthogonal axis normal to the anvil compaction surfaces. Table 1 lists the attributes of the thirteen samples for which thermal conductivity measurements were taken.

3.5 Apparatus Calibration:

It was necessary to calibrate the thermocouple amplifying circuits and the data logger's eight bit signal digitizer. This process involved holding the thermocouples at known temperatures while these temperature values were keyed into the computer for comparison against the corresponding analog to digital conversion values. By bringing the heat stage in contact with the empty sample holder, which allowed thermal contact between the heat stage and the sample thermocouple, the heat stage could be used to heat both the sample and heat stage thermocouples. The digital thermometer in the sample thermocouple amplifying circuit acted as the calibration reference for both thermocouples. An added advantage of having the calibration reference thermocouple located on the working surface of the heat stage was that any temperature gradients between this surface of the heat stage and the heat stage feedback thermocouple would be compensated for automatically. Using

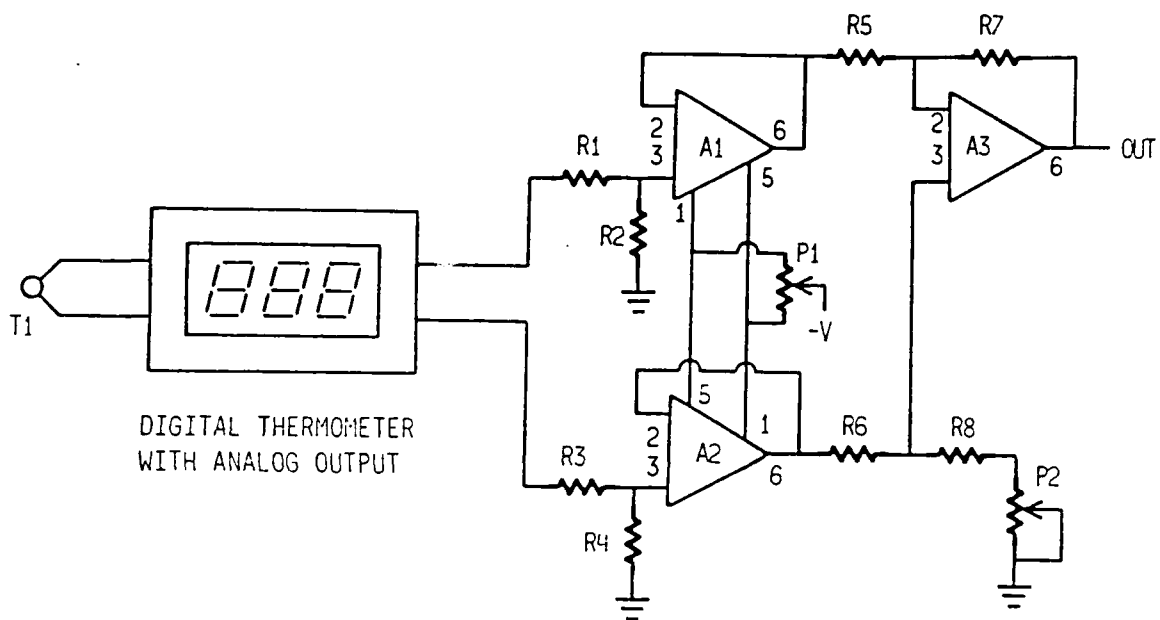


Figure 15. Schematic of sample thermocouple electronics. Component values are listed in Appendix B.

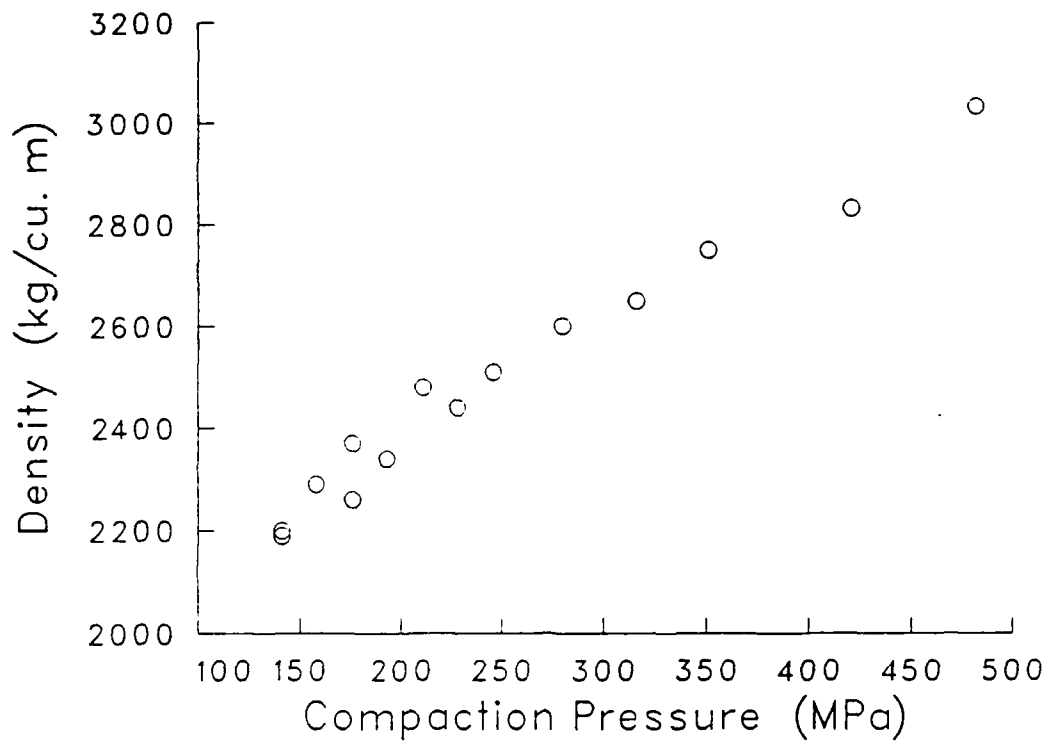


Figure 16. Titanium/graphite powder mixture green compact density versus compaction pressure for 1/2-inch diameter opposed anvil die.

Table 1.
Ti+C Powder Compact Attributes

Sample #	Compact. Force (N)	Compact. Pressure (MPa)	Density (kg/m ³)	Density Ranking
1	22200	176	2260	12
2	17800	141	2200	13
3	17800	141	2190	14
4	20000	158	2290	11
5	22200	176	2370	9
6	26700	211	2480	7
7	35600	280	2600	5
8	24500	193	2340	10
9	31100	246	2510	6
10	28900	228	2440	8
11	44500	351	2750	3
12	40000	316	2650	4
13	53400	421	2830	2
14	>62300	>482	3030	1

the computer program listed and outlined in Appendix C, analog conversion values and their corresponding temperatures were logged while the temperatures of the heat stage and sample thermocouple were ramped over their respective operating temperature ranges. This data was then least squares fit for each thermocouple to a quadratic equation of the form:

$$T = A + B[ADC] + C[ADC]^2 \quad (22)$$

where T is the temperature in degrees Celsius expressed as a function of the analog to digital conversion value ADC and the least squares fitting coefficients A, B and C.³⁰ A plot of the data points and the quadratic fit for each thermocouple were output, as well as the coefficients A, B and C, to allow for an immediate eyeball check on the goodness of fit. Due to the inherently linear response of thermocouples over small temperature ranges, fitting this data to a second order polynomial yielded fits that were sufficiently precise.

This thermocouple calibration procedure was performed daily before thermal conductivity data was taken. Calibrations were generally made on between 15 and 20 data points spread over the temperature range from 20 C to 35 C for the sample thermocouple and 40 C to 60 C for the heat stage thermocouple. The absolute calibration of the digital thermometer used to calibrate the thermocouple systems was verified using ice water and boiling water baths. A MACOR³¹ reference sample was used to check the absolute calibration of the entire thermal conductivity apparatus. This MACOR sample was chosen as a reference material because the thermal conductivity value (1.29 W/m-K) of this material, as provided by the manufacturer, was in the range of measured sample thermal conductivity values. In addition, this reference sample was periodically measured during the course of a data taking session to monitor for any changes in apparatus calibration. Thermal conductivity measurements of the MACOR reference sample using heat stage temperatures ranging from 40 C to 80 C showed no systematic dependence on the heat stage temperature and a relative accuracy of approximately 5%. A 50 C heat stage temperature was used for all thermal conductivity measurements reported here.

3.6 Data Acquisition:

Thermal conductivity data was obtained using the computer program listed and outlined in Appendix D. The thermocouple quadratic fitting equation coefficients determined by the calibration program as well as the time interval between data points were input from the keyboard. Data acquisition timing was controlled by appropriately debounced interrupts to the edge sensitive NMI (nonmaskable interrupt) line of the 6502 microprocessor. Thus the data acquisition rate could be varied by simply adjusting the frequency of a signal generator attached to the NMI line. The sample, at ambient temperature, was centered in the sample holder where it rested on the sample holder thermocouple. To ensure good thermal contact when the heat stage was lowered onto the sample, a thin layer of thermally conducting compound, such as that used in heat sinking power transistors, was spread on the heat stage face of the sample. The heat stage was then brought in contact with the sample while a switch between the frequency generator and the NMI line was simultaneously closed to initiate data acquisition. Temperature measurements of both the sample and the heat stage were stored in computer memory and plotted on the monitor screen in real time. After the sample temperature approached that of the heat stage, data acquisition was terminated by opening the NMI line switch and the recorded data was stored on floppy disk for later analysis.

3.7 Data Analysis:

In the limited temperature range over which the thermal conductivity measurements were made, the thermal conductivity of the tested material can be treated as a constant allowing the situation to be analyzed as linear heat flow in a solid. If it is assumed that no heat flows through any external surface of the sample other than the surface in contact with a heat reservoir, the time dependence of the temperature of a surface a distance L from the surface in contact with the heat reservoir can be expressed as the series:¹¹

$$T(t) = T_r + \frac{4}{\pi} (T_r - T_i) \sum_{n=1}^{\infty} \frac{(-1)^n}{2n-1} \exp(-K(n-\frac{1}{2})^2 \frac{t}{L^2}) \quad (23)$$

where T is the temperature at a time t , $x = L$ represents the surface in contact with the heat reservoir, $x = 0$ represents a surface a distance L from the heat reservoir, T_r is the temperature of the heat reservoir and T_i the initial temperature of the solid at time $t = 0$ when the solid was brought into contact with the heat reservoir. The thermal diffusivity (K) contains the thermal conductivity (k) through the relation:

$$K = k/\rho c \quad (24)$$

where ρ is the mass density and c the specific heat. Using a mass weighted average specific heat for the compressed powder mixture, all parameters in the series expression are known from published values or measurements except the thermal conductivity. The thermal conductivity was determined by using it as the least squares fitting parameter when fitting the temperature-time data of the $x = 0$ surface of the sample to Eq. 23.

The program outlined and listed in Appendix E was used to fit the thermal conductivity data to Eq. 23. Successive approximations were used to determine the value of the thermal conductivity for which the series expression most closely represented the temperature-time data of the $x = 0$ surface. Following the input of the known sample characteristics such as density, specific heat and length, the program fit the thermal conductivity data to an initial thermal conductivity value and determined the sum of the squares of the deviations between the experimental data points and the computed fit. The data was then fit to a new thermal conductivity value about half again as large as the initial value. If the sum of the squares of the deviations for this second fit was larger than for the initial fit the sense of the thermal conductivity variation was reversed. Otherwise, the process of fitting the data to incremented thermal conductivities was continued until the sum of the squares of the deviations of the latest fit exceeded that of the previous fit. This indicated that the incremented thermal conductivity fitting value had passed through the "best fit". At this point the magnitude of the variations of the thermal conductivity fitting value was cut in half, the sense was reversed and the process of comparing sums of squares of the deviations for successive fits was begun again. By repeatedly performing this reversing process, the value of the thermal conductivity which yielded the best fit could be determined with arbitrary precision. In practice this process was repeated seven times which insured fitting uncertainties which were small compared to statistical uncertainties. The temperature-time data for a typical measurement and the best fit to Eq. 23 are shown in Fig. 17 for sample 9 measured perpendicular to the direction of compaction.

One possible source of error in this measurement was the loss of heat through the external surface walls not in contact with the heat reservoir. This undesirable heat loss violates the assumptions inherent in the derivation of Eq. 23. In order to reduce the amount of external surface heat loss, the data was analyzed over a temperature range of only a few degrees above ambient. In this temperature regime the difference between the sample

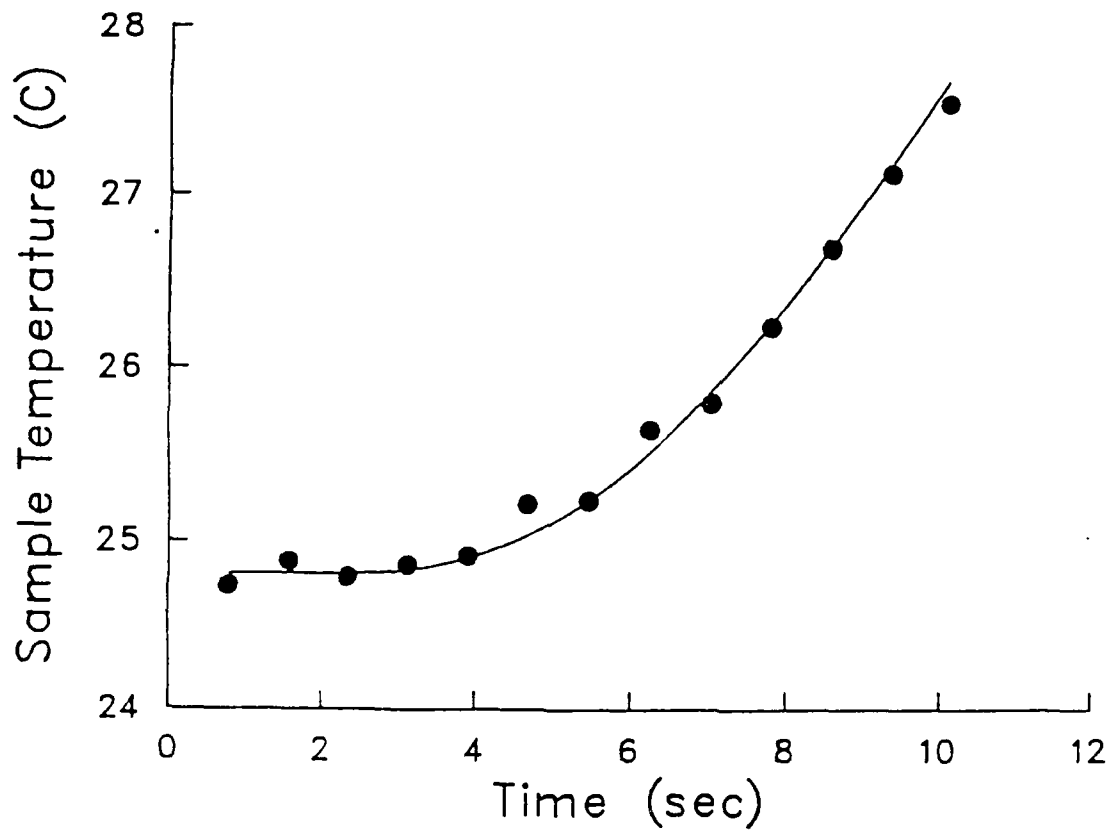


Figure 17. Experimental data of temperature at $x = 0$ surface versus time and plot of Eq. 25 for best fit thermal conductivity value.

and ambient temperatures, which drives the heat loss process, was minimal. In order to ascertain whether the heat loss through external surfaces was a factor, an initially long cylindrical sample was repeatedly measured as its length was incrementally decreased. In this way the surface area of the sample, through which undesirable heat loss could occur, was also being reduced. Since no systematic change in the measured thermal conductivity of this sample with length was observed, it was concluded that heat loss through the external surfaces of these samples was negligible and could be ignored.

4. EXPERIMENTAL RESULTS AND DISCUSSION

Thermal conductivities of mixed titanium and graphite powder compacts, ranging in density from 58% to 81% of maximum theoretical density, were measured in the directions parallel and perpendicular to the compaction direction. These data values are tabulated in Table 2 and plotted in Fig. 18 along with the power series fits as described by Eq. 17. The thermal conductivities of these compacts increased by approximately a factor of four over the range of available densities and a marked anisotropy is evident in the thermal conductivity with respect to the two directions measured. Thermal conductivities in the direction perpendicular to the compaction direction were about twice those in the direction parallel to compaction.

Although a great deal of effort has been directed over the last three quarters of a century towards developing methods for predicting the thermal conductivity of heterogeneous mixtures from the thermal conductivities of the individual components,³² very little experimental data is available on the thermal conductivity of SHS or thermite type powder compacts and its dependence on physical parameters such as density. Butakova et. al.³³ reported on the thermal conductivity of the $2\text{Fe}_2\text{O}_3 + 3\text{Ti} + 2.26\text{TiO}_2$, $2\text{Cr}_2\text{O}_3 + 3\text{Zr} + 2.8\text{ZrO}_2$ and $\text{Cr}_2\text{O}_3 + 2\text{Al} + 0.64\text{Al}_2\text{O}_3$ systems as a function of compact density, percentage dilution by reaction product and particle size. Their results for the dependence of the thermal conductivity on the compact density for these three systems is plotted in Fig. 19. The experimental details of the investigation by Butakova et. al. are similar to that of the authors with both studies measuring the thermal conductivity of samples of approximately the same size and configuration using similar techniques and temperature differentials. Although not explicitly stated, from the description of the experimental details it can be inferred that Butakova and co-workers measured the thermal conductivity of their powder compacts in the direction parallel to the compaction direction. There is no mention of thermal conductivity anisotropy presumably due to the measurements having been made in only one direction. Their experimental results show a characteristic increase in the thermal conductivity with increasing compact density. However, due to the limited information describing the morphology of the powders used in the Butakova study, it is not possible to quantitatively compare the results of this study with that of the authors.

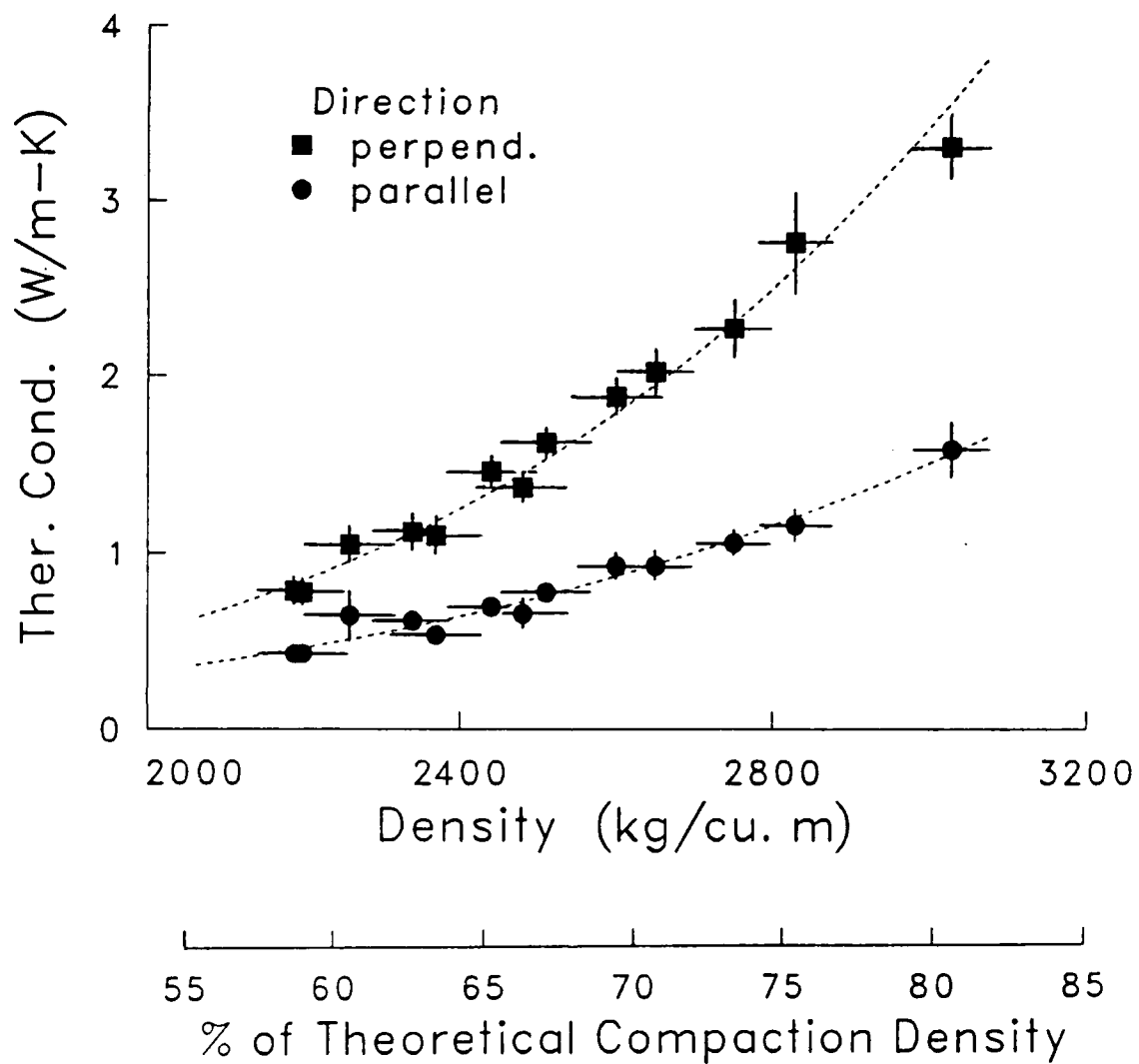


Figure 18. Thermal conductivity of titanium and graphite powder compacts in the directions parallel and perpendicular to the direction of compaction as a function of powder compact density and percent theoretical compaction density.

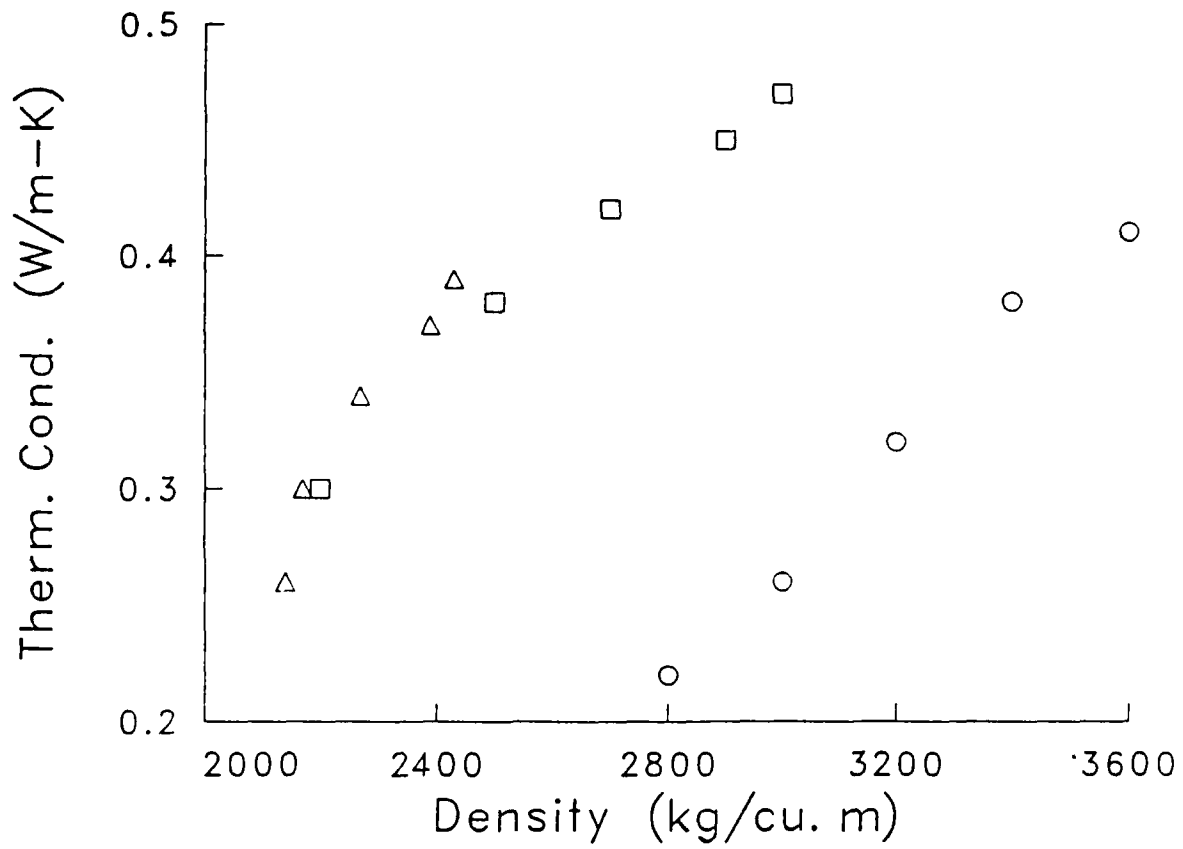


Figure 19. Thermal conductivity versus powder compact density for
 $2\text{Fe}_2\text{O}_3 + 3\text{Ti} + 2.26\text{TiO}_2$ (squares), $2\text{Cr}_2\text{O}_3 + 3\text{Zr} + 2.82\text{ZrO}_2$
(circles) and $\text{Cr}_2\text{O}_3 + 2\text{Al} + 0.64\text{Al}_2\text{O}_3$ (triangles) systems
as measured by Butakova et. al.³³

Table 2
Ti+C Powder Compact Thermal Conductivities

Sample Number	Perpendicular Thermal Conductivity (W/m-K)	Parallel Thermal Conductivity (W/m-K)
1	1.05 ± 0.10	0.65 ± 0.04
2	0.78 ± 0.06	0.43 ± 0.03
3	0.79 ± 0.05	0.43 ± 0.02
5	1.10 ± 0.10	0.54 ± 0.04
6	1.37 ± 0.08	0.66 ± 0.07
7	1.88 ± 0.10	0.93 ± 0.05
8	1.12 ± 0.10	0.62 ± 0.03
9	1.62 ± 0.08	0.78 ± 0.04
10	1.46 ± 0.08	0.70 ± 0.04
11	2.27 ± 0.16	1.06 ± 0.06
12	2.02 ± 0.12	0.93 ± 0.08
13	2.76 ± 0.28	1.16 ± 0.07
14	3.30 ± 0.20	1.58 ± 0.14

The conductivity of heat through solid materials occurs via solid, gaseous and radiative processes and can be expressed as:

$$k = ak_S + bk_G + k_R \quad (25)$$

where k is the total thermal conductivity, k_S is the thermal conductivity of the solid material, k_G is the thermal conductivity of the gas in the voids, k_R is the thermal conductivity due to radiative processes and a and b are geometric factors. All three thermal conduction processes are affected by porosity and thus are density dependent. The solid conductivity is modulated by the geometric factor, a , which takes into account the decrease in the effective cross-sectional area of the bulk solid due to porosity. Gaseous thermal conductivity, which takes place only in the gas filled voids, is inherently dependent on the number of voids and so has a porosity dependence which is expressed through the geometric factor b . The effect of

voids on radiative heat transfer depends on the opacity of the solid to the thermal radiation. For transparent systems, voids can act as photon scattering sites which decrease photon mean free paths thus decreasing the radiative thermal transfer. Solids which are opaque to the thermal radiation, such as the powder compacts studied here, experience little radiation transport within the individual grains. However radiation between powder particles, across the void spaces, can be an important heat transfer mechanism at elevated temperatures and will increase with increasing porosity. Increased porosity acts to decrease solid heat transfer while increasing the amount of gaseous and radiative heat transfer. Since the general trend in the data presented here shows that thermal conductivity increases with decreasing porosity, it is concluded that for these green compacts at the measured temperatures solid heat transfer dominates over the other heat transfer mechanisms and the density dependence of the thermal conductivity of these powder compacts is the result of changes in effective cross-sectional area.

The observed anisotropy of the thermal conductivity of these green compacts can be approached from two different points of view. Either the interaction between adjacent powder particles or the geometry of the pores between the powder particles can be considered as a function of compaction. Consider first the compaction dependence of the powder particle-particle interfaces. The thermal conductivity of powder compacts is generally less than the bulk thermal conductivity of the material in non-powdered form due to contact resistance between powder particles. This contact resistance is the result of reduced area contact between particles due to irregular particle shapes, contact reduction due to microroughness and thermal resistance due to oxide layers. With the application of greater amounts of compacting pressure, the contact area between adjacent particles increases due to particle deformation and thermally insulating oxide layers on the outside of powder particles can be penetrated allowing direct contact between the bulk powder particle material. To the extent that the uniaxial pressure exerted by the opposed anvils is not distributed isostatically in the powder compact, the decrease in the contact resistance with applied pressure will not be the same in all directions.

An additional consideration for the powders used in this study is that non-isostatic pressure is known to orient graphite particles in a direction such that the basal planes of the graphitic two dimensional structure are normal to the pressing axis.³⁴ Since the thermal conductivity of oriented graphite is known to be highly anisotropic, having a much lower value across planes rather than along the planes, this would introduce an anisotropy into the thermal conductivity of the green compact as a whole similar to that observed in molded graphite powder compacts.¹⁷ The effect of non-isostatic compaction pressure on irregular particle shape, microroughness and oxide layers would be to increase the thermal conductivity in the direction parallel to the uniaxial compacting force relative to the thermal conductivity in the perpendicular direction. Conversely, the effect of non-isostatic compaction pressure on graphite particle orientation would decrease the thermal conductivity in the direction parallel to the compaction force relative to the perpendicular direction. Since the observed effect of compaction on the anisotropy of the titanium and graphite powder compact thermal conductivity is to increase the thermal conduction in the direction

perpendicular to the compaction force over that in the parallel direction, it is concluded that the dominant effect of compaction on the thermal conductivity of these green compacts is the orientation of the graphite particles. This description is especially plausible if the relative magnitudes of the thermal conductivities of the individual components in this system are considered. From Reference 17 the thermal conductivity of titanium is listed as 21.9 W/m-K at room temperature while for a highly oriented graphite such as Pyrolytic graphite the thermal conductivity ranges from 1960 W/m-K parallel to the layer planes to 5.73 W/m-K perpendicular to the layer planes. With the values for the thermal conductivity of graphite varying so widely with direction around the thermal conductivity value for titanium, even a small bias in the orientation of the graphite particles with pressure could have a pronounced effect on the directional dependence of the thermal conductivity of the green compact. The orientation of graphite particles with non-isostatic pressure may also lead to an anisotropy in the rate at which these graphite crystals are intercalated by titanium during the SHS reaction. Such an induced anisotropy in mass transfer may mask expected variations in reaction rates due to changes in thermal conductivity.

An alternative scheme for describing the effects of compaction on powder compacts is to focus on the voids between the particles rather than on the particles themselves. With the application of pressure, the density of the green compact is increased due to the reduction in the total volume of the pores in the powder system. Uniaxial forces on powders in dies which prevent powder expansion in a direction transverse to the direction of compaction are not evenly redistributed in all directions to produce an isostatic pressure. Instead, the pressure maintains a dominant uniaxial component in the direction of the compaction force. To the extent that the pressure is non-isostatic, the voids will be deformed in addition to being reduced in volume.³⁵ Since the major component of the non-isostatic pressure for uniaxial compaction would be parallel to the uniaxial compacting force, the largest reduction in pore dimensions would be expected in the direction of the compacting force. This is illustrated graphically in Fig. 20. Pores "flattened" by nonisostatic pressure would therefore present a greater cross-sectional area in the direction of the greatest void dimension reduction. Thus the effective solid cross sectional area per unit area of the green compact would be smaller in the direction parallel to the compaction than in the direction perpendicular to the compaction force. This variation in effective cross sectional area would cause the solid component of the heat conduction to be greater in the direction perpendicular to compaction than in the parallel direction which agrees with the sense of the anisotropy observed for the total thermal conductivity.

If the thermal conductivity anisotropy of these green compacts is indeed the result of the compacting process and not caused by some other powder handling procedure, then the thermal conductivity anisotropy should increase with increasing compaction pressure. The ratio of the thermal conductivities in the directions parallel and perpendicular to the compacting force versus the compaction density are plotted in Fig. 21. In general these data do show an increase in the anisotropy of the green compact thermal conductivity with increasing density or compaction pressure which supports the conclusion that the observed anisotropy is the result of the compaction process. The apparent deviation of the highest density data point from the trend of the

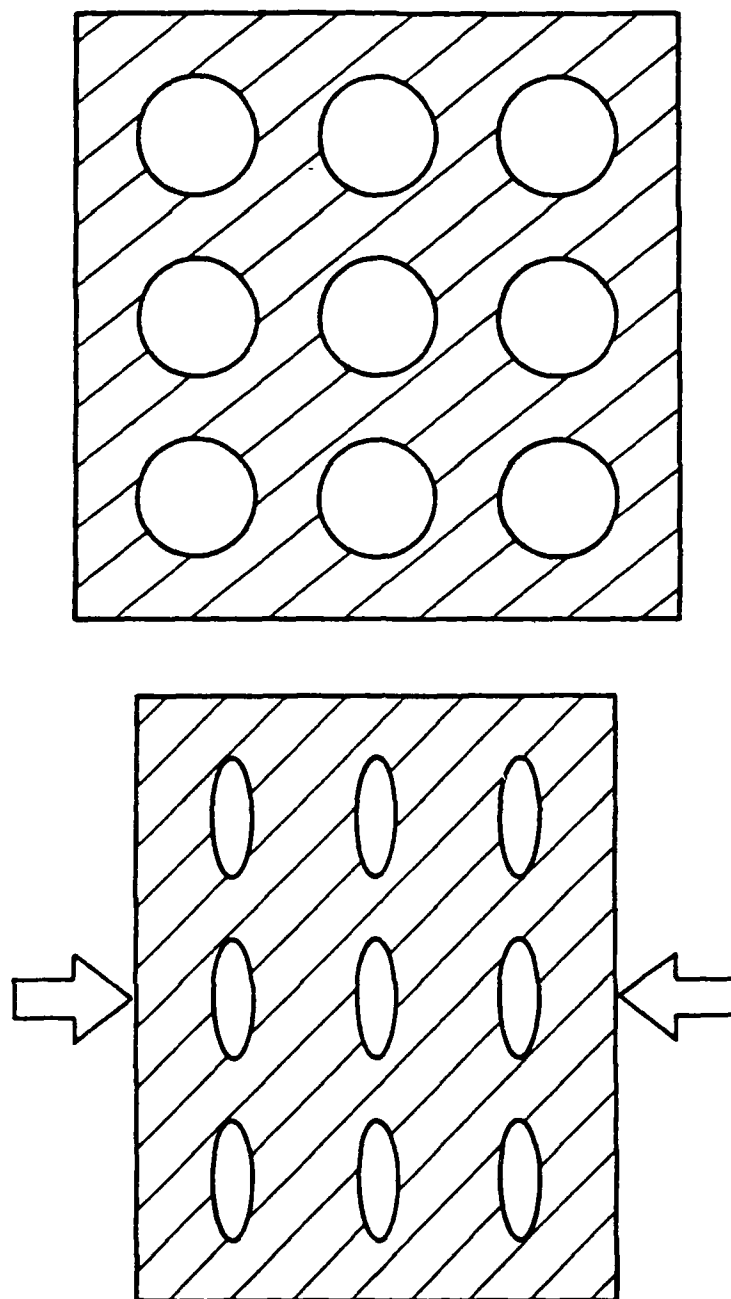


Figure 20. Possible effect of non-isostatic pressure on pore geometry.

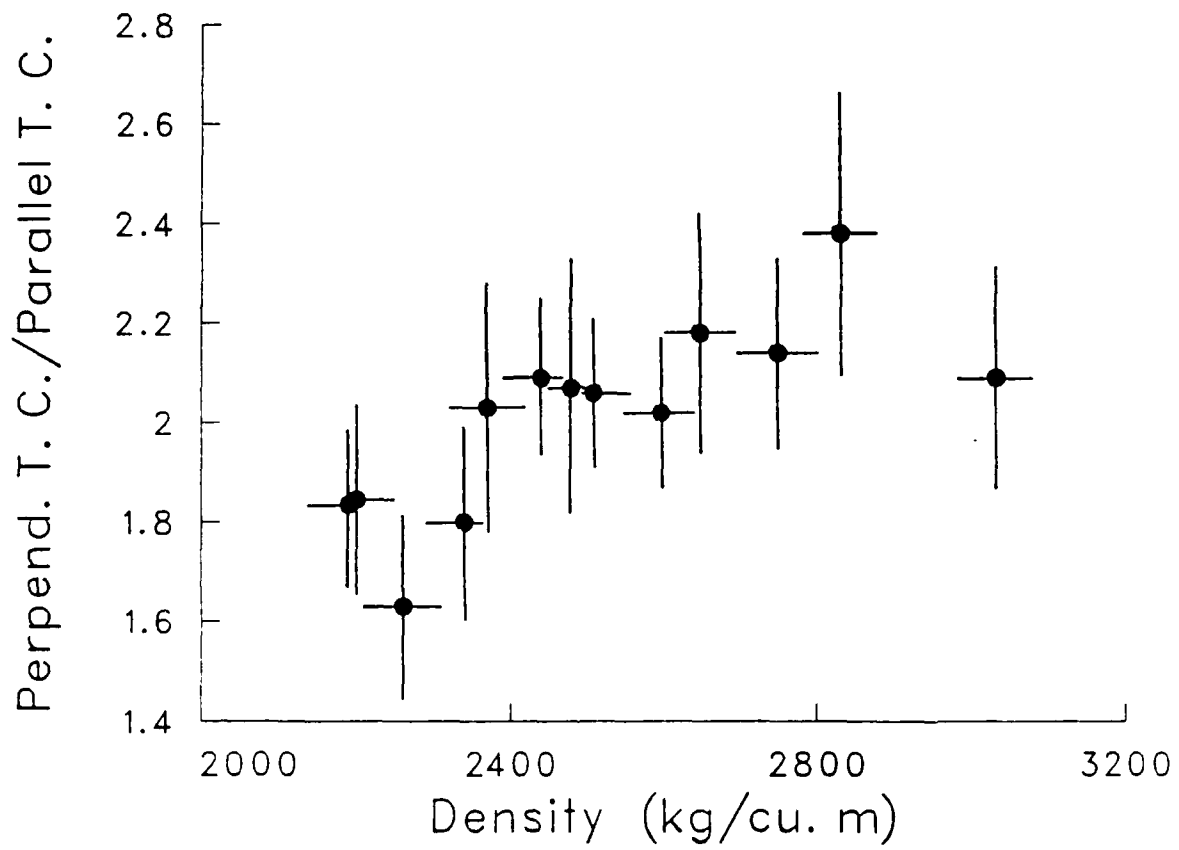


Figure 21. Observed green compact thermal conductivity anisotropy versus density.

other data points may be due to an anomalous compaction event occurring during failure of the compacting die.

The original motivation for measuring the thermal conductivities of titanium and graphite powder compacts of varying densities was to determine if the range of green compact thermal conductivities was of a sufficiently large magnitude as predicted by numerical analysis modeling to be necessary to affect SHS initiation, reaction rates and ultimately final product material properties. Over the range of available densities, the thermal conductivity was found to change by a factor of four in both of the directions measured, Fig. 18. According to the results of the numerical analysis modeling, for ignition by a resistively heated filament, a factor of four change in thermal conductivity can vary titanium carbide SHS reaction initiation times over a wide range of values and even make initiation at lower power levels impossible, Fig. 9. Thus the range of green compact thermal conductivities made available by variations in compact density is broad enough to allow green compacts, or at least the portion of the green compact surrounding the igniting filament, to be tailored for easier ignition.

The numerical analysis modeling of the SHS reaction predicted that a factor of four variation in green compact thermal conductivity would change the reaction zone velocity of titanium and graphite SHS systems that were not mass transfer limited by approximately a factor of three, Fig. 6. The ability to control the SHS reaction zone propagation velocity over such a wide range of values may be particularly convenient if applied to some of the various SHS product densification schemes. Densification methods which simultaneously densify an entire reacted compact^{3,4} require that the entire compact be above the brittle-plastic transition temperature at the time of densification. Such systems would benefit from rapid propagation velocities which allow the entire green compact to synthesize quickly with a minimum of heat loss to any containing vessel. Other densification schemes which densify the reacted material in a continuous process⁵ might benefit from slower reaction rates which would require less critical control over the post-synthesis compaction apparatus. SHS prepared materials which are processed without post-synthesis densification may also benefit from the wide range of reaction rates made possible by variation of the precursor green compact density. The thermal conductivity of a green compact affects the spatial distribution and extent of the reaction zone temperature profile and therefore determines the rate at which the green compact in front of the advancing reaction zone heats up to the synthesis temperature. Highly densified green compacts with high thermal conductivity have broad reaction zone temperature profiles which may allow the green compact to heat up from ambient to reaction temperatures over a relatively long time. Thus high density green compacts may yield SHS prepared materials of higher purity and lower porosity due to the increased outgassing at lower temperatures made possible by the extended temperature profile of the reaction zone. However, SHS reactions which depend on the presence of a gaseous component, such as various hydride and nitride synthesis processes, might benefit from the relatively low outgassing afforded by highly porous green compacts with low thermal conductivities.

The thermal conductivity measurements of the titanium and graphite powder compacts were performed at room temperature. Since the temperature of these green compacts will change by thousands of degrees when being heated from ambient to reaction temperature, it is important to consider how the thermal conductivity of these green compacts will vary as a function of temperature. At high temperatures the thermal conductivity of titanium increases at a moderate rate¹⁶ while the thermal conductivity of graphite decreases significantly.¹⁷ However the titanium and carbon system offers the luxury of working with a material which comes in many forms - namely carbon. In addition to graphite, amorphous forms of carbon such as charcoal, soot and lampblack also exist. Actually these so called amorphous carbons are microcrystalline forms of graphite sometimes containing only a few unit cells of graphite per particle.³⁶ At elevated temperatures the thermal conductivity of the amorphous carbons changes in the sense opposite to that of graphite, increasing with increasing temperatures.^{16,17} So not only can mixed titanium and carbon powder green compact room temperature thermal conductivities be controlled by varying the green compact density, but the variation of the thermal conductivity with temperature can also be manipulated by varying the graphite to amorphous carbon ratio of the powder mixture. This additional degree of control over the green compact thermal conductivity should prove useful in tailoring SHS ignition times, synthesis rates and reaction zone temperature profiles to specific processing applications.

The dependence of SHS propagation velocity on precursor compact density has been studied experimentally for several systems. Maksimov et. al.³⁷ measured the propagation velocity in the aluminium and iron oxide system over a density range of 10% to 70% of theoretical maximum. With increasing powder compact density, the propagation velocity initially decreased to a minimum value at approximately 50% density and then increased rapidly. These investigators noted that the density value for the minimum in propagation velocity coincided with the density value for a measured thermal diffusivity minimum and that the velocity and thermal diffusivity curves exhibited the same general shape. Using the thermal diffusivity relation expressed in Eq. 24, the measured values for thermal conductivity and density and a constant room temperature value for the specific heat, the thermal diffusivity for the titanium and graphite compacts can be determined. The density dependence of this thermal diffusivity in the direction perpendicular to the compaction direction is shown in Fig. 22. Following the correlation noted by Maksimov et. al., the predicted SHS propagation velocity for the titanium and carbon system is plotted as a function of compact density in Fig. 23. Comparison of these two plots shows that the measured thermal diffusivity and the predicted propagation velocity both increase monotonically by approximately the same factor with increasing density.

The dependence of SHS propagation velocity on powder compact density was measured for several titanium containing systems by Rice et. al.³⁸ One of these systems was titanium and carbon with 10% excess titanium. Although the vendors of the powders are listed, the nature of the carbon, graphite or amorphous, is not stated. With increasing compact density Rice and coworkers measured an increase in propagation velocity up to approximately 60% of

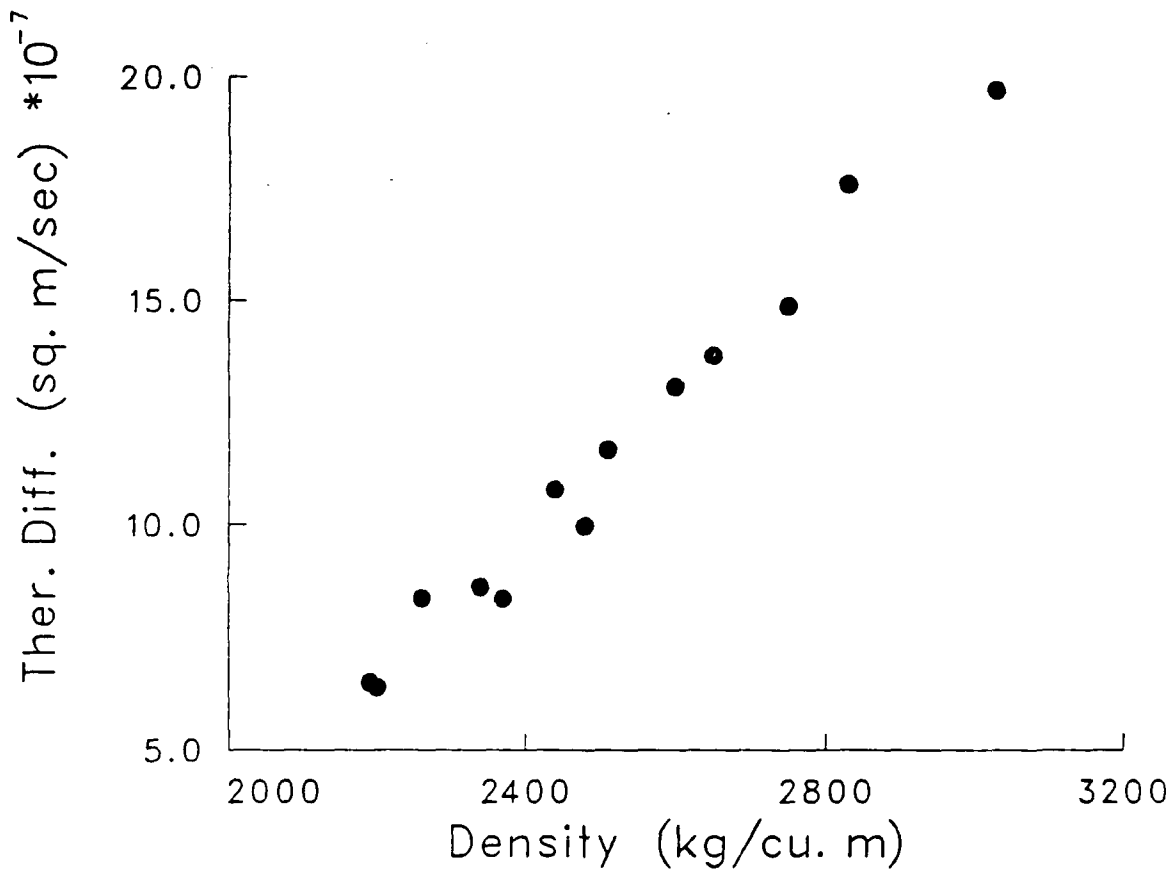


Figure 22. Thermal diffusivity of titanium and graphite powder compacts in the direction perpendicular to the direction of compaction as a function of powder compact density.

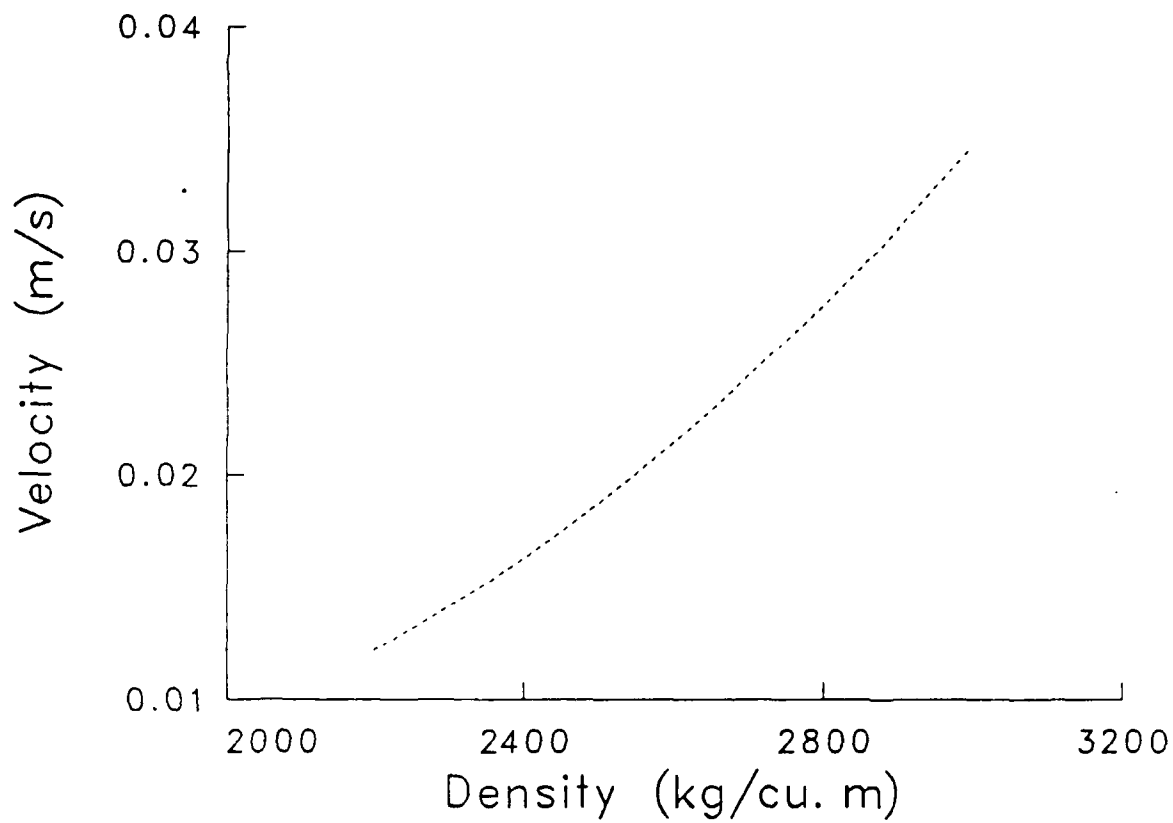


Figure 23. Predicted dependence of SHS propagation velocity on powder compact density for the titanium and carbon system.

theoretical density where propagation velocities dropped off sharply. The initial velocity increase with density was attributed to increased geometric proximity of contact points between powder particles while the high density drop off was explained as being due to excessive dissipation of thermal energy from the reaction front to the green compact. A decrease in propagation velocity with higher compact densities is not consistent with the monotonic dependence predicted by numerical analysis. As noted by Maksimov et. al.³⁷ the conduction of thermal energy from a reacting sample to the surrounding environment can artificially decrease the propagation velocity. The experience of the authors is that when cylindrical titanium and carbon samples are reacted in pressed graphite sample holders, the SHS reaction does not propagate beyond the point of contact between the sample and the holder. Rice et. al. also noted this effect for a related experiment. All the propagation velocity measurements of Rice and coworkers were made on rectangular compacts contained on five sides by a graphite die. It is possible that this configuration might bias SHS propagation velocities by creating a highly nonadiabatic reaction environment. Low density samples may not have been overly affected by reaction in the graphite die because the inherently low thermal conductivity of the powder compact thermally isolated the observed open surface of the rectangular sample from the die. However for higher density samples, with their increased thermal conductivities, a greater portion of the samples volumes may have been subject to heat loss to the die with an eventual decrease in propagation velocity. This possible explanation is supported by the observation that in spite of the wide variety of systems tested using the graphite die sample holder, they all displayed a decrease in propagation velocity at the higher powder compact densities.

5. SUMMARY

A numerical analysis model has been developed and tested for modeling the effects of green compact thermal conductivity on SHS reaction initiation and propagation velocity in the titanium and carbon system. Initiation modeling predicts that the time required to start an SHS reaction using a resistively heated filament of a given power density is strongly dependent on the thermal conductivity of the powder compact. Low filament power levels can lead to unacceptably long ignition times due to excessive heat loss from the portion of the powder compact surrounding the filament to the remainder of the green compact. Conversely, overly high power levels will cause the filament to melt before the SHS reaction is initiated. Acceptable filament power density levels and the predicted ignition times have been calculated over the range of obtainable titanium and graphite powder compact thermal conductivities. Propagation velocity modeling predicts a linear dependence of velocity on green compact thermal conductivity for compacts with conductivities in the upper range of attainable values. For compacts with thermal conductivities in the lower range of attainable values the propagation velocity is predicted to fall off at an increasing rate.

Thermal conductivities of mixed titanium and graphite powder compacts have been measured as a function of compact density to determine if green compact thermal conductivity control via compact density would be a suitable means for controlling SHS reaction initiation, propagation velocity and eventually final product characteristics. Over the range of easily

attainable compact densities, the thermal conductivity of the titanium and graphite powder compacts was found to change by a factor of four, increasing with compact density. When correlated with the modeling results, this factor of four change in thermal conductivity should be sufficient to alter SHS ignition times for certain heating filament power densities by many seconds and vary propagation velocities by at least a factor of three. An anisotropy of the green compact thermal conductivity was also observed which increased with increasing compact density. Thermal conductivities in the direction perpendicular to the uniaxial compacting force were measured to be about twice that in the parallel direction. This green compact thermal conductivity anisotropy is thought to be the result of powder particle orientation and pore deformation resulting from the uniaxial compacting force.

By varying the ratio of crystalline graphite to amorphous carbon used in the titanium and carbon powder mixtures, it should be possible to manipulate the temperature dependence of the thermal conductivities of these green compacts in addition to their room temperature values. This high degree of control over green compact thermal conductivity may result in improved SHS final product characteristics by allowing manipulation of reaction zone temperature profiles which affect outgassing prior to synthesis and product purity. Combined synthesis - compaction processing will also benefit from control of propagation velocities via the compact thermal conductivity.

Other investigators have noted a correlation between the thermal diffusivity and propagation velocity of SHS systems. The measured thermal diffusivities and the predicted propagation velocities for the titanium and carbon system appear to follow the same trend. A systematic investigation of a variety of SHS systems may prove the validity of this correlation. In addition, definitive experimental measurements of propagation velocity as a function of green compact density remain to be performed for the titanium - carbon and many other SHS systems.

REFERENCES

1. Merzhanov, A. G., and Dubovitskiy, F. I., "Towards a Theory of Steady State Combustion of Powder," Doklady Physical Chemistry, pp. 129, 1959.
2. Zavitsanos, P. D., and D'Andrea, J., Study of Self-Propagating Condensed Phase Reactions - TiB₂ Synthesis, Report No. DAAG29-83-C-0017, Army Research Office, Research Triangle Park, NC, February 1985.
3. Riley, M., and Niiler, A., Low Pressure Compaction of SHS Prepared Ceramics and Cermets, Paper presented at DARPA/Army Symposium of Self-Propagating High Temperature Synthesis, Daytona Beach, FL, 21-23 October 1985.
4. Holt, J. B., Bianchini, G., and Kingman, D., Simultaneous Combustion Synthesis and Densification of Refractory Materials, Paper presented at DARPA/Army Symposium on Self-Propagating High Temperature Synthesis, Daytona Beach, FL, 21-23 October 1985.
5. Wallace, J., Richardson, G. Y., and Schrod, D., Simultaneous Densification and Reaction Synthesis in the Ti-C System Through Hot Rolling, Paper presented at DARPA/Army Symposium on Self-Propagating High Temperature Synthesis, Daytona Beach, FL, 21-23 October 1985.
6. Scanes, F. S., The Addition of High Conductivity Materials to Pyrotechnic Compositions, CDE-TP-106, Porton Down, Salisbury, Wilts., United Kingdom, July 1972.
7. Holt, J. B., Kingman, D. D., and Bianchini, G. M., "Kinetics of the Combustion Synthesis of TiB₂," Material Science and Engineering, Vol. 71, pp. 321, May 1986.
8. Holt, J. B., and Munir, Z. A., "Combustion Synthesis of Titanium Carbide: Theory and Experiment," Journal of Materials Science, Vol. 21, pp. 251, January 1986.
9. Kecskes, L. J., and Niiler, A., Gas Evolution During the TiC SHS Reaction, Paper presented at American Ceramic Society 88th Annual Meeting, Chicago, IL, April 1986.
10. Kottke, T., and Niiler, A., Effects of Thermal Conductivity on SHS Reaction Kinetics, Paper presented at DARPA/Army Symposium on Self-Propagating High Temperature Synthesis, Daytona Beach, FL, 21-23 October 1985.
11. Carslaw, H. S., and Jaeger, J. C., Operational Methods in Applied Mathematics, Oxford, New York, NY, 1941.
12. Carslaw, H. S., and Jaeger, J. C., Conduction of Heat in Solids, Oxford, New York, NY, 1946.
13. Weast, R. C., Handbook of Chemistry and Physics, 55th Ed., CRC Press, Cleveland, OH, 1974.

14. Storms, E. K., Refractory Materials Volume 2, Academic Press, New York, NY, 1967.
15. Schulz, B., "Thermal conductivity of porous and highly porous materials," High Temperatures - High Pressures, Vol. 13, pp. 649, 1981.
16. Unvala, B., and Goel, T., Rev. Int. Hautes Temper. et Refract, Vol 7, pp. 341, 1970.
17. Lynch, C. T., Handbook of Materials Science, Vol III, pp. 495, CRC Press, Cleveland, OH, 1975.
18. Riley, M. A., and Niiler, A., Low Pressure Compaction of SHS Prepared Ceramics, BRL-MR-3574, Ballistic Research Laboratory, Aberdeen Proving Ground, MD, 1987.
19. Systems Planning Corporation, "Materials Fabrication by Self-Propagating High-Temperature Synthesis in the Soviet Union, Vol. II," SPC Report 81-4083, December 1982.
20. Wechsler, A. E., "Thermal and Mechanical Properties of Evacuated Powders," Powder Technology, Vol. 3, pp. 163, 1969/70.
21. Klemens, P. G., and Greenberg, I. N., "Radiative Heat Transfer Through Composite Materials," Journal of Applied Physics, Vol. 44, pp. 2992, 1973.
22. Bethin, J., and Williams, W. S., "Ambipolar Diffusion Contribution to High-Temperature Thermal Conductivity of Titanium Carbide," Journal of the American Ceramic Society, Vol. 60, pp. 424, 1977.
23. Novikov, N. P., Borovinskaya, I. P., and Merzhanov, A. G., "Thermodynamic Analysis of Self-Propagating High-Temperature Synthesis Reactions," Combustion Processes in Chemical Technology and Metallurgy, pp. 174, Moscow, USSR, 1975.
24. The word APPLE is a registered trademark of APPLE COMPUTER INC., 10260 Bandley Drive, Cupertino, CA 95014.
25. Melen, R., and Garland, H., Understanding IC Operational Amplifiers, Howard W. Sams and Co., Indianapolis, IN, 1978.
26. Jung, W. G., IC Op Amp Cookbook, Howard W. Sams and Co., Indianapolis, IN, 1980.
27. Atlantic Equipment Engineers, Var Lac Oid Chemical Co., Inc., Division of Micron Metals, Inc., 13 Foster Street, P. O. Box 181, Bergenfield, NJ 07621.
28. Consolidated Astronautics, Inc., P. O. Box 2500, Smithtown, NY 11787.
29. Niiler, A., and Kottke, T., "The TiC Self-Propagating High-Temperature Synthesis Reaction," Army Science Conference Proceedings, Vol 2, pp. 283, 1984.

30. Bevington, P. R., Data Reduction and Error Analysis for the Physical Sciences, McGraw-Hill, Inc., New York, NY, 1969.
31. MACOR is a trademark of Corning Glass Works, Corning, NY 14830.
32. Prakouras, A. G., Vachon, R. I., Crane, R. A., and Khader, M. S., "Thermal Conductivities of Heterogeneous Mixtures," Int. J. Heat Mass Transfer, Vol. 21, pp. 1157, 1978.
33. Butakova, E. A., and Strunina, A. G., "Thermophysical Properties of Some Thermite and Intermetallic Systems," Fizika Goreniya i Vzryva, Vol. 21, No. 1, pp. 71, Jan-Feb 1985; translated to English in Combustion, Explosion, and Shock Waves, July 1985.
34. Reynolds, W. N., Physical Properties of Graphite, Elsevier Publishing Co. Ltd., New York, NY, 1968.
35. Kuhn H., Effects of Porosity on Material Processing, Proceedings of 1976 ASME Applied Mechanics Division Meeting, Salt Lake City, UT, June 14, 1976.
36. Cotton, F., and Wilkinson, G., Advanced Inorganic Chemistry, Interscience Publishers, New York, NY, 1972.
37. Maksimov, E. I., Merzhanov, A. G., and Shkiro, V. M., "Gasless Compositions as a Simple Model for the Combustion of Nonvolatile Condensed Systems", Fizika Goreniya i Vzryva, Vol. 1, No. 4, pp. 22, 1965
38. Rice, R. W., Richardson, G.Y., Kunetz, J. M., Schroeter, T., and McDonough, W. J., "Effects of Self-Propagating Synthesis Reactant Compact Character on Ignition, Propagation and Resultant Microstructure", Ceramics Engineering and Science Proceedings, Vol. 7, No. 7-8, pp. 737, 1986.
39. Selby, S. M., CRC Standard Mathematical Tables, CRC Press, Inc., Cleveland, OH, 1975.

APPENDIX A

SHS Reaction Initiation and Propagation Simulation Software

C THIS PROGRAM SIMULATES THE INITIATION AND PROPAGATION OF AN SHS
C REACTION IN A TITANIUM AND GRAPHITE POWDER COMPACT. THE IDENTITY
C OF THE VOLUME CELLS IS DETERMINED BY NUMBER ACCORDING TO THE
C FOLLOWING ASSIGNMENTS: 1=C+ALPHA TI, 2=TUNGSTEN FILAMENT,
C 3=C+BETA TI, 4=TIC. BEFORE RUNNING THIS PROGRAM, A DATA FILE
C MUST BE CREATED CONTAINING THE ARRAY DIMENSIONS AND IDENTITIES
C OF THE CELL VOLUMES. THE PROGRAM REPGEN.FOR CAN BE USED TO CREATE
C SUCH A DATA FILE.

IMPORTANT VARIABLES:

C BLKCTR SERIAL ID NUMBER OF VOLUME CELL FOR WHICH TEMPERATURE
C CHANGE IS BEING CALCULATED.
C BLKNEI SERIAL ID NUMBER OF VOLUME CELL INTERACTING THERMALLY
C WITH BLKCTR.
C BLOCKID NUMBER REPRESENTING THE MATERIAL OF WHICH VOLUME CELL
C IS ASSUMED TO BE COMPOSED.
C TMPNOW THE PRESENT VOLUME CELL TEMPERATURE.
C TMPNAV THE VOLUME CELL TEMPERATURE AT THE END OF THE LAST
C ITERATIVE TEMPERATURE CALCULATION.
C PLCBRN THE POSITION OF A SELECTED REACTING VOLUME CELL.
C TIMBRN THE TIME ASSOCIATED WITH THE REACTION OF THE RELATED
C PLCBRN VARIABLE VOLUME CELL.
C FILE1 NAME OF DATA FILE CONTAINING ARRAY DIMENSIONS AND
C INITIAL MATERIAL ASSIGNMENTS.
C FILE2 NAME OF FILE CONTAINING POSITION AND REACTION TIME
C OF SELECTED VOLUME CELLS.
C FILE3 NAME OF FILE CONTAINING OPTIONAL NONSTANDARD VOLUME
C CELL TEMPERATURES.
C FILE4 NAME OF FILE CONTAINING VOLUME CELL TEMPERATURES AT
C THE END OF SIMULATION EXERCISE.
C XSIZE SIZE OF VOLUME CELL IN X DIRECTION IN METERS.
C SIMILAR FOR YSIZE AND ZSIZE.
C TMPAMB INITIAL AMBIENT TEMPERATURE OF VOLUME CELLS.
C TIMINT TIME ASSUMED TO PASS BETWEEN ITERATIVE TEMPERATURE
C CALCULATIONS.
C COMDEN DENSITY OF COMPACT AS A PERCENT OF THEORETICAL
C MAXIMUM.
C SETTC THERMAL CONDUCTIVITY OF GREEN COMPACT.
C DENSITY DENSITY OF GREEN COMPACT IN KG PER CUBIC METER.
C POWER POWER DENSITY OF FILAMENT IN WATTS PER METER.
C IXSTOP X COORDINATE OF VOLUME CELL FOR WHICH REACTION STOPS
C FILAMENT HEATING. SIMILAR FOR YSTOP AND ZSTOP.
C IYFILA Y COORDINATE OF FILAMENT. SIMILAT FOR IZFILA.
C IXHALT X COORDINATE FOR OPTIONAL SIMULATION HALT AND DATA
C DUMP INTO FILE4.
C TIMLIM MAXIMUM ALLOWED SIMULATION TIME.
C BLKMAN MASS OF VOLUME CELL WHERE n CORRESPONDS TO MATERIAL
C ASSIGNMENT NUMBER.
C ITOTNUM TOTAL NUMBER OF VOLUME CELLS.

```

C      IXNUM      LENGTH OF ARRAY IN X DIRECTION IN VOLUME CELLS.
C      SIMILAR FOR IYNUM AND IZNUM.
C      IPROP      SERIAL POSITION NUMBER OF VOLUME CELL DESCRIBED BY
C      IXSTOP, IYSTOP AND IZSTOP.
C      IPFLAG     FLAG THAT INDICATES ON OR OFF CONDITION OF FILAMENT.
C      IMFLAG     FLAG THAT INDICATES IF FILAMENT HAS MELTED.
C      IEND       SERIAL POSITION NUMBER OF VOLUME CELL DESCRIBED BY
C      IXHALT, IYHALT AND IZHALT.
C      IXTEST     DETERMINES POSITIONS FOR PLCBRN AND TIMBRN VOLUME
C      CELLS.
C      ITER       ITERATION COUNTER.
C      TIMNOW     PRESENT SIMULATION TIME.
C      Q          TOTAL ENERGY RELEASED BY FILAMENT IN THE TIME
C      INTERVAL TIMINT.

```

```

INTEGER BLKCTR, BLKNEI, BLOCKID, H
DIMENSION BLOCKID(10000), TMPNOW(10000), TMPNAV(10000), H(100), T(100)
DIMENSION TIMBRN(250), PLCBRN(250)
CHARACTER FILE1*35, FILE2*35, FILE3*45, FILE4*45, ANS1*1

C
C      WRITE (6, '( '1' )' )
C
C      WRITE (6, '( '$' ,/, 1X, 'ENTER COMPACT GEOMETRY DATA FILENAME: ' )' )
C      READ (5, '(A)' ) FILE1
C
C      WRITE (6, '( '$' ,/, 1X, 'ENTER OUTPUT FILENAME: ' )' )
C      READ (5, '(A)' ) FILE2
C
C      WRITE (6, '( '$' ,/, 1X, 'ENTER INITIAL TEMP INPUT FILENAME: ' )' )
C      READ (5, '(A)' ) FILE3
C
C      WRITE (6, '( '$' ,/, 1X, 'ENTER FINAL TEMP DUMP FILENAME: ' )' )
C      READ (5, '(A)' ) FILE4
C
C      WRITE (6, '( '$' ,/, 1X, 'ENTER X, Y AND Z BLOCK DIMENSIONS ' )' )
C      WRITE (6, '( '$' , 1X, 'IN MILLIMETERS: ' )' )
C      READ (5, *) XSIZE, YSIZE, ZSIZE
C
C      CONVERTING MILLIMETERS TO METERS
C      XSIZE=XSIZE/1000.
C      YSIZE=YSIZE/1000.
C      ZSIZE=ZSIZE/1000.
C
C      WRITE (6, '( '$' ,/, 1X, 'ENTER AMBIENT TEMPERATURE IN CELSIUS: ' )' )
C      READ (5, *) TMPAMB
C
C      WRITE (6, '( '$' ,/, 1X, 'ENTER TIME BETWEEN ITERATIONS IN SEC: ' )' )
C      READ (5, *) TIMINT
C
C      WRITE (6, '( '$' ,/, 1X, 'ENTER % OF THEORETICAL COMPACT DENS: ' )' )
C      READ (5, *) COMDEN
C
C      WRITE (6, '( '$' ,/, 1X, 'ENTER GREEN COMPACT THERM. COND.: ' )' )

```

```

READ (5,*) SETTC
C
C   CONVERTING PERCENTAGE OF THEORETICAL COMPACTION DENSITY TO AN
C   ACTUAL DENSITY VALUE OF MIXED TI AND C POWDER IN UNITS OF KG/M^3
C   DENSITY=3750*COMDEN/100.
C
WRITE (6,(''$'//,1X,'ENTER LINEAR IGNI POWER IN W/M: '''))
READ (5,*) POWER
C
WRITE (6,(''$'//,1X,'ENTER X,Y,Z OF IGNI OFF BLOCK: '''))
READ (5,*) IXSTOP,IYSTOP,IZSTOP
C
WRITE (6,(''$'//,1X,'ENTER Y AND Z OF FILAMENT: '''))
READ (5,*) IYFILA,IZFILA
C
WRITE (6,(''$'//,1X,'ENTER X,Y AND Z OF IGNITION HALT BLOCK: '''))
READ (5,*) IXHALT,IYHALT,IZHALT
C
WRITE (6,(''$'//,1X,'ENTER MAX ALLOWED RUN TIME: '''))
READ (5,*) TIMLIM
C
C   DETERMINING AND DEFINING MASSES OF DIFFERENT BLOCK TYPES
C   BLKMA1=DENSITY*XSIZE*YSIZE*ZSIZE
C   BLKMA2=19300*XSIZE*YSIZE*ZSIZE
C
OPEN (7,FILE=FILE1, FORM='UNFORMATTED', STATUS='OLD')
READ (7) IXCOM,IYCOM,IZCOM,IXDIE,IYDIE,IZDIE,IYAIR,ITOTNUM
C
C   DETERMINING NUMBER OF BLOCKS IN THE X, Y AND Z DIRECTIONS
C   IXNUM=2*IXDIE+IXCOM
C   IYNUM=IYAIR+IYCOM+IYDIE
C   IZNUM=2*IZDIE+IZCOM
C
C   DETERMINING THE TOTAL NUMBER OF BLOCKS
C   ITOTNUM=IXNUM*IYNUM*IZNUM
C
DO 100 I=1,ITOTNUM,1
    READ (7) BLOCKID(I)
    CONTINUE
100
C
CLOSE (7,STATUS='KEEP')
C
OPEN (7,FILE=FILE2,FORM='FORMATTED',STATUS='NEW')
C
C   CONVERTING FROM POWDER DENSITY TO TOTAL POWER
C   POWER=POWER*IXNUM*XSIZE
C
C   INITIALIZING BLOCK TEMPERATURES
DO 200 I=1,ITOTNUM,1
    TMPNOW(I)=TMPAMB
    TMPSAV(I)=TMPAMB
200 CONTINUE
C
WRITE (6,(''$'//,1X,'ARE NON-INITIAL TEMPS TO BE USED? '''))

```

```

      READ (5,'(A)') ANS1
C
C   OBTAINING NON-INITIAL TEMPERATURES IF REQUIRED
IF (ANS1.NE.'N') THEN
      OPEN (8,FILE=FILE3,FORM='UNFORMATTED',STATUS='OLD')
      DO 864 I=1,ITOTNUM,1
          READ (8) TMPNOW(I),BLOCKID(I)
          TMPSAV(I)=TMPNOW(I)
864      CONTINUE
          END IF
C
      ITER=0
C
C   OBTAINING NON-INITIAL ITERATION NUMBER IF REQUIRED
IF (ANS1.NE.'N') READ (8) ITER
C
      IPROP=(IZSTOP-1)*IXNUM*IYNUM+(IYSTOP-1)*IXNUM+IXSTOP
      IPFLAG=1
      IMFLAG=1
C
C   DETERMINING NON-INITIAL FLAG VALUES IF REQUIRED
IF (ANS1.NE.'N') READ (8) IPFLAG,IMFLAG
C
      CLOSE (8,STATUS='KEEP')
C
      IEND=(IZHALT-1)*IXNUM*IYNUM+(IYHALT-1)*IXNUM+IXHALT
      IXTEST=(IXNUM/2)+1
      IYTEST=IYNUM/2+1
C
C   BEGINNING OF ITERATION SEQUENCE
1000 CONTINUE
C
C   INCREMENT ITERATION COUNTER
      ITER=ITER+1
C
C   DETERMINE TIME SINCE FILAMENT WAS ACTIVATED
      TIMNOW=ITER*TIMINT
C
C   CHECK TO SEE IF TIME EXCEEDS ALLOWED LIMIT
IF (TIMNOW.GT.TIMLIM) THEN
      WRITE (7,*) 'TIME LIMIT EXCEEDED'
      GOTO 9999
      END IF
C
C   IGNITION PROCESS
C
C   DETERMINE WHETHER FILAMENT SHOULD BE SHUT OFF
IF (BLOCKID(IPROP).EQ.4) THEN
      IF (IPFLAG.EQ.1) THEN
          IPFLAG=0
          WRITE (7,*) 'FILAMENT OFF AT ',TIMNOW
          WRITE (6,*) 'FILAMENT OFF AT ',TIMNOW
          END IF
      GOTO 1010

```

```

        END IF
Q=POWER*TIMINT
DO 1010 I=1,IXNUM,1
    IFILA=(IZFILA-1)*IYNUM*IXNUM+(IYFILA-1)*IXNUM+I
    FILSPE=134.+0.0194*(TMPNAV(IFILA)-25.)
    IF (FILSPE.GT.167) FILSPE=167.
    TMPNOW(IFILA)=TMPNOW(IFILA)+(Q/IXNUM)/(BLKMA2*FILSPE)
    IF (TMPNOW(IFILA).GT.3410) THEN
        IF (IMFLAG.EQ.1) THEN
            IMFLAG=0
            WRITE (7,*) 'FILAMENT MELTED AT: ',TIMNOW
            WRITE (6,*) 'FILAMENT MELTED AT: ',TIMNOW
            END IF
        TMPNOW(IFILA)=3410
        END IF
1010     CONTINUE
C
C     DETERMINING ORDER OF BLOCK CONSIDERATION IN A RANDOMIZED MANNER TO
C     AVOID BIASING DUE TO SEQUENCING
KDIR=ITER/2
KDIR=KDIR*2.0
IF (KDIR.EQ.ITER) THEN
    KSTART=1
    KSTOP=IZNUM
    KSTEP=1
    END IF
IF (KDIR.NE.ITER) THEN
    KSTART=IZNUM
    KSTOP=1
    KSTEP=-1
    END IF
DO 1111 K=KSTART,KSTOP,KSTEP
    JDIR=K/2
    JDIR=JDIR*2.0
    IF (KDIR.EQ.ITER.AND.JDIR.EQ.K.OR.KDIR.NE.ITER.
+      AND.JDIR.NE.K) THEN
        JSTART=1
        JSTOP=IYNUM
        JSTEP=1
        END IF
    IF (KDIR.EQ.ITER.AND.JDIR.NE.K.OR.KDIR.NE.ITER.
+      AND.JDIR.EQ.K) THEN
        JSTART=IYNUM
        JSTOP=1
        JSTEP=-1
        END IF
    DO 2222 J=JSTART,JSTOP,JSTEP
        KJSTEP=KSTEP*JSTEP
        IDIR=J/2
        IDIR=IDIR*2.0
        IF (KJSTEP.GT.0.AND.IDIR.EQ.J.OR.KJSTEP.LT.0.
+          AND.IDIR.NE.J) THEN
            ISTART=1
            ISTOP=IXNUM

```

```

        ISTEP=1
        END IF
        IF (KJSTEP.GT.0.AND.IDIR.NE.J.OR.KJSTEP.LT.0.
+         AND.IDIR.EQ.J) THEN
            ISTART=IXNUM
            ISTOP=1
            ISTEP=-1
            END IF
        DO 3333 I=ISTART,ISTOP,ISTEP
            BLKCTR=(K-1)*IXNUM*IYNUM+(J-1)*IXNUM+I
            L=I
300         IF (L.GT.6) THEN
                L=L-6
                GOTO 300
            END IF
            DO 4444 LL=1,6,1
                L=L+ISTEP
                IF (L.GT.6) L=1
                IF (L.LT.1) L=6
C
C     CONSIDERING BLOCK IN POSITIVE X DIRECTION
        IF (L.EQ.1) THEN
            IF (I.EQ.IXNUM) GOTO 4444
            BLKNEI=BLKCTR+1
            ITYPCTR=BLOCKID(BLKCTR)
            ITYPNEI=BLOCKID(BLKNEI)
            TMPCTR=TMPSAV(BLKCTR)
            TMPNEI=TMPSAV(BLKNEI)
            IF (ITYPCTR.EQ.2.AND.ITYPNEI.NE.2.AND.TMPCTR.LE.TMPNEI) GOTO 4444
            CALL SPECHEAT (ITYPCTR,TMPCTR,SPECTR)
            CALL SPECHEAT (ITYPNEI,TMPNEI,SPENEI)
            CALL THERMCON (L,ITYPCTR,TMPCTR,TCCTR,COMDEN,SETTC)
            CALL THERMCON (L,ITYPNEI,TMPNEI,TCNEI,COMDEN,SETTC)
            CALL BLKMASS (ITYPCTR,BLKMASCTR,BLKMA0,BLKMA1,BLKMA2)
            CALL BLKMASS (ITYPNEI,BLKMASNEI,BLKMA0,BLKMA1,BLKMA2)
            TC = (2. * TCCTR * TCNEI) / (TCCTR + TCNEI)
            TMPNOW(BLKCTR)=TMPNOW(BLKCTR)+((TMPNEI-TMPCTR)/(1.+((BLKMASCTR*
+             SPECTR)/(BLKMASNEI*SPENEI))))*(1.-EXP(-(TC*YSIZE*ZSIZE*
+             TIMINT/XSIZE))*(1./(BLKMASNEI*SPENEI)+1./(BLKMASCTR*
+             SPECTR))))
            IF(ITYPCTR.EQ.2.OR.ITYPNEI.EQ.2) TMPNOW(BLKCTR)=TMPNOW(BLKCTR)-
+             ((0.567E-7)*YSIZE*ZSIZE*((TMPCTR+273.)**4.-
+             (TMPNEI+273.)**4.)*TIMINT)/(BLKMASCTR*SPECTR)
            GOTO 4444
            END IF
C
C     CONSIDERING BLOCK IN NEGATIVE X DIRECTION
        IF (L.EQ.2) THEN
            IF (I.EQ.1) GOTO 4444
            BLKNEI=BLKCTR-1
            ITYPCTR=BLOCKID(BLKCTR)
            ITYPNEI=BLOCKID(BLKNEI)
            TMPCTR=TMPSAV(BLKCTR)
            TMPNEI=TMPSAV(BLKNEI)

```

```

IF (ITYPCTR.EQ.2.AND.ITYPNEI.NE.2.AND.TMPCTR.LE.TMPNEI)GOTO 4444
CALL SPECHEAT (ITYPCTR,TMPCTR,SPECTR)
CALL SPECHEAT (ITYPNEI,TMPNEI,SPENEI)
CALL THERMCON (L,ITYPCTR,TMPCTR,TCCTR,COMDEN,SETTC)
CALL THERMCON (L,ITYPNEI,TMPNEI,TCNEI,COMDEN,SETTC)
CALL BLKMASS (ITYPCTR,BLKMASCTR,BLKMA0,BLKMA1,BLKMA2)
CALL BLKMASS (ITYPNEI,BLKMASNEI,BLKMA0,BLKMA1,BLKMA2)
TC = (2. * TCCTR * TCNEI) / (TCCTR + TCNEI)
TMPNOW(BLKCTR)=TMPNOW(BLKCTR)+((TMPNEI-TMPCTR)/(1.+(BLKMASCTR*
+ SPECTR)/(BLKMASNEI*SPENEI)))* (1.-EXP(-(TC*YSIZE*ZSIZE*
+ TIMINT/XSIZE)*(1./(BLKMASNEI*SPENEI)+1./(BLKMASCTR*
+ SPECTR))))
IF(ITYPCTR.EQ.2.OR.ITYPNEI.EQ.2) TMPNOW(BLKCTR)=TMPNOW(BLKCTR)-
+ ((0.567E-7)*YSIZE*ZSIZE*((TMPCTR+273.)**4.-
+ (TMPNEI+273.)**4.)*TIMINT)/(BLKMASCTR*SPECTR)
GOTO 4444
END IF

```

C
C

```

CONSIDERING BLOCK IN POSITIVE Y DIRECTION
IF (L.EQ.3) THEN
IF (J.EQ.IYNUM) GOTO 4444
BLKNEI=BLKCTR+IXNUM
ITYPCTR=BLOCKID(BLKCTR)
ITYPNEI=BLOCKID(BLKNEI)
TMPCTR=TMPNAV(BLKCTR)
TMPNEI=TMPNAV(BLKNEI)
IF (ITYPCTR.EQ.2.AND.ITYPNEI.NE.2.AND.TMPCTR.LE.TMPNEI)GOTO 4444
CALL SPECHEAT (ITYPCTR,TMPCTR,SPECTR)
CALL SPECHEAT (ITYPNEI,TMPNEI,SPENEI)
CALL THERMCON (L,ITYPCTR,TMPCTR,TCCTR,COMDEN,SETTC)
CALL THERMCON (L,ITYPNEI,TMPNEI,TCNEI,COMDEN,SETTC)
CALL BLKMASS (ITYPCTR,BLKMASCTR,BLKMA0,BLKMA1,BLKMA2)
CALL BLKMASS (ITYPNEI,BLKMASNEI,BLKMA0,BLKMA1,BLKMA2)
TC = (2. * TCCTR * TCNEI) / (TCCTR + TCNEI)
TMPNOW(BLKCTR)=TMPNOW(BLKCTR)+((TMPNEI-TMPCTR)/(1.+(BLKMASCTR*
+ SPECTR)/(BLKMASNEI*SPENEI)))* (1.-EXP(-(TC*ZSIZE*XSIZE*
+ TIMINT/YSIZE)*(1./(BLKMASNEI*SPENEI)+1./(BLKMASCTR*
+ SPECTR))))
IF(ITYPCTR.EQ.2.OR.ITYPNEI.EQ.2) TMPNOW(BLKCTR)=TMPNOW(BLKCTR)-
+ ((0.567E-7)*ZSIZE*XSIZE*((TMPCTR+273.)**4.-
+ (TMPNEI+273.)**4.)*TIMINT)/(BLKMASCTR*SPECTR)
GOTO 4444
END IF

```

C
C

```

CONSIDERING BLOCK IN NEGATIVE Y DIRECTION
IF (L.EQ.4) THEN
IF (J.EQ.1) GOTO 4444
BLKNEI=BLKCTR-IXNUM
ITYPCTR=BLOCKID(BLKCTR)
ITYPNEI=BLOCKID(BLKNEI)
TMPCTR=TMPNAV(BLKCTR)
TMPNEI=TMPNAV(BLKNEI)
IF (ITYPCTR.EQ.2.AND.ITYPNEI.NE.2.AND.TMPCTR.LE.TMPNEI)GOTO 4444
CALL SPECHEAT (ITYPCTR,TMPCTR,SPECTR)

```

```

CALL SPECHEAT (ITYPNEI, TMPNEI, SPENEI)
CALL THERMCON (L, ITYPCTR, TMPCTR, TCCTR, COMDEN, SETTC)
CALL THERMCON (L, ITYPNEI, TMPNEI, TCNEI, COMDEN, SETTC)
CALL BLKMASS (ITYPCTR, BLKMASCTR, BLKMA0, BLKMA1, BLKMA2)
CALL BLKMASS (ITYPNEI, BLKMASNEI, BLKMA0, BLKMA1, BLKMA2)
TC = (2. * TCCTR * TCNEI) / (TCCTR + TCNEI)
TMPNOW(BLKCTR)=TMPNOW(BLKCTR)+((TMPNEI-TMPCTR)/(1.+((BLKMASCTR*
+ SPECTR)/(BLKMASNEI*SPENEI))))*(1.-EXP(-(TC*ZSIZE*XSIZE*
+ TIMINT/YSIZE)*(1./(BLKMASNEI*SPENEI)+1./(BLKMASCTR*
+ SPECTR))))
IF(ITYPCTR.EQ.2.OR.ITYPNEI.EQ.2) TMPNOW(BLKCTR)=TMPNOW(BLKCTR)-
+ ((0.567E-7)*ZSIZE*XSIZE*((TMPCTR+273.)**4.-
+ (TMPNEI+273.)**4.)*TIMINT)/(BLKMASCTR*SPECTR)
GOTO 4444
END IF

```

C
C

```

CONSIDERING BLOCK IN POSITIVE Z DIRECTION
IF (L.EQ.5) THEN
IF (K.EQ.IZNUM) GOTO 4444
BLKNEI=BLKCTR+IXNUM*IYNUM
ITYPCTR=BLOCKID(BLKCTR)
ITYPNEI=BLOCKID(BLKNEI)
TMPCTR=TMPNAV(BLKCTR)
TMPNEI=TMPNAV(BLKNEI)
IF (ITYPCTR.EQ.2.AND.ITYPNEI.NE.2.AND.TMPCTR.LE.TMPNEI)GOTO 4444
CALL SPECHEAT (ITYPCTR, TMPCTR, SPECTR)
CALL SPECHEAT (ITYPNEI, TMPNEI, SPENEI)
CALL THERMCON (L, ITYPCTR, TMPCTR, TCCTR, COMDEN, SETTC)
CALL THERMCON (L, ITYPNEI, TMPNEI, TCNEI, COMDEN, SETTC)
CALL BLKMASS (ITYPCTR, BLKMASCTR, BLKMA0, BLKMA1, BLKMA2)
CALL BLKMASS (ITYPNEI, BLKMASNEI, BLKMA0, BLKMA1, BLKMA2)
TC = (2. * TCCTR * TCNEI) / (TCCTR + TCNEI)
TMPNOW(BLKCTR)=TMPNOW(BLKCTR)+((TMPNEI-TMPCTR)/(1.+((BLKMASCTR*
+ SPECTR)/(BLKMASNEI*SPENEI))))*(1.-EXP(-(TC*XSIZE*YSIZE*
+ TIMINT/ZSIZE)*(1./(BLKMASNEI*SPENEI)+1./(BLKMASCTR*
+ SPECTR))))
IF(ITYPCTR.EQ.2.OR.ITYPNEI.EQ.2) TMPNOW(BLKCTR)=TMPNOW(BLKCTR)-
+ ((0.567E-7)*XSIZE*YSIZE*((TMPCTR+273.)**4.-
+ (TMPNEI+273.)**4.)*TIMINT)/(BLKMASCTR*SPECTR)
GOTO 4444
END IF

```

C
C

```

CONSIDERING BLOCK IN THE NEGATIVE Z DIRECTION
IF (L.EQ.6) THEN
IF (K.EQ.1) GOTO 4444
BLKNEI=BLKCTR-IXNUM*IYNUM
ITYPCTR=BLOCKID(BLKCTR)
ITYPNEI=BLOCKID(BLKNEI)
TMPCTR=TMPNAV(BLKCTR)
TMPNEI=TMPNAV(BLKNEI)
IF (ITYPCTR.EQ.2.AND.ITYPNEI.NE.2.AND.TMPCTR.LE.TMPNEI)GOTO 4444
CALL SPECHEAT (ITYPCTR, TMPCTR, SPECTR)
CALL SPECHEAT (ITYPNEI, TMPNEI, SPENEI)
CALL THERMCON (L, ITYPCTR, TMPCTR, TCCTR, COMDEN, SETTC)

```

```

CALL THERMCON (L,ITYPNEI,TMPNEI,TCNEI,CONDEN,SETTC)
CALL BLKMASS (ITYPCTR,BLKMASCTR,BLKMA0,BLKMA1,BLKMA2)
CALL BLKMASS (ITYPNEI,BLKMASNEI,BLKMA0,BLKMA1,BLKMA2)
TC = (2. * TCCTR * TCNEI) / (TCCTR + TCNEI)
TMPNOW(BLKCTR)=TMPNOW(BLKCTR)+((TMPNEI-TMPCTR)/(1.+((BLKMASCTR*
+ SPECTR)/(BLKMASNEI*SPENEI))))*(1.-EXP(-(TC*XSIZE*YSIZE*
+ TIMINT/ZSIZE)*(1./(BLKMASNEI*SPENEI)+1./(BLKMASCTR*
+ SPECTR))))
IF(ITYPCTR.EQ.2.OR.ITYPNEI.EQ.2) TMPNOW(BLKCTR)=TMPNOW(BLKCTR)-
+ ((0.567E-7)*XSIZE*YSIZE*((TMPCTR+273.)**4.-
+ (TMPNEI+273.)**4.)*TIMINT)/(BLKMASCTR*SPECTR)
GOTO 4444
END IF

C
4444 CONTINUE

C
3333 CONTINUE
2222 CONTINUE
1111 CONTINUE

C
CHECKING FOR ANY POSSIBLE TRANSITION TEMPERATURE CHANGES
C
DO 1001 I=1,IXNUM,1
DO 2001 J=1,IYNUM,1
DO 3001 K=1,IZNUM,1
BLKCTR=(K-1)*IXNUM*IYNUM+(J-1)*IXNUM+I
ITYPCTR=BLOCKID(BLKCTR)
TMPCTR=TMPNOW(BLKCTR)

C
FILAMENT - MUST NOT EXCEED TUNGSTEN MELTING POINT.
C
IF (ITYPCTR.EQ.2) THEN
IF (TMPCTR.GT.3410) THEN
IF (IMFLAG.EQ.1) THEN
IMFLAG=0
WRITE (7,*) 'FILAMENT MELTED AT: ',
+ TIMNOW
WRITE (6,*) 'FILAMENT MELTED AT: ',
+ TIMNOW
END IF
TMPNOW(FILA)=3410
END IF
GOTO 5555
END IF

C
CARBON + ALPHA TI TO CARBON + BETA TI TRANSITION
IF (ITYPCTR.EQ.1.AND.TMPCTR.GT.882.AND.TMPCTR.LE.1670.) THEN
TMPNOW(BLKCTR)=TMPNOW(BLKCTR)-72.
BLOCKID(BLKCTR)=3
GOTO 5555
END IF

C

```

```

C      CARBON + ALPHA TI TO TITANIUM CARBIDE
              IF (ITYPCTR.EQ.1.AND.TMPCTR.GT.1670.)THEN
                  TMPNOW(BLKCTR)=TMPNOW(BLKCTR)+TINC1
                  BLOCKID(BLKCTR)=4
C
C      TEST FOR DATA OUTPUT
C
              IF (I.EQ.IXTEST.AND.J.EQ.IYTEST) THEN
                  TIMBRN(K)=TIMNOW
                  PLCBRN(K)=(K-0.5)*ZSIZE
                  WRITE (6,131)
131      FORMAT(/,1X,'REACTED BLOCK ****ALPHA TO TIC*****',/)
              CALL DISPLAY(TIMNOW,IXNUM,IYNUM,IZNUM,BLOCKID,TMPNOW,IXTEST,IYTEST)
                  END IF
                      GOTO 5555
                  END IF
C
C      CARBON + BETA TI TO TITANIUM CARBIDE
              IF (ITYPCTR.EQ.3.AND.TMPCTR.GT.1670.)THEN
                  TMPNOW(BLKCTR)=TMPNOW(BLKCTR)+TINC2
                  BLOCKID(BLKCTR)=4
C
C      TEST FOR DATA OUTPUT
C
              IF (I.EQ.IXTEST.AND.J.EQ.IYTEST) THEN
                  TIMBRN(K)=TIMNOW
                  PLCBRN(K)=(K-0.5)*ZSIZE
                  WRITE (6,132)
132      FORMAT(/,1X,'REACTED BLOCK ****BETA TO TIC*****',/)
              CALL DISPLAY(TIMNOW,IXNUM,IYNUM,IZNUM,BLOCKID,TMPNOW,IXTEST,IYTEST)
                  END IF
                      GOTO 5555
                  END IF
C
5555      CONTINUE
3001      CONTINUE
2001      CONTINUE
1001      CONTINUE
C
C      TRANSFER TEMPERARY TEMPERATURES TO PERMANENT STORAGE
C
DO 7777 I=1,ITOTNUM,1
    TMPNAV(I)=TMPNOW(I)
7777      CONTINUE
C
CHECK FOR PERIODIC DISPLAY OF ARRAY TEMPERATURES
IDUMP=(ITER*100)/(1./TIMINT)
IDUMP=IDUMP*(1./TIMINT)/100
IF (IDUMP.EQ.ITER) CALL DISPLAY(TIMNOW,IXNUM,IYNUM,IZNUM,BLOCKID,
+
    TMPNOW,IXTEST,IYTEST)
C
C      TEST FOR COMPLETION OF SHS REACTION
C

```

```

IF (BLOCKID(IEND).EQ.4) THEN
    WRITE (7,*) 'REACTION COMPLETED'
C
    OPEN (8,FILE=FILE4,FORM='UNFORMATTED',STATUS='NEW')
    DO 975 I=1,ITOINUM,1
        WRITE (8) TMPNOW(I),BLOCKID(I)
975    CONTINUE
        WRITE (8) ITER
        WRITE (8) IPFLAG,IMFLAG
        CLOSE (8,STATUS='KEEP')
C
        GOTO 9999
    END IF
C
    GOTO 1000
C
    END OF ITERATION SEQUENCE
C
9999 CONTINUE
C
    WRITING REACTION POSITION INFO TO FILE
    DO 717 K=1,IZNUM,1
        WRITE (7,*) TIMBRN(K),PLCBRN(K)
717    CONTINUE
        CLOSE(7,STATUS='KEEP')
    STOP
    END
C
C
C
C
*****
C
    SUBROUTINE TO DETERMINE THE SPECIFIC HEAT OF A BLOCK
    SUBROUTINE SPECHEAT (ITYP,TMP,SPE)
C
C
C
    CARBON + ALPHA TITANIUM
    IF (ITYP.EQ.1) THEN
        CC = 1430. + 0.356 * (TMP + 273.) - 7.33E7 /
+          (TMP + 273.)**2.
        CTI = 458 + 0.22 * (TMP + 273.)
        SPE = (CC + 4.*CTI) / 5.
        GOTO 99
    END IF
C
C
    FILAMENT
    IF (ITYP.EQ.2) THEN
        SPE = 134.+0.0194*(TMP-25.)
        IF(SPE.GT.167) SPE=167
        GOTO 99
    END IF
C
C
    CARBON + BETA TITANIUM
    IF (ITYP.EQ.3) THEN
        CC = 1430. + 0.356 * (TMP + 273.) - 7.33E7 /

```

```

+           (TMP + 273.)**2.
      CTI = 654
      SPE = (CC + 4. * CTI) / 5.
      GOTO 99
      END IF

C
C   TITANIUM CARBIDE
      IF (ITYP.EQ.4) THEN
+           SPE = 825. + 0.056 * (TMP + 273.) - 2.5E7 /
           (TMP + 273.)**2.
      GOTO 99
      END IF

C
99  CONTINUE
      RETURN
      END

C
C *****
C
C   SUBROUTINE TO DETERMINE THE THERMAL CONDUCTIVITY OF A BLOCK
      SUBROUTINE THERMCON (L,ITYP,TMP,TC,COMDEN,SETTC)

C
C
C   GREEN COMPACT
      IF (ITYP.EQ.1.OR.ITYP.EQ.3) THEN
          TC=SETTC
          GOTO 98
          END IF

C
C   FILAMENT
      IF(ITYP.EQ.2) THEN
          TC=100
          GOTO 98
          END IF

C
C   TITANIUM CARBIDE
      IF (ITYP.EQ.4) THEN
          TC=100
          GOTO 98
          END IF

C
98  CONTINUE
      RETURN
      END

C
C *****
C
C   SUBROUTINE TO DETERMINE BLOCK MASSES
      SUBROUTINE BLKMASS (ITYPCTR,BLKMAS,BLKMA0,BLKMA1,BLKMA2)

C
      IF (ITYPCTR.EQ.1.OR.ITYPCTR.EQ.3.OR.ITYPCTR.EQ.4) BLKMAS = BLKMA1
      IF (ITYPCTR.EQ.2) BLKMAS = BLKMA2

C

```

```

RETURN
END
C
C *****
C
C   SUBROUTINE TO DISPAY ARRAY ID AND TEMPERATURE
C   SUBROUTINE DISPLAY (TIMNOW,IXNUM,IYNUM,IZNUM,BLOCKID,TMPNOW,IXTEST,
+       IYTEST)
C
C   DIMENSION BLOCKID(10000),TMPNOW(10000),H(100),IT(100)
C   INTEGER BLOCKID,H
C
C       WRITE (6,'(/,1X,''TIMNOW = ',F9.6)')TIMNOW
C       IF(IZNUM.GT.15) GOTO 545
C       DO 505 JJ=1,IYNUM,1
C           DO 606 KK=1,IZNUM,1
C               IDISP=(KK-1)*IXNUM*IYNUM+(JJ-1)*IXNUM+
+                   IXTEST
C               H(KK)=BLOCKID(IDISP)
C               IT(KK)=TMPNOW(IDISP)/100.
606          CONTINUE
C               WRITE (6,3) (H(KK),KK=1,IZNUM),(IT(KK),KK=1,IZNUM)
3              FORMAT(1X,<IZNUM>I2,2X,<IZNUM>(I2,1X))
505          CONTINUE
C
C       GOTO 599
545      CONTINUE
C       IF (IZNUM.GT.25) GOTO 565
C       DO 525 JJ=1,IYNUM,1
C           DO 626 KK=1,IZNUM,1
C               IDISP=(KK-1)*IXNUM*IYNUM+(JJ-1)*IXNUM+IXTEST
C               H(KK)= BLOCKID(IDISP)
626          CONTINUE
C               WRITE (6,4) (H(KK),KK=1,IZNUM)
4              FORMAT (1X,<IZNUM>I2)
525          CONTINUE
C       WRITE (6,'(/)')
C
C       DO 515 JJ=1,IYNUM,1
C           DO 616 KK=1,IZNUM,1
C               IDISP=(KK-1)*IXNUM*IYNUM+(JJ-1)*IXNUM+IXTEST
C               IT(KK)=TMPNOW(IDISP)/100.
616          CONTINUE
C               WRITE (6,5) (IT(KK),KK=1,IZNUM)
5              FORMAT (1X,<IZNUM>(I2,1X))
515          CONTINUE
C       GOTO 599
C
C       CONTINUE
565      DO 636 KK=1,IYTEST,1
C           IDISP=(KK-1)*IXNUM*IYNUM+(IYTEST-1)*IXNUM+IXTEST
C           IT(KK)=TMPNOW(IDISP)/100.
636          CONTINUE
C
C

```

```
WRITE (6,6) (IT(KK),KK=1,IYTEST)
C
599 FORMAT (1X,<IYTEST>(I2,1X))
C
CONTINUE
RETURN
END
```

APPENDIX B

Electronic Component Values

Component values for schematic diagram illustrated in Fig. 14. Resistance values are given in ohms and capacitance values are given in microfarads.

A1:	LM310	A2:	LM310	A3:	LM307
A4:	LM725	A5:	LM741	A6:	LF351
A7:	LF351	R1:	2.2k	R2:	3.3M
R3:	2.2k	R4:	3.3M	R5:	1K
R6:	1k	R7:	100k	R8:	97.6k
R9:	1k	R10:	100k	R11:	100k
R12:	100k	R13:	100k	R14:	51k
R15:	220	R16:	20k	R17:	20k
R18:	20k	R19:	51	R20:	10k
R21:	10k	R22:	10k	R23:	10k
R24:	10k	R25:	10k	P1:	1k
P2:	5k	P3:	100k	P4:	100k
C1:	0.01	C2:	0.01	C3:	0.001
C4:	0.047	D1:	1N4001	D2:	1N4001
T1:	thermocouple				

Component values for schematic illustrated in Fig. 15. Resistance values are given in ohms.

A1:	LF351	A2:	LF351	A3:	LF351
R1:	2.2k	R2:	3.3M	R3:	2.2k
R4:	3.3M	R5:	1k	R6:	1k
R7:	100k	R8:	97.6k	P1:	10k
P2:	5k	T1:	thermocouple		

APPENDIX C

Thermal Conductivity Apparatus Calibration Program

The following program was used to calibrate the thermocouple systems of the thermal conductivity apparatus by correlating the analog to digital conversion values from the thermocouples with temperature reference points read from the digital thermometer and entered manually from the keyboard. These data were then fit to a second order polynomial where the dependent variable, the temperature, was expressed as a power series of the independent variable, the conversion values.

The architecture of this software is a foreground BASIC program from which background machine language routines are accessed as required. Functions which do not require high speed such as screen updating, reference temperature input, mathematical calculations, maintaining heat stage temperature and outputting final results are handled conveniently in the BASIC format. The machine language routines were used for monitoring the keyboard for which high speed was an advantage.

Variable List:

- ST(i,j): heat stage temperature where i is the counter which correlates to the digital thermometer input and j is a counter which is used for data averaging. For each temperature, or value of i, fifteen analog to digital conversion are taken and later averaged.
- PT(i,j): sample temperature where counters have the same meaning as for ST(i,j).
- RS(i): actual heat stage temperature as read from the digital thermometer and entered on the keyboard.
- RP(i): actual sample temperature as read from the digital thermometer and entered on the keyboard.
- SA(i): average of the fifteen analog to digital conversions of the heat stage thermocouple signal taken at each temperature.
- PA(i): average of the fifteen analog to digital conversions of the sample thermocouple signal taken at each temperature.
- SS(i): heat stage temperature statistical error.
- PS(i): sample stage temperature statistical error.
- SU(i): heat stage temperature total error.
- FU(i): sample stage temperature total error.
- DS: total number of heat stage temperature data points to be used in the least squares fit.
- DP: total number of sample stage temperature data points to be used in the least squares fit.
- XP: x axis screen counter used for plotting conversion values during calibration data entry.
- SP: internal computer set point against which heat stage analog to digital conversion values are compared for heat stage temperature regulation.

Program Outline:

9000: LOMEM set to 16384 (\$4000) to allow the primary high resolution graphics page, with memory mapping from \$2000 to \$4000, to be used without interference.

9500 to 10150: various screen preparations and variable dimensioning and initialization.

10200: BASE set to 49344 (\$C0C0) which is Device Select base address for peripheral slot 4.

15000 to 15025: USR() jump vector \$4000 POKEd to \$A through \$C.

15030 to 15235: machine language keystroke monitor routine POKEd into memory beginning at address \$4000.

20000: jump to machine code routine which returns with any keystroke value in location \$5000 (20480).

20100 to 20700: screen output and decision sequence on keystroke monitor.

30000 to 32000: BASIC subroutine entered after data acquisition is complete which calculates average temperature and conversion values, determines statistical uncertainties and summed matrix elements necessary for quadratic least squares fit, calculates and outputs quadratic equation coefficients and finally plots data points along with the fitting equation.

40000 to 42000: BASIC foreground subroutine which averages ten analog to digital conversions from the heat stage thermocouple, compares this value to a set point value previously entered into the computer via the keyboard and toggles the heat stage heater on or off depending on the magnitude of the conversion value average compared to the set point value. In addition, an average conversion value is determined for the sample thermocouple and both thermocouple conversion values are plotted on the high resolution graphics screen.

50000 to 50600: a short BASIC subroutine which allows the heat stage internal computer set point value to be changed. This set points determines the steady stage temperature of the heat stage.

60000 to 60900: a BASIC subroutine which is accessed when data acquisition is requested via the keystroke monitor. This subroutine accepts input of the present digital thermometer reading from the keyboard and then inputs fifteen analog to digital conversion values from both the heat stage and sample thermocouple systems.

Program Listing:

```
9000 LOMEM: 16384
9500 HOME
9550 PRINT ""
9560 FOR I = 1 TO 24
9570 PRINT
9580 NEXT I
10000 DIM ST(20,15),PT(20,15),RS(20),RP(20)
10010 DIM SA(20),PA(20),SS(20),PS(20)
10020 DIM SU(20),PU(20)
10100 HGR
10105 HCOLOR= 3
10110 HPLOT 0,0 TO 279,0 TO 279,159 TO 0,159 TO 0,0
10120 SP = 1
10130 XP = 1
10140 DP = 0
```

```

10150 DS = 0
10200 BASE = 49344
15000 POKE 10,76
15005 REM POKE $000A,$4C (JSR)
15010 POKE 11,0
15015 REM POKE $000B,$00 ($00)
15020 POKE 12,64
15025 REM POKE $000B,$40 ($40)
15030 POKE 16384,173
15035 REM POKE $4000,$AD (LDA)
15040 POKE 16385,0
15045 REM POKE $4001,$00 ($00)
15050 POKE 16386,192
15055 REM POKE $4002,$C0 ($C0)
15060 POKE 16387,48
15065 REM POKE $4003,$30 (BMI)
15070 POKE 16388,6
15075 REM POKE $4004,$06 ($06)
15080 POKE 16389,169
15085 REM POKE $4005,$A9 (LDA)
15090 POKE 16390,0
15095 REM POKE $4006,$00 ($00)
15100 POKE 16391,141
15105 REM POKE $4007,$8D (STA)
15110 POKE 16392,0
15115 REM POKE $4008,$00 ($00)
15120 POKE 16393,80
15125 REM POKE $4009,$50 ($50)
15130 POKE 16394,96
15135 REM POKE $400A,$60 (RTS)
15140 POKE 16395,173
15145 REM POKE $400B,$AD (LDA)
15150 POKE 16396,0
15155 REM POKE $400C,$00 ($00)
15160 POKE 16397,192
15165 REM POKE $400D,$C0 ($C0)
15170 POKE 16398,141
15175 REM POKE $400E,$8D (STA)
15180 POKE 16399,16
15185 REM POKE $400F,$10 ($10)
15190 POKE 16400,192
15195 REM POKE $4010,$C0 ($C0)
15200 POKE 16401,141
15205 REM POKE $4011,$8D (STA)
15210 POKE 16402,0
15215 REM POKE $4012,$00 ($00)
15220 POKE 16403,80
15225 REM POKE $4013,$50 ($50)
15230 POKE 16404,96
15235 REM POKE $4014,$60 (RTS)
20000 Z = USR (0)
20100 KEY = PEEK (20480)
20200 PRINT "TYPE A TO ENTER NEW TEMP. SETPOINT"
20210 PRINT "TYPE D TO ENTER TEMP DATA POINT ";DS;" ";DP

```

```

20220 PRINT "TYPE C TO TERMINATE DATA ENTRY"
20250 FOR T = 1 TO 500: NEXT T
20300 IF KEY = 0 THEN GOTO 40000
20400 IF KEY = 193 THEN GOTO 50000
20500 IF KEY = 196 THEN GOTO 60000
20600 IF KEY = 195 THEN GOTO 30000
20700 GOTO 20000
30000 PRINT : PRINT : PRINT : PRINT ""
30005 PRINT "ENTER UNCERTAINTY IN DIGITAL"
30010 INPUT "THERMOMETER READINGS: ";EU
30011 PRINT : PRINT : PRINT
30012 PRINT "ONE MOMENT PLEASE...": PRINT
30020 FOR I = 1 TO DP
30025 PA(I) = 0
30030 FOR J = 1 TO 15
30050 PA(I) = PA(I) + PT(I,J)
30060 NEXT J
30066 PA(I) = PA(I) / 15
30070 NEXT I
30071 FOR I = 1 TO DS
30072 SA(I) = 0
30073 FOR J = 1 TO 15
30074 SA(I) = SA(I) + ST(I,J)
30075 NEXT J
30076 SA(I) = SA(I) / 15
30077 NEXT I
30100 FOR I = 1 TO DP
30110 PS(I) = 0
30120 FOR J = 1 TO 15
30140 PS(I) = PS(I) + (PT(I,J) - PA(I)) ^ 2
30150 NEXT J
30170 PS(I) = SQR (PS(I) / 15)
30180 NEXT I
30181 FOR I = 1 TO DS
30182 SS(I) = 0
30183 FOR J = 1 TO 15
30184 SS(I) = SS(I) + (ST(I,J) - SA(I)) ^ 2
30185 NEXT J
30186 SS(I) = SQR (SS(I) / 15)
30187 NEXT I
30200 FOR I = 1 TO DP
30220 PU(I) = SQR (EU ^ 2 + PS(I) ^ 2)
30230 NEXT I
30240 FOR I = 1 TO DS
30250 SU(I) = SQR (EU ^ 2 + SS(I) ^ 2)
30260 NEXT I
30300 A0 = 0:A1 = 0:B0 = 0:B1 = 0
30310 C0 = 0:C1 = 0:D0 = 0:D1 = 0
30320 E0 = 0:E1 = 0:F0 = 0:F1 = 0
30330 G0 = 0:G1 = 0:H0 = 0:H1 = 0
30350 FOR I = 1 TO DP
30360 A1 = A1 + 1 / PU(I) ^ 2
30370 B1 = B1 + PA(I) / PU(I) ^ 2
30380 C1 = C1 + RP(I) / PU(I) ^ 2

```

```

30390 D1 = D1 + PA(I) * RP(I) / PU(I) ^ 2
30400 E1 = E1 + PA(I) ^ 2 / PU(I) ^ 2
30410 F1 = F1 + PA(I) ^ 2 * RP(I) / PU(I) ^ 2
30420 G1 = G1 + PA(I) ^ 3 / PU(I) ^ 2
30430 H1 = H1 + PA(I) ^ 4 / PU(I) ^ 2
30440 NEXT I
30445 FOR I = 1 TO DS
30450 A0 = A0 + 1 / SU(I) ^ 2
30452 B0 = B0 + SA(I) / SU(I) ^ 2
30454 C0 = C0 + RS(I) / SU(I) ^ 2
30456 D0 = D0 + SA(I) * RS(I) / SU(I) ^ 2
30458 E0 = E0 + SA(I) ^ 2 / SU(I) ^ 2
30460 F0 = F0 + SA(I) ^ 2 * RS(I) / SU(I) ^ 2
30462 G0 = G0 + SA(I) ^ 3 / SU(I) ^ 2
30464 H0 = H0 + SA(I) ^ 4 / SU(I) ^ 2
30470 NEXT I
30500 Z0 = A0 * (E0 * H0 - G0 ^ 2) - B0 * (B0 * H0 - G0 * E0)
      + E0 * (B0 * G0 - E0 ^ 2)
30510 Z1 = A1 * (E1 * H1 - G1 ^ 2) - B1 * (B1 * H1 - G1 * E1)
      + E1 * (B1 * G1 - E1 ^ 2)
30520 AS = (C0 * (E0 * H0 - G0 ^ 2) - D0 * (B0 * H0 - G0 * E0)
      + F0 * (B0 * G0 - E0 ^ 2)) / Z0
30530 AP = (C1 * (E1 * H1 - G1 ^ 2) - D1 * (B1 * H1 - G1 * E1)
      + F1 * (B1 * G1 - E1 ^ 2)) / Z1
30540 BS = (A0 * (D0 * H0 - F0 * G0) - B0 * (C0 * H0 - F0 * E0)
      + E0 * (C0 * G0 - D0 * E0)) / Z0
30550 BP = (A1 * (D1 * H1 - F1 * G1) - B1 * (C1 * H1 - F1 * E1)
      + E1 * (C1 * G1 - D1 * E1)) / Z1
30560 CS = (A0 * (E0 * F0 - G0 * D0) - B0 * (B0 * F0 - G0 * C0)
      + E0 * (B0 * D0 - E0 * C0)) / Z0
30570 CP = (A1 * (E1 * F1 - G1 * D1) - B1 * (B1 * F1 - G1 * C1)
      + E1 * (B1 * D1 - E1 * C1)) / Z1
30600 PRINT ""
31000 PRINT : PRINT : PRINT
31100 PRINT "FOR THE STAGE: A = ";AS
31110 PRINT "          B = ";BS
31120 PRINT "          C = ";CS
31130 INPUT "ENTER ANY LETTER TO CONTINUE...      ";A$
31140 PRINT "FOR THE PELLET: A = ";AP
31150 PRINT "          B = ";BP
31160 PRINT "          C = ";CP
31170 INPUT "ENTER ANY LETTER TO CONTINUE...      ";A$
31200 PRINT : PRINT : PRINT
31210 PRINT "PLOT OF STAGE CALIBRATION."
31220 HGR
31230 H$PLOT 0,0 TO 279,0 TO 279,159 TO 0,159 TO 0,0
31235 YBIG = 0:XBIG = 0
31240 FOR I = 1 TO DS
31250 IF RS(I) > YBIG THEN YBIG = RS(I)
31260 IF SA(I) > XBIG THEN XBIG = SA(I)
31270 NEXT I
31280 YLIT = 100:XLIT = 100
31290 FOR I = 1 TO DS
31300 IF RS(I) < YLIT THEN YLIT = RS(I)

```

```

31310 IF SA(I) < XLIT THEN XLIT = SA(I)
31320 NEXT I
31350 FOR I = 1 TO DS
31360 X = (SA(I) - XLIT) * 277 / (XBIG - XLIT) + 1
31370 Y = 158 - ((RS(I) - YLIT) * 157 / (YBIG - YLIT))
31380 HPLOT X + 1,Y - 1
31385 HPLOT X,Y - 1
31390 HPLOT X + 1,Y + 1
31395 HPLOT X,Y + 1
31400 HPLOT X - 1,Y + 1
31405 HPLOT X - 1,Y
31410 HPLOT X - 1,Y - 1
31415 HPLOT X + 1,Y
31420 HPLOT X,Y
31430 NEXT I
31450 HCOLOR= 3
31500 FOR I = 1 TO 278
31510 X = XLIT + ((I - 1) / 277) * (XBIG - XLIT)
31520 Y = AS + BS * X + CS * X ^ 2
31525 Y = 158 - 157 * (Y - YLIT) / (YBIG - YLIT)
31527 IF Y < 0 THEN Y = 0
31529 IF Y > 159 THEN Y = 159
31530 HPLOT I,Y
31540 NEXT I
31550 PRINT : PRINT
31560 INPUT "ENTER ANY LETTER TO CONTINUE... ";AS
31600 PRINT : PRINT
31610 PRINT "PLOT OF SAMPLE TC CALIBRATION."
31620 HGR
31630 HPLOT 0,0 TO 279,0 TO 279,159 TO 0,159 TO 0,0
31640 YBIG = 0:XBIG = 0
31650 FOR I = 1 TO DP
31660 IF RP(I) > YBIG THEN YBIG = RP(I)
31670 IF PA(I) > XBIG THEN XBIG = PA(I)
31680 NEXT I
31700 YLIT = 255:XLIT = 255
31710 FOR I = 1 TO DP
31720 IF RP(I) < YLIT THEN YLIT = RP(I)
31730 IF PA(I) < XLIT THEN XLIT = PA(I)
31740 NEXT I
31745 HCOLOR= 3
31750 FOR I = 1 TO DP
31760 X = (PA(I) - XLIT) * 277 / (XBIG - XLIT) + 1
31770 Y = 158 - ((RP(I) - YLIT) * 157 / (YBIG - YLIT))
31780 HPLOT X + 1,Y - 1
31790 HPLOT X,Y - 1
31800 HPLOT X + 1,Y + 1
31810 HPLOT X,Y + 1
31820 HPLOT X - 1,Y + 1
31830 HPLOT X - 1,Y
31840 HPLOT X - 1,Y - 1
31850 HPLOT X + 1,Y
31860 HPLOT X,Y
31870 NEXT I

```

```

31880 HCOLOR= 3
31900 FOR I = 1 TO 278
31910 X = XLIT + ((I - 1) / 277) * (XBIG - XLIT)
31920 Y = AP + BP * X + CP * X ^ 2
31930 Y = 158 - 157 * (Y - YLIT) / (YBIG - YLIT)
31940 IF Y < 0 THEN Y = 0
31950 IF Y > 159 THEN Y = 159
31960 HPLOT I,Y
31970 NEXT I
32000 END
40000 POKE BASE + 4,0
40100 A = 0
40200 FOR I = 1 TO 10
40300 B = PEEK (BASE + 1)
40400 A = A + PEEK (BASE + 3)
40500 NEXT I
40600 A = A / 10
40700 IF A > SP THEN B = PEEK (BASE + 5)
40800 IF A < = SP THEN POKE BASE + 5,0
40900 POKE BASE + 4,1
41000 C = 0
41100 FOR I = 1 TO 10
41200 B = PEEK (BASE + 1)
41300 C = C + PEEK (BASE + 3)
41400 NEXT I
41500 C = C / 10
41510 IF XP < > 279 THEN GOTO 41600
41520 HGR
41530 HPLOT 0,0 TO 279,0 TO 279,159 TO 0,159 TO 0,0
41535 HPLOT 1,158 - 157 * (SP / 255) TO 278,158 - 157 * (SP /
255)
41540 XP = 1
41600 HPLOT XP,158 - 157 * (A / 255)
41700 HPLOT XP,158 - 157 * (C / 255)
41800 XP = XP + 1
41900 FOR T = 1 TO 1000: NEXT T
42000 GOTO 20000
50000 HCOLOR= 0
50100 HPLOT 1,158 - 157 * (SP / 255) TO 278,158 - 157 * (SP /
255)
50200 HCOLOR= 3
50300 PRINT : PRINT : PRINT : PRINT ""
50350 PRINT "PRESENT SET POINT: ";SP: PRINT
50400 INPUT "ENTER NEW TEMP. SETPOINT: ";SP
50500 HPLOT 1,158 - 157 * (SP / 255) TO 278,158 - 157 * (SP /
255)
50600 GOTO 20000
60000 PRINT : PRINT : PRINT : PRINT : PRINT ""
60002 INPUT "TEMP FOR STAGE OR PELLET? (S OR P) ";K$
60003 IF K$ = "P" THEN GOTO 60450
60004 IF K$ = "S" THEN GOTO 60008
60006 GOTO 60000
60008 PRINT : PRINT : PRINT
60010 PRINT "ENTER DIGITAL THERMOMETER READING:"

```

```
60012 PRINT
60015 INPUT "INPUT 999 TO ABORT. ";RS(DS + 1)
60020 IF RS(DS + 1) = 999 THEN GOTO 20000
60090 DS = DS + 1
60100 FOR I = 1 TO 15
60200 POKE BASE + 4,0
60300 B = PEEK (BASE + 1)
60400 ST(DS,I) = PEEK (BASE + 3)
60410 NEXT I
60420 GOTO 20000
60450 PRINT : PRINT : PRINT
60455 PRINT "ENTER DIGITAL THERMOMETER READING:"
60460 PRINT
60465 INPUT "INPUT 999 TO ABORT. ";RP(DP + 1)
60470 IF RP(DP + 1) = 999 THEN GOTO 20000
60475 DP = DP + 1
60480 FOR I = 1 TO 15
60500 POKE BASE + 4,1
60600 B = PEEK (BASE + 1)
60700 PT(DP,I) = PEEK (BASE + 3)
60800 NEXT I
60900 GOTO 20000
```

APPENDIX D

Thermal Conductivity Data Acquisition Program

The following program was used to gather thermal conductivity data. As with the previous calibration program, the architecture of this program is a foreground BASIC program with background interrupt driven high speed machine language routines. The foreground BASIC program was used to monitor keystrokes, update graphic and text displays, perform mathematical calculations and dump acquired data to floppy disks for long term storage. When signaled by an interrupt on the 6502 microprocessor NMI line, 255 data values were read from both the sample and heat stage thermocouples. These values were then stored in specific address locations to be PEEKed by the BASIC program once control returned to the foreground level.

Memory Allocation:

- \$4000 to \$408D: machine code program which reads 255 data values for both thermocouples, adds these values and stores the sums in memory locations \$4311 and \$4321.
- \$4100 to \$41FF: storage location for 255 data values read from sample thermocouple system.
- \$4200 to \$42FF: storage location for 255 data values read from heat stage thermocouple system.
- \$4300: data acquisition flag.
- \$4310 to \$4311: summing locations for sample thermocouple data.
- \$4320 to \$4321: summing locations for heat stage thermocouple data.
- \$4400 to \$4413: keystroke monitor machine language program.
- \$4500: keystroke value memory location.

Program Outline:

- 9000: LOMEM set to 20480 (\$5000) to keep primary high resolution memory area clear and to allocate space for machine language routines.
- 9500 to 10130: high resolution screen accessed, variables DIMensioned and initialized.
- 10200: BASE set to 49344 (\$C0C0) with is the Device Select base address for peripheral slot 4.
- 11000: reset data acquisition flag.
- 15000: DATA statement for NMI jump vector definition.
- 15100 to 15200: Data statements for interrupt driven machine language data acquisition routine.
- 15400: DATA statement for USR() jump vector definition.
- 15500: DATA statement for machine language keystroke monitor routine.
- 16000 to 17500: POKEing loops for the about DATA statements.
- 19000 to 20604: quadratic equation thermocouple calibration coefficients, heat stage setpoint temperature and time between data acquisitions entered from the keyboard.
- 20610 to 20620: horizontal line corresponding to the set point temperature is plotted on screen.

20700: series reversion³⁹ performed to determine analog to digital conversion setpoint corresponding to entered temperature setpoint.
 39900 to 40850: heat stage analog to digital conversion read in and converted to a temperature value. Current to tungsten heating filament in heat stage turned on or off depending on the relative magnitude of the conversion value to the setpoint value.
 40900 to 41600: sample stage analog to digital conversion read in and converted to a temperature value.
 41700 to 41900: converted temperature values printed out to text screen.
 42000 to 42100: data acquisition flag address (\$4300) surveyed for recent data acquisition. If new data is available for processing a jump is made to line 50000.
 43000 to 45000: machine language keystroke monitor is accessed using a USR() call and the keystroke storage location \$4500 is checked. If the "S" key has been pressed, data acquisition stops and the program jumps to 5500.
 50000 to 52000: portion of the BASIC foreground program which accesses data obtained by the machine language data acquisition routine. Data counter is incremented by one, data flag is reset, time of latest data point is calculated, data is PEEKed in from memory locations, converted from hexadecimal to decimal, averaged, converted to a temperature value and plotted to the high resolution screen.
 55000 to 63010: portion of the BASIC foreground program which is entered after data acquisition is complete. If the data is to be stored on disk, the storage filename is entered from the keyboard. The data is stored on the disk, read back off the disk and then checked for self-consistency. If all the data storage is in order, the data is listed to the screen and to program exited.

Program Listing:

```

9000 LOMEM: 20480
9500 HOME
9510 VTAB 10
9520 PRINT " THERMAL CONDUCTIVITY DATA ACQUISITION"
9530 PRINT ""
9540 FOR T = 1 TO 1000: NEXT T
9550 PRINT ""
9560 FOR I = 1 TO 24
9570 PRINT
9580 NEXT I
10000 DIM S(255),P(255),SH(255)
10050 DIM TP(255),TS(255)
10075 DIM T(255),TT(255)
10100 HGR
10105 HCOLOR= 3
10110 HPLOT 0,0 TO 279,0 TO 279,159 TO 0,159 TO 0,0
10130 XP = 0
10200 BASE = 49344
11000 POKE 17152,0
15000 DATA 76,0,64
15100 DATA 32,74,255,169,1,141,196,192
15110 DATA 162,255,160,10,136,208,253,173
15120 DATA 193,192,173,194,192,201,128,48
15130 DATA 249,173,195,192,157,0,65,202

```

```

15140 DATA 208,232,160,255,136,208,253,169
15150 DATA 0,141,196,192,162,255,160,10
15160 DATA 136,208,253,173,193,192,173,194
15170 DATA 192,201,128,48,249,173,195,192
15180 DATA 157,0,66,202,208,232
15181 DATA 169,0,141,17,67,141,16,67
15182 DATA 141,33,67,141,32,67,162,255
15183 DATA 24,173,16,67,125,0,65,141
15184 DATA 16,67,173,17,67,105,0,141
15185 DATA 17,67,202,208,235,162,255,24
15186 DATA 173,32,67,125,0,66,141,32
15187 DATA 67,173,33,67,105,0,141,33
15188 DATA 67,202,208,235
15189 DATA 32,221
15190 DATA 251,169,255,141,0,67,32,63
15200 DATA 255,64
15400 DATA 76,0,68
15500 DATA 173,0,192,48,6,169,0,141,0,69,96,173,0,192,141,1
      6,192,141,0,69,96
16000 FOR I = 1 TO 3
16100 READ A
16200 POKE 1018 + I,A
16300 NEXT I
16400 FOR I = 1 TO 142
16500 READ A
16600 POKE 16383 + I,A
16700 NEXT I
16800 FOR I = 1 TO 3
16900 READ A
17000 POKE 9 + I,A
17100 NEXT I
17200 FOR I = 1 TO 21
17300 READ A
17400 POKE 17407 + I,A
17500 NEXT I
19000 PRINT : PRINT : PRINT :
20000 PRINT "ENTER THERMOCOUPLE CALIBRATION"
20100 INPUT "COEFFICIENTS FOR HEAT STAGE: ";S1,S2,S3
20200 PRINT : PRINT : PRINT
20300 PRINT "ENTER THERMOCOUPLE CALIBRATION"
20400 INPUT "COEFFICIENTS FOR PELLET: ";P1,P2,P3
20450 PRINT : PRINT : PRINT
20500 PRINT "ENTER HEAT STAGE SET POINT"
20600 INPUT "IN DEGREES CELSIUS: ";SS
20601 PRINT : PRINT
20602 PRINT "ENTER TIME BETWEEN DATA"
20604 INPUT "POINTS IN SECONDS: ";TIME
20610 Z = 158 - (157 * SS / (1.2 * SS))
20620 H PLOT 1,Z TO 279,Z
20700 SD = (1 / S2) * (SS - S1) - (S3 / (S2 ^ 3)) * ((SS - S1) ^ 2)
39900 REM SET ADC CHANNEL 0
40000 POKE BASE + 4,0
40300 B = PEEK (BASE + 1)
40400 A = PEEK (BASE + 3)

```

```

40500 FV = S1 + S2 * A + S3 * A * A
40700 IF FV > SS THEN B = PEEK (BASE + 5)
40800 IF FV < = SS THEN POKE BASE + 5,0
40850 A = FV
40900 POKE BASE + 4,1
41200 B = PEEK (BASE + 1)
41300 C = PEEK (BASE + 3)
41600 C = P1 + P2 * C + P3 * C ^ 2
41700 PRINT : PRINT
41800 PRINT "HEAT STAGE TEMP: ";A
41850 PRINT "
S TO STOP"
41900 PRINT "PELLET TEMP: ";C
42000 A = PEEK (17152)
42100 IF A = 255 THEN GOTO 50000
43000 Z = USR (0)
43100 A = PEEK (17664)
43200 IF A = 211 THEN GOTO 55000
45000 GOTO 40000
50000 XP = XP + 1
50100 POKE 17152,0
50150 T(XP) = TIME * XP
50200 A = (256 * PEEK (17169) + PEEK (17168)) / 255
50700 P(XP) = P1 + P2 * A + P3 * A ^ 2
50800 A = (256 * PEEK (17185) + PEEK (17184)) / 255
51300 S(XP) = S1 + S2 * A + S3 * A ^ 2
51350 AA = 158 - 157 * P(XP) / (1.2 * SS)
51420 HPLOT XP,AA
51500 BB = 158 - 157 * S(XP) / (1.2 * SS)
51520 HPLOT XP,BB
52000 GOTO 40000
55000 PRINT : PRINT : PRINT
55050 INPUT "SAVE THESE DATA IN A FILE? (Y OR N)";A$
55100 IF A$ = "N" THEN GOTO 63000
55200 PRINT : PRINT : PRINT
55300 INPUT "ENTER NAME OF FILE: ";F$
55400 D$ = CHR$ (4)
55450 PRINT D$;"OPEN";F$
55475 PRINT D$;"DELETE";F$
55500 PRINT D$;"OPEN";F$
55600 PRINT D$;"WRITE";F$
55700 PRINT XP
55800 FOR I = 1 TO XP
55900 PRINT P(I)
55950 PRINT S(I)
55960 PRINT T(I)
56000 NEXT I
56100 PRINT D$;"CLOSE";F$
56200 PRINT D$;"OPEN";F$
56300 PRINT D$;"READ";F$
56400 INPUT XT
56500 FOR I = 1 TO XT
56600 INPUT TP(I)
56650 INPUT TS(I)
56660 INPUT TT(I)

```

```

56700 NEXT I
56800 PRINT D$;"CLOSE";F$
56810 TEXT
56850 PRINT : PRINT "XP: ";XP;" XT: ";XT
56900 IF XP - XT > 0.01 THEN GOTO 60000
57000 FOR I = 1 TO XP
57010 PRINT
57050 PRINT "I: ";I;" S: ";S(I);" TS: ";TS(I)
57100 IF S(I) - TS(I) > 0.01 THEN GOTO 60000
57150 PRINT "I: ";I;" P: ";P(I);" TP: ";TP(I)
57200 IF P(I) - TP(I) > 0.01 THEN GOTO 60000
57220 PRINT "I: ";I;" T: ";T(I);" TT: ";TT(I)
57240 IF T(I) - TT(I) > 0.01 THEN GOTO 60000
57300 NEXT I
58000 PRINT : PRINT : PRINT
58050 PRINT " DATA STORAGE COMPLETE"
58100 GOTO 63000
60000 PRINT : PRINT : PRINT : PRINT ""
61000 PRINT " ERROR IN DATA STORAGE"
63000 A = PEEK (BASE + 5)
63010 END

```

APPENDIX E

Thermal Conductivity Data Analysis Program

The following program was used to analyze the thermal conductivity temperature-time data by fitting these data to the series expression of Eq. 23. A successive approximation formalism was used in which the thermal conductivity was varied as the single least squares fitting parameter. By repeatedly reversing the sense and decreasing the magnitude of the thermal conduction variations, the fitting uncertainties of the thermal conductivity were reduced to a magnitude that was small compared to statistical uncertainties. The program is written entirely in BASIC.

Variable List:

P(i): recorded sample temperature for the ith acquisition interval.
S(i): recorded heat stage temperature for the ith acquisition interval.
T(i): time associated with the ith acquisition interval.
F(i): value of temperature-time fitting equation at a time corresponding to the time of the ith acquisition interval.
SK(i): value of the ith series element.
R2(i): sum of the square of the deviations between the temperature-time data and the current fit by equation 3.
DE: mass density of the sample.
SH: specific heat of the sample.
LE: length of the sample.
TC: thermal conductivity currently being used for data fitting.
MT: temperature range above ambient for which the data is to be fit to equation *1.
F\$: data filename.
XP: initially the total number of data acquisition time intervals in data file. Later changed to the total number of data acquisition intervals in the temperature range above ambient for which data is being fit.
BS: largest recorded heat stage temperature in data fitting temperature range.
LS: smallest recorded heat stage temperature in data fitting temperature range.
BP: largest recorded sample temperature in data fitting temperature range.
LP: smallest recorded sample temperature in data fitting temperature range.
TA: ambient sample temperature.
TS: average heat stage temperature.
PM: constant equal to $4*(TS-TA)/\#$
EM: constant equal to $\#\#/(DE*SH*LE*LE)$
GF: goodness to fit parameter used to terminate computation of series value.
STC: same as TC.
CTC: current variation increment of thermal conductivity value.

Program Outline:

14000: LOMEM set to 16384 (\$4000) to allow the primary high resolution graphics screen to be utilized without interference.

15000 to 20700: Variables DIMensioned and graphics screen accessed.

21000 to 22400: Sample mass density, specific heat, length, starting thermal conductivity, temperature fitting range and data filename entered from keyboard.

25000 to 25700: Data read from data file.

25800 to 25830: Number of data points in temperature fitting range determined.

25900 to 26250: Data within temperature fitting range listed to screen.

26300 to 26400: High resolution graphics screen accessed and bordered.

28000 to 28600: Average heat stage temperature, largest and smallest heat stage and sample temperatures determined.

28800 to 28900: Commonly used constants calculated.

30000: Goodness of fit parameter defined. This parameter was used to determine when the series computation could be truncated. When the value of the most recently calculated series elements was less than the first series element times the goodness of fit parameter, the series computation was terminated.

31000: Beginning of the loop associated with the number of successive approximation steps.

31010 to 31030: Loop to clear variable array used to store values of the sums of the squares of the deviations for successive single parameter fits to the experimental data points.

31050: Thermal conductivity increment magnitude determined.

31060: Sense of thermal conductivity increment determined.

31070: Beginning of the loop which determines the sum of the squares of the deviations between the experimental data and the fit to that data for the present thermal conduction fitting value.

31100: Jump to subroutine which plots experimental data points in the high resolution graphics screen.

31200: Beginning of loop to calculate values of fitting curve associated with each experimental value data acquisition time.

31250: Summing variable cleared.

31300: Beginning of loop to determine summation value. Maximum number of allowed series elements is twenty if series is not truncated by goodness of fit (GF) parameter.

31400: Magnitude of series element calculated.

31500 to 31600: Sense of the series element determined.

31600: Series element value added to summing variable.

31700: Most recent series element compared to goodness of fit parameter to determine if series computation is to be terminated.

31900: Value of fitting curve associated with the time of the experimental data point acquisition is calculated.

31920 to 32000: Value of fitting curve plotted on graphics screen.

32200 to 32350: Value of the sum of the squares of the deviations is computed.

32370 to 32380: Parameters of recent fit to experimental data output to the screen.

32400 to 32500: Most recent and previous sum of the squares of the deviations compared to determine if the test thermal conductivity value has passed through the best fit thermal conductivity value. 32600 to 32650: Test thermal

conductivity value is incremented.

32700: Jump to subroutine which erases most recent fit values from the graphics screen.

33000 to 35100: Determined best fit thermal conductivity value and experimental test parameters output to the text screen.

Program Listing:

```
14000 LOMEM: 16384
15000 DIM P(255),S(255),T(255),F(255),SK(20),R2(10)
20000 HOME
20100 VTAB 10
20200 PRINT " THERMAL CONDUCTIVITY DATA FITTING"
20300 PRINT "": REM BELL
20320 FOR T = 1 TO 1000: NEXT T
20400 FOR I = 1 TO 24
20500 PRINT
20600 NEXT I
20700 HGR
21000 PRINT "ENTER MASS DENSITY OF SAMPLE (GM/CC)": PRINT
21100 INPUT DE
21200 PRINT : PRINT
21300 PRINT "ENTER SPECIFIC HEAT OF SAMPLE (J/GM*C)": PRINT
21400 INPUT SH
21500 PRINT : PRINT
21600 PRINT "ENTER LENGTH OF SAMPLE (CM)": PRINT
21700 INPUT LE
21800 PRINT : PRINT
21900 PRINT "ENTER STARTING THER. COND. (J/SEC*CM*C)": PRINT
22000 INPUT TC
22100 PRINT : PRINT
22110 PRINT "ENTER TEMP FITTING RANGE (C)": PRINT
22120 INPUT MT
22130 PRINT : PRINT
22200 PRINT "ENTER DATA FILENAME": PRINT
22300 INPUT F$
22400 PRINT : PRINT
25000 D$ = CHR$(4)
25100 PRINT D$;"OPEN";F$
25200 PRINT D$;"READ";F$
25300 INPUT XP
25400 FOR I = 1 TO XP
25500 INPUT P(I),S(I),T(I)
25600 NEXT I
25700 PRINT D$;"CLOSE";F$
25800 TEXT
25810 FOR I = 1 TO XP
25820 IF P(I) > MT + P(1) THEN XP = I - 1: GOTO 25900
25830 NEXT I
25900 PRINT "NUMBER OF DATA POINTS: ";XP: PRINT
26000 FOR I = 1 TO XP
26100 PRINT "P(";I;")=";P(I);" S(";I;")=";S(I);" T(";I;")=";
T(I)
26200 NEXT I
```

```

26210 PRINT ""
26220 FOR T = 1 TO 3000: NEXT T
26250 PRINT : PRINT : PRINT
26300 HGR
26350 HCOLOR= 3
26400 HPLOT 0,0 TO 279,0 TO 279,159 TO 0,159 TO 0,0
28000 A = 0
28020 BS = 0
28040 LS = 999
28050 BP = 0
28060 LP = 999
28100 FOR I = 1 TO XP
28200 A = A + S(I)
28300 IF S(I) > BS THEN BS = S(I)
28400 IF S(I) < LS THEN LS = S(I)
28420 IF P(I) < LP THEN LP = P(I)
28440 IF P(I) > BP THEN BP = P(I)
28500 NEXT I
28550 TA = (P(1) + P(2)) / 2
28600 TS = A / XP
28800 PM = 4 * (TS - TA) / 3.1416
28900 EM = 3.1416 * 3.1416 / (DE * SH * LE * LE)
30000 GF = 0.001
30050 STC = TC
31000 FOR DIR = 1 TO 7
31010 FOR I = 1 TO 10
31020 R2(I) = 0
31030 NEXT I
31050 CTC = STC / (2.1 ^ DIR)
31060 IF DIR / 2 = INT (DIR / 2) THEN CTC = - CTC
31070 FOR PASS = 1 TO 10
31100 GOSUB 50000
31200 FOR I = 1 TO XP
31250 SM = 0
31300 FOR K = 1 TO 20
31400 SK(K) = (1 / (2 * K - 1)) * EXP ( - TC * (K - 1 / 2) *
(K - 1 / 2) * EM * T(I))
31500 IF K / 2 = INT (K / 2) THEN SM = SM + SK(K): GOTO 31700
31600 SM = SM - SK(K)
31700 IF SK(K) < GF * SK(1) THEN K = 20
31800 NEXT K
31900 F(I) = TS + PM * SM
31920 Y = 158 - ((F(I) - LP) * YM + 10)
31940 IF Y < 0 THEN GOTO 32100
31960 IF Y > 159 THEN GOTO 32100
32000 HPLOT I * XM,Y
32100 NEXT I
32200 FOR L = 1 TO XP
32300 R2(PASS) = R2(PASS) + ABS (P(L) - F(L)) * ABS (P(L) -
F(L))
32350 NEXT L
32370 PRINT "DIR = ";DIR;" PASS = ";PASS;" CTC = ";CTC
32380 PRINT " TC = ";TC;" R2 = ";R2(PASS)
32400 IF PASS = 1 THEN GOTO 32600

```

```

32500 IF R2(PASS) > R2(PASS - 1) THEN PASS = 10: GOTO 32700
32600 TC = TC + CTC
32650 IF TC < = 0 THEN TC = 0.00001
32700 GOSUB 55000
32800 NEXT PASS
32900 NEXT DIR
33000 PRINT : PRINT
34000 PRINT ""
35000 PRINT "FINAL THERMAL COND: ";TC - CTC
35010 PRINT
35020 PRINT " STAGE TEMP MIN,AVE,MAX"
35040 PRINT " ";LS,TS,BS
35041 PRINT
35042 PRINT "AMBIENT TEMPERATURE: ";P(1): PRINT
35043 PRINT "TIME BETWEEN DATA POINTS: ";T(1): PRINT
35044 PRINT "NUMBER OF DATA POINTS: ";XP: PRINT
35045 PRINT "MAXIMUM SAMPLE TEMP: ";P(XP)
35046 PRINT
35047 PRINT "DATA FILENAME: ";F$: PRINT
35050 GOSUB 55000
35060 GOSUB 50000
35065 HCOLOR= 3
35070 FOR I = 1 TO XP
35080 HPLOT I * XM,158 - ((F(I) - LP) * YM + 10)
35090 NEXT I
35100 END
50000 HCOLOR= 3
50100 XM = 278 / (XP + 1)
50200 YM = 120 / (BP - LP)
50300 FOR I = 1 TO XP
50320 Y = 158 - ((P(I) - LP) * YM + 10)
50340 IF I < > 1 THEN GOTO 50500
50400 HPLOT I * XM,Y
50450 GOTO 50600
50500 HPLOT TO I * XM,Y
50600 NEXT I
50700 RETURN
55000 HCOLOR= 0
55100 FOR I = 1 TO XP
55150 Y = 158 - ((F(I) - LP) * YM + 10)
55160 IF Y > 159 THEN GOTO 55300
55170 IF Y < 0 THEN GOTO 55300
55200 HPLOT XM * I,Y
55300 NEXT I
55400 RETURN

```

DISTRIBUTION LIST

<u>No. of Copies</u>	<u>Organization</u>	<u>No. of Copies</u>	<u>Organization</u>
2	Administrator Defense Technical Info Center ATTN: DTIC-FDAC Cameron Station, Bldg 5 Alexandria, VA 22304-6145	1	Commander US Army Aviation Systems Command ATTN: AMSAV-ES 4300 Goodfellow Blvd St. Louis, MO 63120-1798
10	C.I.A. OIR/DB/Standard GE47 HQ Washington, DC 20505	1	Director US Army Aviation Research and Technology Activity Ames Research Center Moffett Field, CA 94035-1099
1	HQDA ATTN: DAMA-ART-M Washington, DC 20310	1	Commander US Army Communication- Electronics Command ATTN: AMSEL-ED Fort Monmouth, NJ 07703-5000
1	Commander US Army Material Command ATTN: AMCDRA-ST 5001 Eisenhower Avenue Alexandria, VA 22333-0001	1	Commander US Army Communication- CECOM R&D Technical Library ATTN: AMSEL-IM-L (Reports Section) B.2700 Fort Monmouth, NJ 07703-5000
2	Commander U. S. Army Armament Research, Development & Engr Center ATTN: SMCAR-MSI SMCAR-TDC Picatinny Arsenal, NJ 07801-5001	1	Commander US Army Missile Command Research, Development, and Engineering Center ATTN: AMSMI-R Redstone Arsenal, AL 35898
1	Commander Fire Control & Small Caliber Weapons Systems Lab ATTN: DRSMC-SCM Dr. William Ebihara Picatinny Arsenal, NJ 07801-5001	1	Commander USA Missile & Space Intelligence Center ATTN: AMSMI-YDL Redstone Arsenal, AL 35898-5500
2	Commander U. S. AMCCOM ARDEC CCAC Benet Weapons Laboratory ATTN: SMCAR-CCB-TL Watervliet, NY 12189	1	Commander US Army Tank Automotive Command ATTN: AMSTA-TSL Warren, MI 48397-5000
1	Commander US Army Armament, Munition and Chemical Command ATTN: AMSMC-IMP-L Rock Island, IL 61299-7300	1	Director U.S. Army TRADOC Analysis Center ATTN: ATAA-ATOR-TSL White Sands Missile Range NM 88002-5502

AD-A194 692

THERMAL CONDUCTIVITY EFFECTS ON SHS (SELF-PROPAGATING
HIGH-TEMPERATURE SY. (U) ARMY BALLISTIC RESEARCH LAB
ABERDEEN PROVING GROUND MD T KOTTKE ET AL. MAR 88
BRL-TR-2889

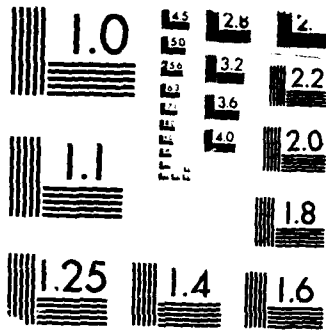
2/2

UNCLASSIFIED

F/G 28/13

NL





MICROCOPY RESOLUTION TEST CHART
BUREAU OF STANDARDS-1963-A

<u>No. of Copies</u>	<u>Organization</u>	<u>No of Copies</u>	<u>Organization</u>
1	Commandant US Army Infantry School ATTN: ATSH-CD-CS-OR Fort Benning, GA 31905-5400	5	AFATL/DOIL (Tech Info Center) Eglin AFB, FL 32542-5438
1	Commander LABCOM ATTN: AMSLC-ASSE 2800 Powder Mill Road Adelphi, MD 20783-1145	1	National Bureau of Standards ATTN: D. S. J. Schneider Room A257. Bldg 223 Washington, DC 20234
1	Commander US Army Development and Employment Agency ATTN: MODE-ORO Fort Lewis, WA 98433-5000	4	Director Los Alamos National Laboratory ATTN: Dr. R. Behrens, MST-3C348 Dr. Karl F. Wylie, MS G780 Dr. D. Sandstrom, MS-G756 Dr. S. E. Caldwell P. O. Box 1663 Los Alamos, NM 87545
1	Commander US Army Foreign Science and Technical Center ATTN: Mr. Joey F. Crider 220 Seventh Street, NE Charlottesville, VA 22901	2	Director Lawrence Livermore National Lab ATTN: Dr. J. B. Holt, L-369 Dr. D. Maiden, MS-L71 P. O. Box 808 Livermore, CA 94550
5	Commander Army Materials Technology Laboratory ATTN: AMXMR-OM Dr. James W. McCauley Dr. Kenneth Gabriel Ms. Theresa M. Resetar ATTN: AMXMR-MCP Dr. Dennis Viechnicki Watertown, MA 02172	1	Director Sandia National Laboratory Applied Mathematics Div 8231 ATTN: Dr. Stephen B. Margolis Livermore, CA 94550
3	Commander US Army Research Office ATTN: Dr. Iqbal Ahmad Dr. Andrew Crowson Dr. Robert Reeber P. O. Box 12211 Res Triangle Park, NC 27709	1	AIRTRON Division ATTN: Dr. John Ings 200 East Hanover Ave. Morris Plains, NJ 07950
2	Commander Naval Research Laboratory Dr. W. Henshaw Code 6372 Washington, DC 20234	1	ALCOA Laboratory ALCOA Tech Center ATTN: Dr. Aaron J. Becker Alcoa Center, PA 15069
1	AFWL/SUL Kirtland AFB, NM 87117	1	General Sciences, Inc. ATTN: Dr. P. D. Zavitsanos P. O. Box 185 Norristown, PA 10401
		1	Lockheed Palo Alto Research Laboratory ATTN: Dr. Alexander P. Hardt 3251 Hanover Street Palo Alto, CA 94304

No. of
Copies

Organization

- 2 Martin Marietta Laboratories
ATTN: Dr. Dennis C. Nagle
Dr. Stephen R. Winzer
Mr. Michael Riley
1450 South Rolling Road
Baltimore, MD 21227
- 1 Systems Planning Corp.
ATTN: Mr. William W. Frankhouser
1500 Wilson Blvd.
Arlington, VA 22209
- 1 Terra Tek, Inc.
ATTN: Raymond A. Cutler
400 Wakara Way
Salt Lake City, UT 84108
- 2 Defense Advance Research
Project Agency
ATTN: Dr. P. A. Parrish
Dr. Gene Farnum
1400 Wilson Blvd.
Arlington, VA 22209
- 2 Georgia Institute of Tech
ATTN: Ms. Kathryn V. Logan
Dr. Jesse D. Walton
EES/EMSL
Atlanta, GA 30332
- 1 Rice University
ATTN: Dr. John Margrave
Vice President
Advance Studies Research
P. O. Box 2692
Houston, TX 77252
- 1 State University of New York
ATTN: Dr. Vladimir Hlavacek
Amherst Campus
Furnas Hall 507
Buffalo, NY 14260
- 1 University of California
ATTN: Dr. Zuhair Munir
College of Engineering
Davis, CA 95616

Aberdeen Proving Ground

Dir, USAMSSA
ATTN: AMXSY-D
AMXSY-MP, H. Cohen
Cdr, USATECOM
ATTN: AMSTE-SI-F
Cdr, CRDC, AMCCOM
ATTN: SMCCR-RSP-A
SMCCR-MU
SMCCR-SPS-IL

USER EVALUATION SHEET/CHANGE OF ADDRESS

This Laboratory undertakes a continuing effort to improve the quality of the reports it publishes. Your comments/answers to the items/questions below will aid us in our efforts.

1. BRL Report Number _____ Date of Report _____

2. Date Report Received _____

3. Does this report satisfy a need? (Comment on purpose, related project, or other area of interest for which the report will be used.) _____

4. How specifically, is the report being used? (Information source, design data, procedure, source of ideas, etc.) _____

5. Has the information in this report led to any quantitative savings as far as man-hours or dollars saved, operating costs avoided or efficiencies achieved, etc? If so, please elaborate. _____

6. General Comments. What do you think should be changed to improve future reports? (Indicate changes to organization, technical content, format, etc.) _____

CURRENT ADDRESS Name _____
 Organization _____
 Address _____
 City, State, Zip _____

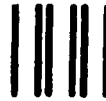
7. If indicating a Change of Address or Address Correction, please provide the New or Correct Address in Block 6 above and the Old or Incorrect address below.

OLD ADDRESS Name _____
 Organization _____
 Address _____
 City, State, Zip _____

(Remove this sheet, fold as indicated, staple or tape closed, and mail.)

FOLD HERE

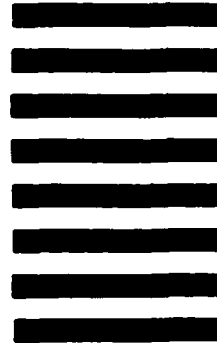
Director
US Army Ballistic Research Laboratory
ATTN: DRXBR-OD-ST
Aberdeen Proving Ground, MD 21005-5066



NO POSTAGE
NECESSARY
IF MAILED
IN THE
UNITED STATES

OFFICIAL BUSINESS
PENALTY FOR PRIVATE USE, \$300

BUSINESS REPLY MAIL
FIRST CLASS PERMIT NO 12062 WASHINGTON, DC
POSTAGE WILL BE PAID BY DEPARTMENT OF THE ARMY



Director
US Army Ballistic Research Laboratory
ATTN: DRXBR-OD-ST
Aberdeen Proving Ground, MD 21005-9989

FOLD HERE

END

DATE

FILMED

8-88

DTIC